Electrospinning of porous composite materials for hydrogen storage application

By

Perushini Annamalai

BSc Chemistry (Honours)-University of KwaZulu-Natal

A thesis submitted in fulfilment of the requirements for the degree of Magister Scientiae in the Department of Chemistry, University of the Western Cape.

Supervisors:

Prof Leslie F. Petrik

Dr Nicholas M. Musyoka

Dr Henrietta W. Langmi

November 2016

Abstract

Due to the rapid depletion of fossil fuel reserves and the production of environmentally harmful by-products such as carbon dioxide, there is an urgent need for alternate sustainable clean energy. One of the leading candidates in this endeavour is hydrogen, which can be used as an energy carrier since it has a high energy density, zero emissions and is produced from non-depletable resources such as water. The major challenge hindering a hydrogen economy is the lack of safe and effective storage technologies for mobile applications. A prospective solution to this problem lies in the use of porous powdered materials, which adsorb the hydrogen gas. However, the integration of these powdered materials into a storage tank system, results in the pipelines being contaminated during filling cycles. This necessitates the shaping of the porous powdered materials. Among the many shaping techniques available, the electrospinning technique has been proposed as a promising technology since it is a versatile process that is easily scaled-up making it attractive for the applications of the study. Furthermore, the electrospinning process enables the synthesis of nano-sized fibres with attractive hydrogen sorption characteristics. In this regard, the current study employs the electrospinning technique to synthesise electrospun composite fibres for mobile hydrogen storage applications.

After electrospinning three polymers, polyacrylonitrile (PAN) was selected as the most suitable polymer because it yielded bead-free electrospun fibres. However, the diameter of the PAN fibres was large/thick which prompted further optimisation of the electrospinning parameters. The optimised electrospinning conditions that yield unbeaded fibres within the desired diameter range (of 300-500 nm) were a PAN concentration of 10 wt%, a flow rate of 0.4 mL/h, a distance of 10 cm between the needle tip and collector plate, and an applied voltage of 8 kV. The study then progressed to the synthesis and characterisation of the pristine porous powdered materials which adsorb hydrogen gas. The porous powdered materials investigated were commercial zeolite 13X, its synthesised templated carbon derivative (ZTC) and Zr (UiO-66) and Cr (MIL-101) based metal-organic frameworks (MOFs). ZTC was synthesised via liquid impregnation coupled with chemical vapour deposition (CVD), and the MOFs were synthesised by the modulated solvothermal method. Analysis of the ZTCs morphology and phase crystallinity show that the carbon templated process using zeolites was successful, however, ZTC was amorphous compared to crystalline zeolite template. The BET surface area was assessed with the aid of nitrogen sorption

isotherms for both zeolite 13X and ZTC, and values of 730 and 2717 m^2/g, respectively were obtained. The hydrogen adsorption capacity for zeolite 13X was 1.6 wt% and increased to 2.4 wt% in the ZTC material at 77 K and 1 bar. The successful synthesis of well defined, crystalline MOFs was evident from X-ray diffraction and morphological analysis. The BET surface area and hydrogen adsorption for Zr MOF were 1186 m^2/g and 1.5 wt%, respectively at 77 K and 1 bar. Cr MOF had a BET surface area of 2618 m^2/g and hydrogen adsorption capacity of 1.9 wt% at 77 K and 1 bar.

The main focus of the study was to synthesise electrospun composite fibres that can adsorb hydrogen gas and thus provide significant insight in this field of research. As such it examined composite fibres that incorporates porous powdered materials such as zeolite 13X, ZTCs, UiO-66 (Zr) MOF and MIL-101 (Cr) MOF and investigated their ability to adsorb hydrogen gas, which have not been reported previously. The synthesis of composite fibres was achieved by incorporating the porous powdered materials into the PAN resulting in a polymeric blend that was then electrospun. Morphological analysis illustrated that the porous powdered materials were successfully supported by or incorporated within the PAN fibres, forming composite fibres. The BET surface area of the 40 wt% zeolite-PAN and 12.5 wt% ZTC-PAN composite fibres were 440 and 1787 m^2/g respectively. Zr MOF and Cr MOF composite fibres had a BET surface area of 815 and 1134 m^2/g, respectively. The BET surface area had reduced by 40, 34, 31 and 57% for zeolite 13X, ZTC, Zr MOF and Cr MOF, respectively after these porous powdered materials were incorporated into PAN. The hydrogen adoption capacity for 40 wt% zeolite-PAN, 12.5 wt% ZTC-PAN, 20 wt% Zr MOF-PAN and 20 wt% Cr MOF-PAN composite fibres was 0.8, 1.8, 0.9 and 1.1 wt%, respectively. This decrease was attributed to the limited amount of porous powdered materials that could be incorporated into the fibres since only 40 wt% of zeolite 13X, 12.5 wt% of ZTC and 20 wt% of the MOFs were loaded into their respective composite fibres. This was due to the fact that incorporation of greater amounts of porous powdered materials resulted in a viscous polymeric blend that was unable to be electrospun.

It is evident from the study that electrospinning is a versatile process that is able to produce composite fibres with promising properties that can potentially advance the research in this field thus providing a practical solution to the problem of integrating loose powdered materials into an on-board hydrogen storage system.

Keywords

Zeolites
Zeolite templated carbons

Metal-organic frameworks

Electrospinning

Composite fibres

Hydrogen storage

Declaration

I, Perushini Annamalai declare that the dissertation entitled *"Electrospinning of porous composite materials for hydrogen storage"* is to the best of my understanding my own work unless referenced and that neither the whole nor any part of this dissertation has ever been submitted for any other degree or diploma to a tertiary institution or examination board.

Perushini Annamalai

30 November 2016

Acknowledgements

Garretty once said that "a mother's love is the fuel that enables a normal human being to do the impossible"; this is a true testament to my achievements thus far.

Last but not least a very special thank you to the host of family and close friends who has supported and encouraged me through this time, I am eternally grateful to have each and every one of you in my life.

Dedication

I dedicate this work to my late Grandfather

Mr Terence Davan

Your life was the epitome of altruism and I hope to follow in your footsteps with this work as it is a step towards changing the world.

Table of Contents

Chapter Three

Chapter Four

Chapter Five

Chapter Six

Chapter Seven

List of Figures

List of Tables

List of Equations

UNIVERSITY *of the*

WESTERN CAPE

Nomenclature

BET =   Brunauer-Emmett-Teller

CVD =   Chemical Vapour Deposition

DMF =   N,N-dimethylformamide

DOE =   Department of Energy

FAU =   Faujasite

FTIR =   Fourier Transform Infrared Spectroscopy

HF =   Hydroflouric acid

HySA =   Hydrogen South Africa

MIL=   Matérial Institute Lavoiser

MOF =   Metal-organic frameworks

PAA =   Poly-acrylic acid

PAN =   Poly-acrylonitrile

PSMA =   Poly-styrene-alt-maleic anhydride

PXRD =   Power X-ray diffraction

SEM =   Scanning Electron Microscopy

TGA =   Thermal Gravimetric Analysis

UiO=   University of Oslo

ZTC =   Zeolite templated carbon
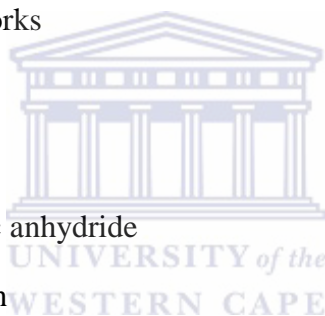
Achievements

The subject matter was submitted as peer-reviewed journal articles for publication:

1. Ren, J., Musyoka, N.M., Annamalai, P., Langmi, H.W., North, B.C. and Mathe, M., (2015). Electrospun MOF nanofibers as hydrogen storage media. *International Journal of Hydrogen Energy,* **40** (30), pp. 9382-9387.

2. Annamalai, P., Musyoka, N.M., Ren, J., Langmi, H.W., Mathe, M., Bessarabov, D. and Petrik, L.F., (2016). Electrospun zeolite templated carbon composite fibres for hydrogen storage applications. *Research on Chemical Intermediates*. (Accepted).

The subject matter was presented at several conference proceedings:

1. P. Annamalai, N. M. Musyoka, H.W. Langmi, J. Ren, and L.F. Petrik, Electrospinning of zeolitic fibre composites for hydrogen storage applications, 17th SACI Inorganic Chemistry Conference, Grahamstown, South Africa, 28 June-2 July 2015. Poster Presentation.

2. P Annamalai, NM Musyoka, HW Langmi and D Bessarabov, Electrospinning of composite fibres for hydrogen storage applications. HySA Technical Meeting 2015, Cape Town, South Africa, 17-18 August 2015. Poster Presentation.

3. P. Annamalai, N. M. Musyoka, H.W. Langmi, J. Ren, and L.F. Petrik, Electrospinning of zeolitic fibre composites for hydrogen storage applications, 5th CSIR Emerging Researcher Symposium, Pretoria, South Africa. 8-9 October 2015. Poster Presentation.

4. P. Annamalai, N. M. Musyoka, H.W. Langmi, J. Ren, and L.F. Petrik, Synthesis and characterisation of electrospun porous composite materials for hydrogen storage application, 1st SACI North Section Young Chemist Symposium, Limpopo, South Africa. 23 November 2016. Oral Presentation.

5. N.M. Musyoka, J. Ren, P. Annamalai, H.W. Langmi, B. C. North, M. Mathe and L. F. Petrik, Synthesis of porous electrospun nanofiber composites for hydrogen storage applications, 1st European Conference on Metal Organic Frameworks and Porous Polymers, Kongresshotel Potsdam am Templiner See (nearby Berlin), Germany, 11-14 October 2015. Poster Presentation.

6. J. Ren, P. Annamalai, N. M. Musyoka, H. W. Langmi, B. C. North, M. Mathe, D. Bessarabov, Electrospun Preparation and Hydrogen Storage Properties of Sodalite-type Zr-fumarate Metal-Organic Framework, 6th International Conference on Advanced Nanomaterials, Aveiro, Portugal, 20-22 July 2015. Poster Presentation.

Other journal article publications during Master's study:

1. Musyoka, N.M., Ren, J., Annamalai, P., Langmi, H.W., North, B.C., Mathe, M. and Bessarabov, D. (2015). Synthesis of a hybrid MIL-101 (Cr)/ZTC composite for hydrogen storage applications. *Research on Chemical Intermediates,* **42**, pp. 1-9.
2. Medina, P., Zheng, H., Fahlman, B., Annamalai, P., Swartbooi, A., Roux, L. and Mathe, M. (2015). $Li_4Ti_5O_{12}$/graphene nanoribbons composite as anodes for lithium ion batteries. *SpringerPlus,* **4** (1), pp. 1-7.

Chapter One

Introduction

This chapter serves to establish the basis for the study by outlining the reason humanity is facing global devastation together with a proposed solution to curb the effects of global warming. It will focus on transportation and an alternative fuel option. Then the chapter will detail all relevant information as to the reason for the study and how it will be approached. It then goes on to highlight the scope of the study and how the thesis is structured.

1.1 Broad context

Existence on our planet is dependent on a delicately balanced global ecosystem, a tip in this balance results in cataclysmic effects (Vitousek et al., 1997). Case in point, the high concentration of greenhouse gases in the atmosphere such as carbon dioxide, which is problematic because it is directly linked to global warming and climate change (Conte et al., 2001). An increase in carbon dioxide emissions was seen after the fossil fuel capitalisation during the 20th century, when its concentration was estimated to have increased by a staggering 30% from 280 to 370 ppm (Conte et al., 2001; Armaroli & Balzani, 2007; Houghton et al., 2001). Human activities such as agriculture, mining as well as in the energy sector contribute the highest amount of greenhouse gas emissions (Houghton, 2009; Pegels, 2010).

Humankind has encountered many challenges over the centuries; however, the most significant challenge is the accessibility of energy (Evans et al., 2009). The direct correlation between economic growth and energy demand leaves developing countries like South Africa dependent on fossil fuels as a dominant source, since it is cheap and highly accessible, however, fossil fuel reserves are finite and rapidly diminishing (Armaroli & Balzani, 2007; Pegels, 2010; Evans et al., 2009; Dincer, 2000). This exploitation of fossil fuels resulted in a 1.1% contribution to the global carbon dioxide emissions a decade ago (Pegels, 2010); WRI, 2014). The important question is how do we improve the living standards for people and not compromise the environment? Scientists believe that the solution lies in the use of renewable energy sources, for instance solar and wind energy (Armaroli & Balzani, 2007; Pegels, 2010).

The energy yield from solar and wind sources are impermanent hence the necessary storage of excess energy during low supply periods are usually done by batteries (Agbossou et al., 2001). However, this storage option is limiting due to a loss of 1-5% of energy capacity per hour (Agbossou et al., 2001). Current research for viable storage of excess energy is exploring the employment of hydrogen, which is produced via electrolysis from this excess electrical energy, the hydrogen is then supplied to a fuel cell that provides electricity during high demand periods (Agbossou et al, 2001; Chan, 2007).

Hydrogen, as an energy carrier, is easily produced and simply converted to electricity via fuel cell technology, as compared to solar and wind energy, which first needs to be transformed into electricity in order to be, transported effectively (Jiménez et al., 2012). A hydrogen economy sounds remarkable because it provides energy that is not harmful to the environment; it is produced in a variety of ways such as from non-depletable resources like water and it has a high energy density (Nishihara & Kyotani, 2012; Yang et al., 2012). Although hydrogen can be used to power portable electronic devices and in the distribution of generated power, it is mainly used as a fuel for transport (Solomon & Banerjee, 2006).

A person's inclination to be mobile is what drives the transport sector to consume 25% of the global energy (Mori & Hirose, 2009). South Africa is highly reliant on imported crude oil since it is the primary source of fuel for transportation, which averaged at 3% (amounting to 8 million tonnes) per annum a decade post-apartheid (Thambiran & Diab, 2011; Wabiri & Amusa, 2010). The transport sector contributes approximately 9% of the total greenhouse gas emissions in South Africa, which is mainly due to road transport (Thambiran & Diab, 2011). With 79% of crude oil supplied by the Middle East, a region prone to geopolitical turmoil, together with the oil crisis in 1973 and the air pollutants and greenhouse gases from road transportation, alternative resources need to be explored to ensure energy security as well as a reduction in adverse environmental effects (Wabiri & Amusa, 2010; Demirdoven & Deutch, 2004; Lund, 2007; Lund & Kempton, 2008; Liaquat et al., 2010).

The transition from internal combustion engines to hydrogen fuelled vehicles may seem easy due to the many advantages it presents, however, on-board hydrogen storage for automotive applications is challenging due to it being a low density gas (Solomon & Banerjee, 2006; Mori & Hirose, 2009). At ambient temperatures and pressures, hydrogen has a low volumetric density implying that for mobile applications, hydrogen gas will require an enormous on-board storage unit for the vehicle to travel an adequate distance (Yang et al.,

2012; Bimbo et al., 2013). For instance, driving a distance of 400 km requires approximately 4 kg of hydrogen for a fuel cell vehicle; this amount of hydrogen gas will fill up a 45 m^3 tank at room temperature and 1 bar pressure (Zhao et al., 2008). Herein lays the major challenge for the realisation of a hydrogen economy (Jordá-Beneyto et al., 2007).

A variety of storage options are already in existence, which are high pressure compressed gas, cryogenic liquid hydrogen, metal hydrides and physical adsorption on solid porous materials (Jiménez et al., 2012; Yang et al., 2012). However, none of these options satisfy the US Department of Energy on-board storage requirements for 2020, that is a gravimetric and volumetric capacity of 1.8 kWh/kg (0.055 kg H_2/kg system) and 1.3 kWh/kg (0.040 kg H_2/L system) respectively, these measurements include the tank, storage medium and accessories (Zhao et al., 2008; Jordá-Beneyto et al., 2007; US DOE, 2015). The on-board storage system needs to have the highest volumetric density, with the least amount of material used. Also, the uptake of hydrogen must be reversible and the system must be cost effective (Jiménez et al., 2012).

In line with the South African National Development Plan to reduce greenhouse gas emissions, the Department of Science and Technology established a strategy branded as Hydrogen South Africa (abbreviated, HySA), which involves research, development and innovation of hydrogen and fuel cell technologies. HySA Infrastructure, a division of HySA, is aimed at researching and developing technologies, processes and products for hydrogen production, storage and distribution. This study constitutes part of the research undertaken at HySA Infrastruture.

1.2 Problem statement

Strategies that propagate the use of sustainable energy begins with research into renewable energy, followed by the development of innovative technologies and materials to be implemented worldwide, thereby being the final step of a global energy evolution (Su & Centi, 2013). Following the various research done on storage options for hydrogen fuelled vehicles, inadequate strategies that do not meet the necessary storage capacity, safety and cost requirements are available. However, a niche area that many scientists would say looks promising is the physisorption of hydrogen on porous nanomaterials (Yang et al., 2012; Nishihara et al., 2009). Intensive studies on physical adsorption of hydrogen on porous materials such as zeolites, templated carbons and metal-organic frameworks (MOFs) have

illustrated their potential for attractive storage capacities (Yang et al., 2012; Jordá-Beneyto et al., 2007; Nishihara et al., 2009). For mobile applications these porous, powdered materials need to be confined in a tank, a part of the hydrogen storage system, like a petroleum tank. However, various complications arise due to these porous materials being nano- or micro-scaled powders. For instance, the volumetric capacity is affected by the low packing density of the powders and contamination of the pipes can occur during charge and discharge cycles. In addition, powdered materials are difficult to handle since they are easily blown around (Ren et al., 2015b).

1.3 Motivation and research questions

The transition from producing these porous materials in a laboratory to integrating them in a storage system is challenging since they are produced in powder form. By shaping these powdered materials one can successfully integrate these materials into a storage system for mobile applications (Ren et al., 2015). A variety of shaping techniques are available to date such as granulation, pelletisation, templating methods and a combination of templating and activation techniques. Electrospinning is a versatile, easily up-scaled technique that utilises a high voltage source that causes a polymer solution to be drawn out of a needle onto a metal collector plate resulting in fibres (Fu et al., 2011; Cavaliere et al., 2011; Megelski et al., 2002; Ren & North, 2014).

Although electrospinning was discovered over a century ago, much attention is being paid to this process recently due to the production of fibres with micro- and nano-scale features necessary for the improvement of energy storage (Cavaliere et al., 2011). Morphology of the fibres is highly dependent on the manner in which they are electrospun. For instance, in the production of composite fibres (involving the porous materials being incorporated into the polymer and then electrospun) evaporation of the solvent during electrospinning and the removal of solvent trapped in the pores during the degassing process lead to the creation of pores (Ren et al., 2015b; Schwieger et al., 2016; Srinivasan et al., 2006).

Electrospinning is able to produce composite fibres with the necessary properties that will advance the research in this field and furthermore create a product that will be implemented in real life applications (Cavaliere et al., 2011). The research done on electrospun composite fibres was limited and only incorporated select materials such as silicalite-1, MCM-41 and SBA-15, zeolitic imidazolate framework (ZIF-8), MIL-101 (Fe-based) and UiO-66 metal-

organic frameworks (MOFs) (Di et al., 2008; Ostermann et al., 2011; Srinivasan et al., 2006; Wu et al., 2012; Armstrong et al., 2015; Zhao et al., 2016). Therefore this study will provide significant insight in the field because it examines composite fibres that incorporate porous materials such as zeolite 13X, zeolite templated carbons (ZTCs) and MIL-101 (Cr) MOF which have not been studied previously. Furthermore, the study will analyse the aforementioned composite fibres for hydrogen adsorption which also has not been done before. The study endeavours to ascertain answers to the following research questions:

- Can the electrospun composite fibres adsorb hydrogen?
- Can pores be created on PAN fibres if they are placed under vacuum?
- Does the hydrogen storage capacity increase with weight percent of porous materials incorporated into the composite fibres?
- Does heat treatment affect the composite fibres?

1.4 Objectives

The overall aim of the study is to produce electrospun composite fibres and to investigate their proclivity for hydrogen adsorption. To attain this aim, the objectives of the study were envisaged as follows:

1. To perform experiments aimed at optimising electrospinning parameters and also identify the best polymeric material.
2. To synthesise electrospun composite fibres whereby different porous powders such as zeolites, ZTCs and MOFs will be incorporated into the polymer and then electrospun.
3. To thoroughly characterise the resulting materials and test them for their hydrogen uptake capacity.

1.5 Hypotheses

1. During electrospinning when the solvent evaporates resulting in fibres on the collector plate, the fibres are not completely free of solvent. It is hypothesised that placing the PAN fibres under a high vacuum of 10^{-7} bar will remove any solvent in the fibres thereby creating pores.
2. It is further hypothesised that porous hydrogen storage materials in powder form can be encapsulated in the polymeric fibres and still adsorb hydrogen. The hydrogen

adsorption capacity will increase as the increment weight percent of powder is increased.

1.6 Research approach

The approach to achieving the goals of the study began with the literature review to assess the state-of-art of the electrospinning process and identify research gaps in order to structure the study. From literature, polymers suitable for electrospinning were selected, knowledge about the assembly of a bench scale electrospinning setup was obtained and the conditions that affect the electrospinning process identified. The research approach consisted of four stages; firstly, the polymer selection whereby a suitable polymer was determined. Secondly, the optimisation of electrospinning parameters for that suitable polymer. Thirdly, the synthesis of the porous powdered materials, and finally, the production of the composite fibres.

In order to produce composite fibres a suitable polymer needed to be selected first, hence three polymers were chosen namely; poly-styrene-alt-maleic anhydride (PSMA), poly-acrylic acid (PAA) and poly-acrylonitrile (PAN) along with the corresponding solvent system, and thereafter electrospun. The resultant polymer fibres were analysed visually during the electrospinning process and via scanning electron microscopy (SEM) to assess if there was bead formation. In order to control the morphology and diameter of the fibres; one needs to understand the principles of electrospinning and the parameters that govern the success of the process (Huang et al., 2003). Hence the second step was to optimise the electrospinning parameters by varying each parameter for PAN (suitable polymer selected from the previous step) to obtain a baseline condition. The varied parameters were:

- Polymer concentration
- Applied voltage
- Flowrate of the polymer solution
- Distance between the needle tip and collector plate

According to literature, stabilisation improves the mechanical strength of the fibres thus the fibres underwent thermal treatment (Lee et al., 2012).

The crux of the study was the production of composite fibres whereby the highest amount of porous powders that store hydrogen was incorporated into the polymer without compromising its ability to be electrospun. The porous powdered materials were:

- Zeolite 13X

- ZTCs

- MOFs specifically MIL-101 (Cr) and UiO-66 (Zr)

Since the study focuses on the shaping of porous powdered materials without considerably compromising their hydrogen storage capacity, the effect of porous powdered material loading percent was investigated. The loading percentage range for each porous powdered material was identified whereby the porous powdered materials were incorporated and periodically incremented. It is known that by incorporating the porous powdered materials into PAN fibres, there will be a reduction in surface area and thus a concomitant reduction in the hydrogen storage capacity because a 100 weight percent loading cannot be achieved (Ostermann et al., 2011). It is by this thinking that the creation of porosity in the polymer nanofibres was investigated by placing the fibres under a high vacuum (10^{-7} bar) to remove any solvent trapped from the electrospinning process.

At each stage of the experimental approach the as-synthesised samples were characterised via SEM to analyse the surface morphology and to measure diameter of the fibres. Powder X-ray diffraction (XRD) was used to determine phase crystallinity and thermal studies were done by thermal gravimetric analysis (TGA) to determine the temperature at which the materials decompose. Since Brunauer-Emmett-Teller (BET) surface area and hydrogen storage capacity are directly correlated, both were measured. Then the structural changes in the materials were analysed via Fourier transform infrared spectroscopy (FTIR).

1.7 Scope and delimitations

A bench scale electrospinning unit was employed, because of financial constraints. Therefore, small batches of fibres were produced. Initial investigations resulted in the use of PAN as the polymer of choice to produce composite fibres. ZTCs are of interest for hydrogen storage because they are robust materials that possess a high surface area. Zeolite 13X was utilised because it served as a sacrificial template from which the ZTCs were synthesised. Zr MOF and Cr MOF were used because they are thermally and chemically stable. In addition, Cr MOF is synthesised from a green route and both MOFs possess high surface areas. Measurements for hydrogen storage capacity were done at 1 bar pressure because that was the pressure limit of the instrument available. Due to the exceedingly high temperatures at which carbonisation takes place, carbon fibres were not produced for the study because such

temperatures would destroy the porous powdered materials used in preparing the composite fibres.

1.8 Thesis structure

Chapter one introduces the topic of research, thus stating its relevance and gives an outline of the background and rationale of the study. It will briefly discuss how the study was executed to achieve the objectives and prove the hypotheses. It further outlines the scope and delimitations. Finally, it ends with a road map of the structure of the thesis.

Chapter two is an in-depth literature review highlighting the physical properties of hydrogen, its production methods, and the advantages and disadvantages of the current hydrogen storage technologies available, that is compressed high pressure gas cylinders, cryogenic liquid hydrogen, chemisorption with chemical hydrides and physisorption on porous materials. Thereafter relevant information about the porous powdered materials, including zeolites, ZTCs and MOFs used in the production of the composite fibres are given. The chapter progresses further by explaining the reason why it is important to shape these porous powdered materials, and outlines shaping techniques available with an elaboration of electrospinning process and parameters. The chapter concludes by highlighting previous studies done on the production of electrospun composite fibres with particular attention to the porous powdered materials used in this study.

Chapter three is the experimental section where all details and conditions pertaining to the production and characterisation of the materials are given.

Chapter four is the polymer selection and optimisation, it discusses why and how the suitable polymer (PAN) was selected for the production of composite nanofibres. This chapter also presents and discusses the results from the optimisation of electrospun PAN fibres as well as the morphological, structural, thermal, surface area and hydrogen analysis.

Chapter five presents the analysis of the pristine porous powdered materials and discusses the most important results applicable to the characterisation of the pristine porous materials that adsorb hydrogen gas.

Chapter six is the analysis of the composite fibres whereby a full discussion of the results pertaining to the synthesised electrospun composite fibres is given.

Chapter seven will conclude the findings of this research and contain recommendations for future work.

Chapter summary

In hopes of setting the context of the study, the chapter began with an overview of the link between carbon dioxide concentrations and global warming, explaining the rationale for the use of hydrogen as a fuel for automotive vehicles. Strong evidence illustrates that solid-state porous materials is a promising solution for the hydrogen storage bottleneck for mobile applications. Shaping of the porous solid-state materials is a necessary step for integrating the materials into a hydrogen storage system which provided a motivation for the study.

Electrospinning is a versatile shaping technique that incorporates porous materials into fibres thereby producing composite fibres. The chapter then highlighted how the study was approached to answer the research questions and hypotheses, and achieve the objectives set out. Thereafter scope of the study was outlined along with infrastructure limitations. The chapter concluded with how the thesis is structured by briefly describing what each chapter entails.

The next chapter is an in-depth literature survey on research that was done on aspects pertaining to the study.

Chapter Two
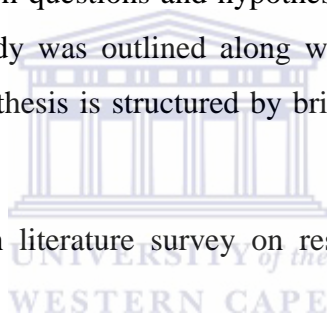
Literature Review

The chapter provides insight into previous studies and findings pertaining to this particular research topic. It begins with a brief introduction of hydrogen and then focuses on the current hydrogen storage technologies with particular attention being paid to the adsorption of hydrogen on porous materials, highlighting the use of zeolites, templated carbons and MOFs specifically the types used in this study.

The chapter goes on further to discuss the rationale behind shaping the powdered materials and highlights available shaping techniques paying particular attention to electrospinning, discussing the process, history and parameters. The chapter ends with research done on electrospun zeolite, carbon or MOF composite fibres.

2.1 Hydrogen

Hydrogen, being the lightest and abundantly available element is said to be the energy carrier for the 21st century, since it is pollution free when produced from renewable energy sources (Jain, 2009). Ubiquitous sources of hydrogen on earth include natural gas, biomass and water since pure hydrogen is not available naturally in large quantities (Klell, 2006). Production of hydrogen via steam reforming, partial oxidation and gasification technologies of natural gas involves the conversion to syngas and then hydrogen, whereas biomass needs to be converted to biogas first then syngas and then hydrogen (Conte et al., 2001; Turner, 2004). An alternative, more sustainable method to produce hydrogen is the splitting of water into hydrogen and oxygen with the aid of an electrolyser; electrolysis can be driven by solar energy thus making it sustainable but it occurs on a small scale (Zeng & Zhang, 2010).

Widespread infrastructure needs to be in place for the transport, distribution and storage of hydrogen for it to be an energy carrier for automotive fuel cell vehicles (Mori & Hirose, 2009). The typical supply route for hydrogen depicted in Figure 2.1, involves the hydrogen being produced at a plant then transported via two storage mechanisms (that is gas or liquid) to the hydrogen fuelling station. Thereafter it is converted or remains in the same phase when being transferred into the fuel cell vehicle depending on the on-board storage of fuel cell vehicles. Although the preferred method of hydrogen storage is as low pressure gas, since it is produced

in gaseous form, this is not possible due to hydrogen being a low density gas (Mori & Hirose, 2009).
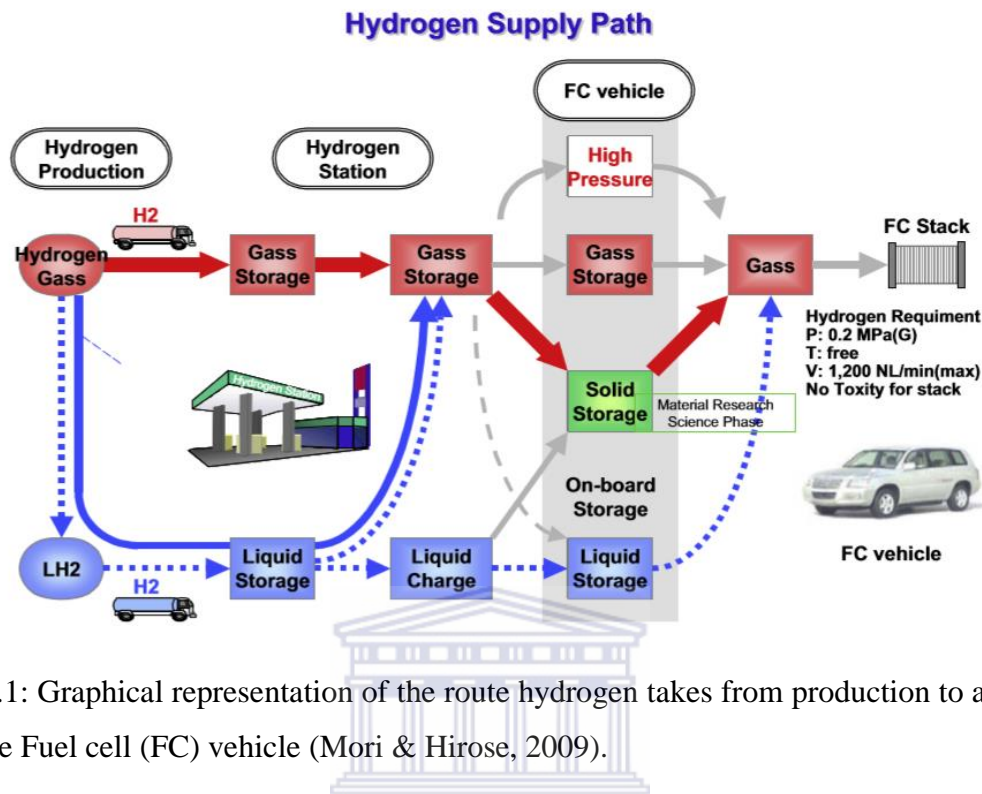
Figure 2.1: Graphical representation of the route hydrogen takes from production to application that is the Fuel cell (FC) vehicle (Mori & Hirose, 2009).

The significant on-board storage issues will govern the evolution of the energy and transportation sectors from fossil fuels to hydrogen (Berry & Aceves, 1998). The economic investment in hydrogen fuel cell vehicles is dependent on the type of on-board storage implemented which is able to satisfy stringent criteria, in terms of performance, range, cost and safety among other aspects (Berry & Aceves, 1998).

2.2 Current hydrogen storage technologies

Aceves et al (2000) states practical storage options for hydrogen include compressed high pressure gas cylinders, cryogenic liquid hydrogen and metal hydride absorption, each with its own benefits and drawbacks. However, a more favourable route to store hydrogen is the physisorption of hydrogen gas on porous materials such as zeolites, templated carbons and MOFs (Yürüm et al., 2009; Hirscher et al., 2010). This section will explain the storage mechanism of each technology and outline their advantages and disadvantages.

2.2.1 Compressed high pressure gas cylinders

The typical and extensively studied technology for on-board hydrogen storage is high pressure gas cylinders, which utilise high pressure cylinders to contain compressed hydrogen gas at 350 or 700 bar thereby increasing the energy density (Hua et al., 2011; O'Malley et al., 2014). There are four types of vessels to store hydrogen gas, categorised according to their composition. It began with steel cylinders (type I) at atmospheric pressure which was impractical for on-board storage because it took up a considerable amount of space and it was heavy (Mori & Hirose, 2009; Ewald, 1998). Thereafter type II cylinders which consisted of metal liner hoop wrapped with a glass fibre reinforced polymer (GFRP) were developed, however, these cylinders could not withstand the high pressures necessary for hydrogen storage (Mori & Hirose, 2009; Barthélémy et al., 2016). It is the US DOE on-board requirements of a gravimetric and volumetric capacity of 0.055 kg H_2/kg system and 0.040 kg H_2/L system, respectively that prompted the development of type III and IV composite cylinders specifically designed for high pressures (Mori & Hirose, 2009; Barthélémy et al., 2016; Zheng et al., 2012).

The difference between type III and IV cylinders is that they have a metal or plastic liner, respectively but both are fully wrapped with carbon fibre/epoxy resin (Mori & Hirose, 2009; Zheng et al., 2012; Hu et al., 2008). Although both cylinders are designed for hydrogen storage type IV is more favourable because it is able to endure 15 000 refuelling cycles between 20-875 bar (Villalonga et al., 2009). People are enthusiastic about this storage option because it has almost fulfilled the gravimetric targets and is close to meeting volumetric targets, however feasibility and large scale production requires a notable cost reduction (O'Malley et al., 2014). The general public's perception of the use of hydrogen is that hydrogen is not safe because of the Hindenburg disaster in 1937, which is a major drawback since it will determine whether hydrogen fuel cell vehicles will be accepted into the public domain (Schulte et al., 2004). Compressed hydrogen gas cylinders run the risk of a fire due to the flammable polymer-reinforced composite on the cylinders as well as the hazardous effects of leakage of hydrogen from stationary vehicles (Hu et al., 2008; Schulte et al., 2004; Utgikar & Thiesen, 2005).

2.2.2 Cryogenic liquid hydrogen

Storing hydrogen in its liquid form is quite beneficial because it contains a higher energy density; it is compact and can be easily and economically transported; however these benefits are outweighed by the disadvantages (Sherif et al., 1997). The use of liquid hydrogen is

restricted due to the high energy consumption for liquefaction as well as the high evaporation rate during transporting, refuelling and the absorption of heat when pressurised rapidly (Aceves et al., 2000; Aceves et al., 2010). By improving these restrictions, liquid hydrogen will be a promising option. Such improvements include reliquefying hydrogen that has evaporated and the use of cyro-compressed tanks (Berry & Aceves, 1998; Sherif et al., 1997). The interesting concept of cryo-compressed storage of hydrogen originates from the combination of existing technologies, compressed and liquid hydrogen whereby hydrogen is stored in a pressurised tank at cryogenic temperatures (Ahluwalia et al., 2010). The current cyro-compressed system (Gen-3) was assessed and resulted in remarkable achievements; the 2015 US Department of Energy gravimetric and volumetric targets were met but it is not yet viable in terms of cost, efficiency and safety (Ahluwalia et al., 2010).

2.2.3 Chemisorption with metal hydrides

The basic principle involved in the metal hydride storage mechanism in the production of metal hydrides is the absorption of atomic hydrogen by the metal which is then chemically bonded by the intermetallic phase of a metal under specific conditions (Jain, 2009; Ross, 2006). Conventional metal hydrides are more favourable because additional supply of energy is not required as in the case of liquid hydrogen. In addition, there is no loss of hydrogen due to evaporation and hydrogen is supplied at an optimal constant pressure making it safe compared to the aforementioned storage options (Güther & Otto, 1999). Sakintuna et al (2007) reported that metal hydrides have the leading hydrogen storage capacity of 6.5 H atoms/cm^3 for MgH_2 in contrast to 0.99 H atoms/cm^3 for compressed hydrogen gas and 4.2 H atoms/cm^3 for liquid hydrogen. However, metal hydrides are too heavy and have slow kinetics during desorption, and thus are not suitable for automotive vehicle on-board storage (David, 2005). Development of light metal alloys are underway but an alternative storage option that is safe and practical for on-board storage is the adsorption of hydrogen on porous materials (Sakintuna et al., 2007).

2.2.4 Physisorption on porous materials

The physisorption storage mechanism is based on the ability of hydrogen gas molecules to adsorb onto porous materials. The porous materials are advantageous because they are light weight, the kinetics for hydrogen adsorption are fast, and some materials are inexpensive to synthesise. The physisorption of hydrogen gas on porous materials is supposed to be safe for automobile applications since it is aimed at storing hydrogen at ambient conditions (Thomas,

2007; Yang et al., 2010). However, reasonable storage capacities can only be obtained at cryogenic temperatures (77 K) and high pressures (20 bar), because the hydrogen molecules are adsorbed on the pore walls by weak van der Waals forces (Thomas, 2007; Li et al., 2012). Therefore intensive studies have been carried out on tuning porous materials such as zeolites, carbons and meta-organic frameworks to meet the targets since they illustrate a potential for attractive hydrogen storage capacities (Yang et al., 2012; Jordá-Beneyto et al., 2007; Nishihara et al., 2009). This is due to the fact that these materials exhibit high surface areas and distinctive microporosity (Zhao et al., 2008).

The size of the pore channels is important for hydrogen storage capacities due to the interaction between the walls of the pore channel and the hydrogen gas. For instance, macropores (pore width greater than 50 nm) are too wide therefore the gas may pass through the pore channel without adsorbing to the wall. Micropores (width less than 2 nm) and mesopores (width between 2 and 50 nm) are more desirable for hydrogen storage since the pore channel is narrower allowing the hydrogen gas to better interact with the pore wall and adsorb (Li et al., 2012; Fu et al., 2011). Although there are different types of the aforementioned materials for hydrogen storage the literature review will focus on zeolites, templated carbons as well as Zr- and Cr-MOFs. These materials were chosen because zeolites are thermally stable and excellent templating agents for the synthesis of templated carbons, which are robust, high surface area materials. The MOFs were chosen because they possess high surface areas and furthermore, both Zr MOF and Cr MOF are thermally and chemically stable and the Cr-MOF is synthesised via a green synthetic route.

2.2.4.1 Zeolites

Zeolites, commonly referred to as molecular sieves, are aluminosilicate materials that are highly crystalline and consist of interconnected cavities and molecular pores that are highly stable and can be produced from a variety of feedstocks (Langmi et al., 2005; Li et al., 2012). There are a wide variety of zeolites available. Weitkamp et al. (1995) observed that sodalite cages in the zeolitic framework structure promotes higher hydrogen uptake capacity and the work was corroborated by Li et al. (2012) who stated that zeolite X is favourable for hydrogen storage due to the encapsulation of hydrogen occurring in the small sodalite cages rather than the supercages of the zeolite microporous faujasite framework illustrated in Figure 2.2.
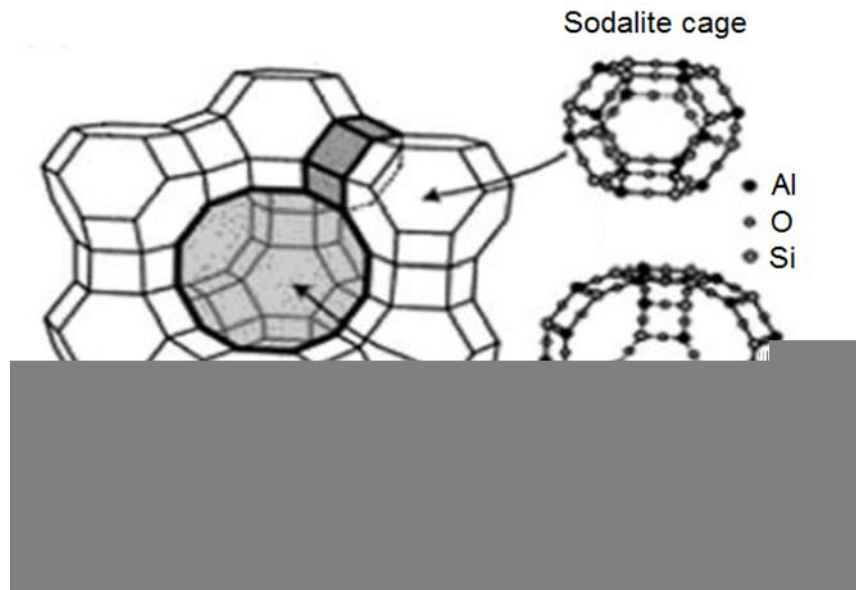
Figure 2.2: Zeolite X faujasite (FAU) framework depicting the supercage and the sodalite (β) cage (Li et al., 2012).

Coal fly ash, a common waste of the mining industry is used to produce zeolites rendering the zeolitization process inexpensive and also serve as an attractive route for beneficiating the coal combustion waste (Ma et al., 2014; Li & Yang, 2006; Babajide et al., 2012).

The interest in zeolites as a hydrogen storage media began over twenty years ago since zeolite pore channel width can be easily controlled with the exchange of ions producing zeolites that are more susceptible to high hydrogen storage capacities (Weitkamp et al., 1995). This observation initiated Langmi and colleagues to investigate the effect different cations (adsorption sites) and the framework structure would have on the hydrogen storage capacity and it was found that zeolites X and Y are not affected by the large cations blocking pores thereby not compromising the gravimetric hydrogen uptake capacity of 2.19 wt% at 77 K and 15 bar for CaX which correlated to the BET surface area of 669 m^2/g (Langmi et al., 2005).

Since hydrogen storage capacity is dependent on the density of cations exchanged in the structure, Li and Yang (2006) investigated the effect the exchange of Li^+, K^+ and Na^+ cations have on the hydrogen uptake capacity for X zeolites that have less silica in the structure. This investigation deduced that the interaction energy between the hydrogen and the cations was highest for Li^+ and lowest for K^+ because of the radius of the cation. There was a hydrogen uptake capacity of 1.5 wt% at 77 K and 1 bar and a BET surface area of 717 m^2/g for the low silica X zeolite with the Li^+ cation (Li & Yang, 2006). Although zeolites may seem like a

prospective material for hydrogen storage, the BET surface area and hydrogen adsorption capacity to date are quite low, therefore more promising materials could be carbons and MOFs.

2.2.4.2 Zeolite templated carbons

Zeolite templated carbons (ZTCs) as the name suggests are carbons that utilise zeolites as a sacrificial template, proving to be beneficial since control of porosity is easy and the pore channels are more ordered and uniform affording easy access for carbon precursors (Yang et al., 2012); Nishihara et al., 2009). The templation process is quite simple; firstly, the channel of the zeolite template is impregnated with a liquid carbon precursor followed by polymerisation and partial carbonisation. Secondly, the templation process is complete when the zeolite/carbon composite (from the first stage) is subjected to chemical vapour deposition (CVD) thereby being exposed to another carbon precursor usually a gas at high temperatures. The final stage is the detemplation that is the removal of the zeolite template often obtained by acid washing. A general schematic of the process can be seen below in Figure 2.3 (Masika & Mokaya, 2013).
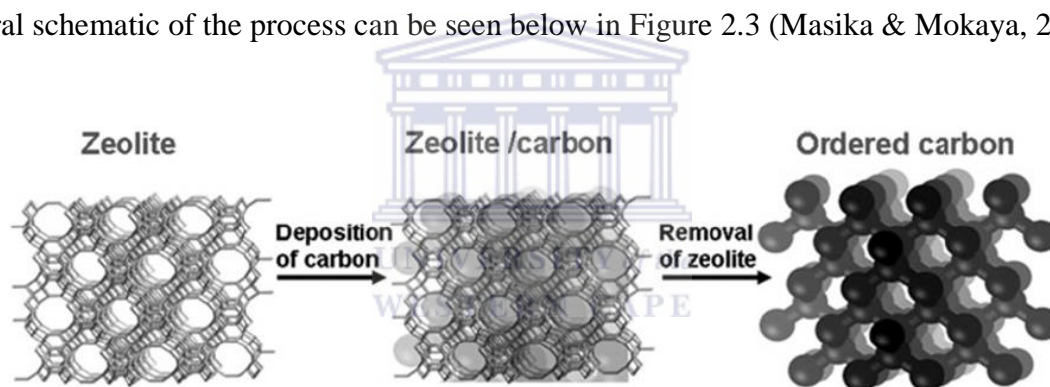
Figure 2.3: General graphical depiction of the templation of zeolite (adapted from Yang et al., 2012; Nishihara et al., 2009).

According to Nishihara et. al. (2009) templated carbons are more promising hydrogen storage material when compared to carbon nanotubes and carbon nanofibres, since templated carbons are highly microporous with large micropore volumes and surface areas. The aforementioned CVD method was used to prepare templated carbons and a BET surface area of greater than 2000 m^2/g, a micropore volume of greater than 0.8 cm^3/g and a 5.4 wt% hydrogen uptake at 77 K and 20 bar was reported (Yang et al., 2012; Alam & Mokaya, 2010). Chen and colleagues (2007) synthesised templated carbons via a similar vapour phase deposition process with a surface area of 2500 m^2/g, micropore volume of 0.2 cm^3/g and a hydrogen uptake of 2 wt% at 77 K and 1 bar. Masika and Mokaya (2013) reported a ZTC synthesised via the CVD process

with a surface area of 3332 m^2/g, a pore volume of 1.66 cm^3/g and a hydrogen uptake of 7.3 wt% at 77 K and 20 bar. With similar characteristics to carbons MOFs are also leading contenders in the race of materials for physisorption of hydrogen due to the higher surface areas (Zhao et al., 2008).

2.2.4.3 Metal-organic frameworks

Metal-organic frameworks are compounds consisting of metal clusters and organic linkers, and are extremely porous, highly crystalline and large surface area materials (Klein et al., 2009; Abid et al., 2012). Thus they are under intensive consideration for hydrogen storage applications (Yang et al., 2010; Ren et al., 2015b). Hirscher et al. (2010) stated that the hydrogen uptake is dependent on the surface area and not the structural composition of the different MOFs. However, Somayajulu Rallapalli et al. (2013) disagrees, stating that the structure of the surface and the pore geometry are the influencing factors for hydrogen adsorption.

MIL-101, a chromium-based MOF (that will be referred to as Cr MOF henceforth), has an empirical formula of [Cr(O)-X (benzene-1,4-dicarboxylate)$_3$ (H$_2$O)$_2$] where X= OH or F and consists of a rigid terephthalate ligand with octahedral trimeric chromium (III) clusters which is illustrated in Figure 2.4 (Zhao et al., 2015). Since HF is dangerous and toxic for large scale synthesis, Zhao et al. utilised the non-fluorinated method to synthesise Cr MOF thereby replacing HF with other acids and deduced that nitric and acetic acids were the best substitutes which yielded Cr MOF with a surface area greater than 3100 m^2/g and 2700-2800 m^2/g, respectively which were less than the fluorinated synthesis method which yielded a surface area of 4000 m^2/g (Latroche et al., 2006; Ren et al., 2014).
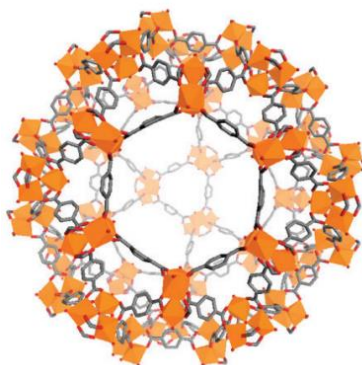
Figure 2.4: Crystal structure of Cr-MOF where Cr (orange polyhedrone), C (grey), O (red) and for clarity purposes H was omitted (Lee et al., 2009).

The thermal and chemical instabilities of most MOFs is what prompted the research and development of various MOFs, among them is UiO-66 which is a Zr based MOF (hereafter referred to as Zr MOF) consisting of a Zr metal centre bridged to 12 benzene-1,4-dicarboxylate (BDC) linkers forming a close packed cubic structure (Figure 2.5) (Kandiah et al., 2010; Wu et al., 2013). Its thermal and chemical stabilities exceed those of most MOFs due to the high affinity between Zr-O ligands as well as the close packed structure (Zhao et al., 2013). It is due to these reasons that the Zr MOF was tested as an adsorbent for hydrogen, which yielded excellent surface area and hydrogen uptake capacities like 1434 m^2/g and 1.6 wt%, respectively at 1 bar and 77 K (Abid et al., 2012). Zhao et al. (2013) synthesised Zr-MOFs with a surface area of 1358 m^2/g and a hydrogen uptake of 3.35 wt% at 18 bar and 77 K.
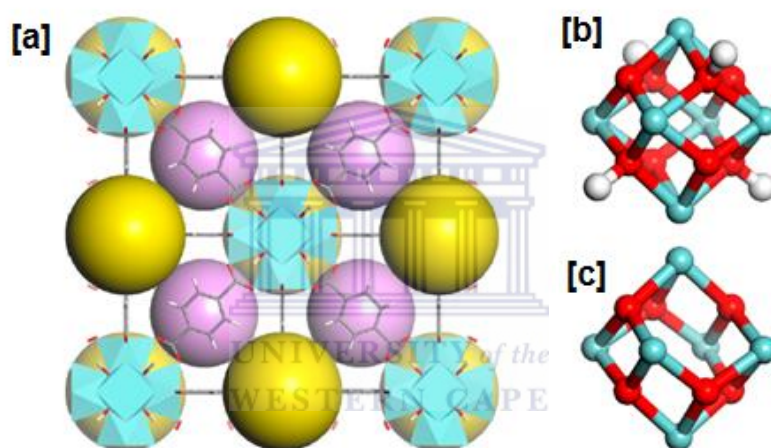
Figure 2.5: Crystal structure of Zr-MOF (a) depicting the different elements as Zr (cyan), C (grey), O (red) and H (white). The pores on the Zr MOF are denoted by yellow (located on octahedral site) and pink (located on the tetrahedral site). The hydroxylated (b) and dehydroxylated (c) Zr_6-cluster are also illustrated (Wu et al., 2013).

The development of the aforementioned materials illustrates the promising possibility of a hydrogen economy, however, when these powdered materials are to be applied practically in a hydrogen storage system, they need to undergo further processing (which is referred to as shaping) prior to system integration depicted in Figure 2.6 (Ren et al., 2015b). Some of the existing shaping techniques will be highlighted in the next section.
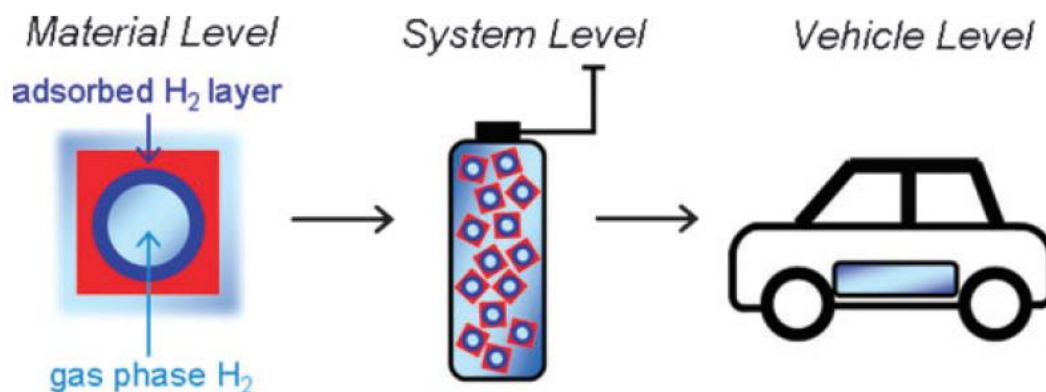
Figure 2.6: Graphical representation of the porous powdered materials at the different levels (Yang et al., 2010).

2.3 Shaping techniques available for powders

The integration of these porous powdered materials in hydrogen fuel cell vehicles is challenging, because; (1) they are powders which have a low packing density compromising the volumetric capacities, (2) pipelines may become contaminated during charge and discharge cycles, and (3) loose powders are difficult to handle since they can be blown away (Ren et al., 2015). Generally the powdered materials are mixed with a binder and shaped into granules or fibres; however mechanical force (no binder) is used to shape monoliths (O'Neill et al., 2010).

Ardelean et al. (2013) prepared Cr-MOF monoliths by mechanically pressing the Cr-MOF powders with a pressure of 120 MPa and the effect shaping had on the hydrogen uptake capacity was studied. A general schematic of the pressing technique is illustrated in Figure 2.7a. In terms of gas adsorption the induced transformation after compression is irreversible and a reduction in surface area and hydrogen uptake was prominent (Ardelean et al., 2013). Since pressing is not aided by a binder there is a possibility that the monolith may crack, and together with small scale production and the probable damage to the structure or surface texture of the porous materials, are limiting factors for mechanical pressing (Ren et al., 2015).

An alternative shaping technique that will overcome the aforementioned drawbacks of mechanical pressing is granulation (Figure 2.7b) a process whereby the porous powders are mixed with a binder and shaped into pellets (Ren et al., 2015; Liu et al., 2012). The aid of binders is beneficial due to the shaping being done easily without excess pressure being placed on the powdered materials. However, the amount of porous powders incorporated into the binder for shaping is limited and for hydrogen adsorption applications the binder may be a

diffusional barrier (Ren et al., 2015). Ren and colleagues studied the effect granulation had on the hydrogen storage capacity of MOFs and reported that pellets can be produced at large scale and easily transferred to a hydrogen storage tank due their spherical nature. The simulated tumbler drum and drop test were used to assess the breakage of the pellets which amounted to zero breakage, nevertheless, the surface area and hydrogen uptake capacity for the pellets were lower than that of the powdered MOFs.
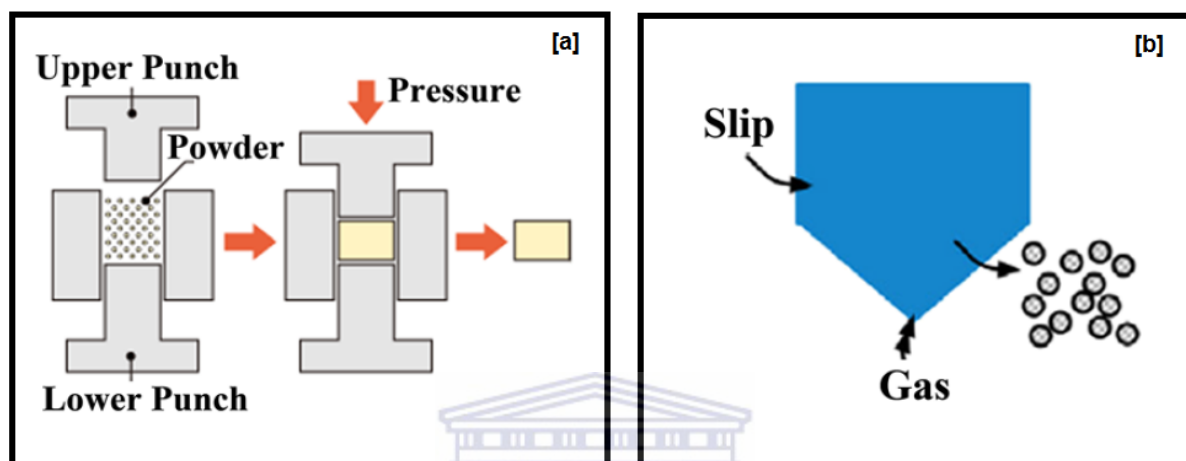
Figure 2.7: Schematic diagram depicting the mechanical pressing process (a) and the granulation process (b) utilised to shape porous powdered materials into monoliths and pellets respectively (adapted from Ren et al., 2015; Akhtar et al., 2014).

Complimentary to granulation is electrospinning, which is a versatile technique that produces ultra-thin continuous fibres (Cavaliere et al., 2011). Electrospinning is advantageous because it is a simple, easily scaled up process but more importantly it enables the production of fibres with properties that are best suited for hydrogen adsorption (Cavaliere et al., 2011; Megelski et al., 2002; Inayat et al., 2012; Elahi et al., 2013). Such properties include continuous ultrathin nano-scaled diameter fibres with a high surface area (Chung et al., 2005; Im et al., 2009; Han et al., 2005; Ding et al., 2002). Since electrospinning is the shaping technique adopted for the study, this review will dive deeper into the process in the next section.

2.4 Electrospinning process

The electrospinning process utilises a high voltage source that causes a polymer solution to be drawn out of a needle onto a metal collector plate resulting in fibres (Almuhamed et al., 2014). A typical electrospinning unit is made up of a high electric voltage meter, a syringe pump with

a syringe and needle as well as a metal collector as illustrated in Figure 2.8 (De Schoenmaker et al., 2013).
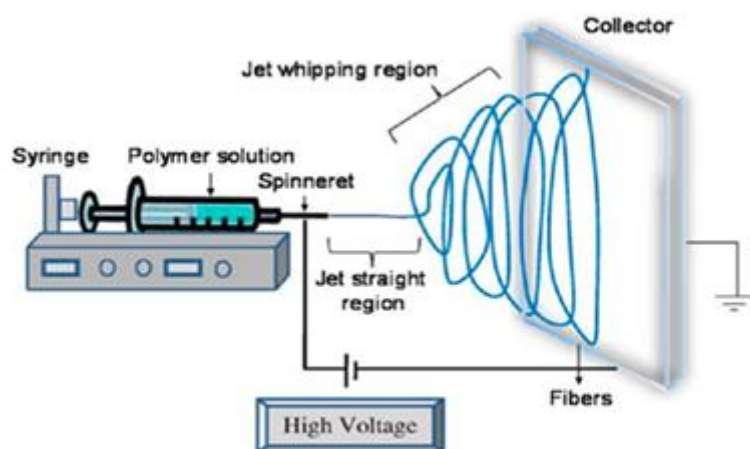
Figure 2.8: schematic diagram of the electrospinning unit (Richard-Lacroix & Pellerin, 2013).

An increase in repulsion charge on the surface of the droplet of polymer solution pumped out of a needle tip is caused by an increase in the electric voltage applied to the drop, resulting in the droplet transforming into the shape of a cone, often referred to as a Taylor cone (Shenoy et al., 2005). Once the charge repulsion surpasses the surface tension, the droplet transforms into a stream of polymer solution spiralling towards the collector during which the solvent evaporates and a mesh of electrospun fibres forms on a collector (Shenoy et al., 2005).

2.4.1 Electrospinning history

In 1897 Rayleigh was the first to observe electrostatic spinning technique known as electrospraying which was then studied by Zeleny in 1914. However, it was only by 1934 that Formhals patented the process and apparatus which used a moving collector to draw out spun threads of a cellulose acetate and acetone mixture. But an aggregated web structure was produced due to the short distance between the needle and collector together with insufficient drying time. This gave rise to his second patent in 1940, where the distance between the needle and collector was adjusted allowing more time for the fibres to dry and the production of fibres via electrostatic forces was reported (Bhardwaj & Kundu, 2010; Subbiah et al., 2005; Jacobs et al., 2010). The term electrospinning was coined after Taylor studied the jet formation in 1969 and found that 49.3 degree angle is necessary for the balance of the surface tension and electrostatic forces of the polymer to form a stream. Therefore the conical shape of the jet was termed the Taylor cone. Numerous modifications to the apparatus and parameters used to

electrospin were done over the years to give the universal electrospinning unit used today (Subbiah et al., 2005). However, now the main focus of research surrounding the electrospinning process is based on the diameter and morphology of the fibres since the rise in the early 90s of nano-scaled materials (Huang et al., 2003).

2.4.2 Electrospinning parameters

The morphology and diameter of the fibres are dependent on the parameters under which they are electrospun, categorised as solution, processing and ambient conditions. For instance a common defect amongst electrospun fibres is beads, which are not desired in this study since they reduce the surface area of the fibre and inhibit gas from accessing the porous powdered materials (Zuo et al., 2005). Since it is important to understand the materials and parameters for electrospinning in order to achieve the desired materials a discussion of the polymers used in this study that is PSMA, PAN and PAA as well as the parameters applied will be presented in the following sub-sections.

2.4.2.1 Polymers

The chemically versatile copolymer that is PSMA is formed from two moieties namely nonpolar polystyrene (PS) and a polar maleic acid (MA) (Figure 2.9 for reaction scheme). Cécile and Hsieh (2009) studied the solubility of the PSMA and the two moieties in different solvents and reported that the adoption of co-solvents, DMF and acetone was necessary to dissolve PSMA.
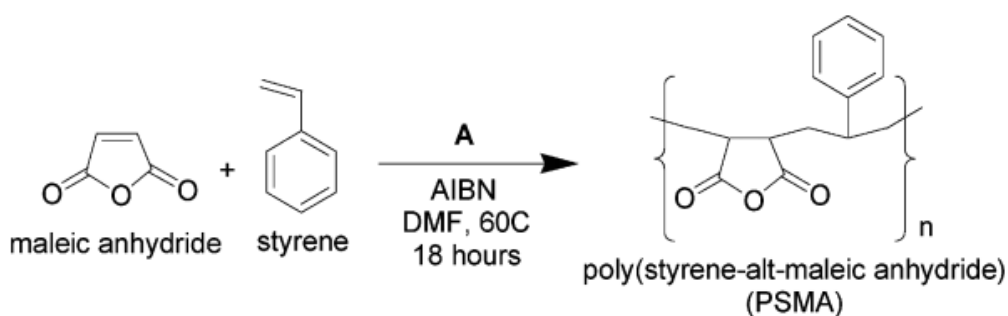
Figure 2.9: Reaction scheme for the synthesis of PSMA (Henry et al., 2006).

PAA is a polyelectrolyte, (implying that it has charges in aqueous solutions) consisting of a hydrocarbon backbone (non-polar) and carboxylic side groups (polar) structure presented in Figure 2.10 (Li & Hsieh, 2005). In order for fibres to form during electrospinning, it is imperative that the polymer contains adequate molecular chain entanglement for the formation

of fibres, which was reported by Li & Hsieh (2005). They showed that PAA dissolved in N,N-Dimetylformamide (DMF) has a high molecular chain entanglement.
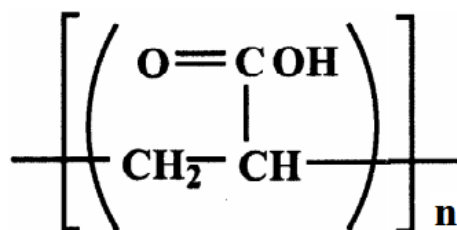
Figure 2.10: Structure of PAA (adapted from Li et al., 2002) .

PAN is the most studied electrospun polymer to date, since it is the best precursor for the production of carbon fibres due to the high carbon yield (Wang & Kumar, 2006; Nataraj et al., 2012). PAN contains bulky nitrile groups (illustrated in Figure 2.10) that give rise to the stiff chains and dissolves well in DMF (Yamane et al., 1997).
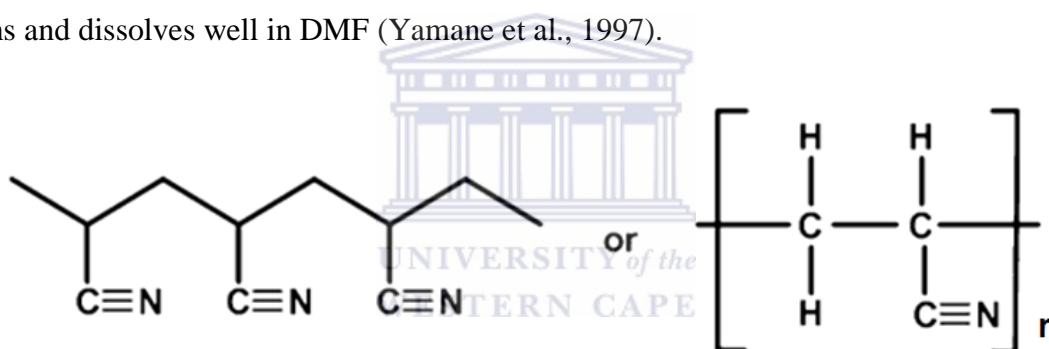
Figure 2.10: Structure of PAN (Rahaman et al., 2007).

2.4.2.2 Solution parameters

The viscosity of the polymer solution which is dependent on the concentration as well as the surface tension form part of solution parameters. Adequate chain entanglement, an attribute of structural and concentration properties of the polymer is a necessary requirement for the formation of fibres (Li & Hsieh, 2005; Wang & Kumar, 2006). The morphology of fibres are determined by the viscosity of the solution. An appropriate viscosity of the solution is required in order for electrospinning to take place because a very low viscosity does not yield smooth fibres and the polymeric solution jet will not be able to discharge from the needle if the viscosity is too high (Li & Wang, 2013). Non-beaded fibres result if the concentration and viscosity are high but the surface tension and solution conductivity are low, making them

inversely correlated to each other (Gupta et al., 2005; Wang et al., 2007). If the polymer has a low molecular weight it will be subject to electrospraying since the fluid breaks into droplets (McKee et al., 2004).

2.4.2.3 Processing parameters

Processing parameters are subdivided into the applied voltage, flowrate of the polymer solution, the distance between the tip of the needle and the collector plate, and the collector. The applied voltage and the flowrate are dependent on the viscosity of the polymer solution, resulting in a high applied voltage and flowrate if the viscosity is high (Shenoy et al., 2005). The polymer solution jet will only occur when the applied voltage has surpassed the surface tension of the solution (Chowdhury & Stylios, 2010). The distance between the needle tip and collector plate is important because, if the distance is too short, there will not be enough time for the solvent to evaporate and instead of dry fibres forming on the collector plate the fibres will intersect and bond, causing a cohesive porous structure to form (Gibson et al., 2001). The collector has to be made of a metal for electricity conduction purposes. The collectors are either stationary which yield randomly aligned fibres or rotating causing the fibres to be drawn out, hence they are more aligned (Carnell et al., 2008).

2.4.2.4 Ambient parameters

Temperature and humidity are commonly referred to as ambient parameters and are interdependent. Wang et al. found a decrease in the viscosity and surface tension with an increase in temperature favouring the formation of thinner fibre diameters (Wang et al., 2007). Humidity has an effect on the diameter and surface of the fibre which is partially dependent on the polymer and solvent utilised. An interesting observation is that water condensation as a result of humidity may cause pores to appear on the fibres (De Schoenmaker et al., 2013).

2.5 Electrospun composite fibres

Since the crux of the study is the production of composite electrospun fibres, it is essential that work done previously by other researchers be highlighted in the review. To date, only a few studies have been reported on composite electrospun fibres containing porous materials. Ostermann et al. (2011) were the first to produce MOF-polymer composite fibres where the zeolitic imidazolate framework (ZIF-8) was mixed with polyvinylpyroldine (PVP) and electrospun. It was reported that as the amount of ZIF-8 was added to the PVP the surface areas

increased. For instance, the 22 wt% and 56 wt% ZIF-8 in PVP yielded a surface area of 180 and 530 m^2/g which was however still lower when compared to the surface area of 960 m^2/g for the ZIF-8 alone (Ostermann et al., 2011). This is due to the polymer acting as a diffusional barrier around the MOF particles depending on how thick the polymer layer is (Wu et al., 2012). Armstrong and colleagues prepared nanofibres composites with Zr MOF and poly(vinyl cinnamate) (PVCi) by incorporating the Zr MOF into the PVCi then electrospinning and thereafter subject the composite fibres to a secondary growth of Zr-MOF (Armstrong et al., 2015). The composite membrane was analysed after the secondary growth and it had a BET surface area of 430 m^2/g, which was lower than the BET surface area of the pristine Zr-MOF of 1188 m^2/g. Gas permeation studies (helium, argon, nitrogen and sulfure hexafluoride) were conducted on the composite membrane. Srinivasen et al. (2006) electrospun zeolites and PVA. The PVA was a structure directing agent and was later removed by calcination, because they wanted to place the zeolites onto a sensor device for gas sensing applications. Zeolitic hollow composite fibres were also produced by Di and colleagues with the aid of PVP for catalysis applications (Di et al., 2008). It is important to note that even though these studies state that the composite fibres produced can be used for gas adsorption none of them conducted hydrogen adsorption capacity of the materials.

Chapter summery
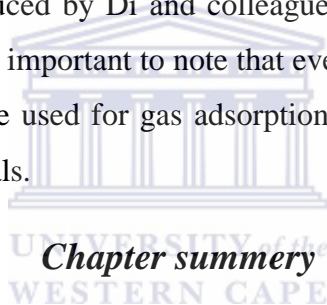
Although hydrogen is said to be the solution to the energy problem since it is abundant and can be produced via eco-friendly methods, its realisation is still faced with the challenge of on-board storage for automotive applications. This is due to the stringent performance, range, safety and cost criteria that the on-board storage technology needs to adhere to. There are four main on-board storage technologies available to date including compressed high pressure gas cylinders, cryogenic liquid hydrogen, chemisorption with metal hydrides and physisorption on porous materials, however, none fully satisfy the US DOE 2020 targets yet.

Compressing hydrogen gas at 350 and 700 bar in type IV tanks is close to fulfilling the gravimetric and volumetric targets but the polymer reinforced resin tanks are flammable and high pressure hydrogen gas tanks do not sit well with the public due to the Hindenburg disaster. Liquefying the hydrogen is more advantageous since it contains a higher energy density but it requires an exorbitant amount of energy and money to liquefy hydrogen. Although the US DOE 2020 gravimetric and volumetric targets are met by cryo-compressed storage technology it is not cost effective or safe. The absorption of hydrogen gas into metal hydrides are safe

compared to compressed and liquid hydrogen but it is not recommended for on-board automotive vehicle storage due to mass constraints and the slow kinetics during desorption. The most promising solution to the on-board storage challenge is the physisorption of hydrogen gas onto porous materials such as zeolites, zeolite templated carbons and MOFs. These porous materials are safe to use for on-board storage and reasonably inexpensive to synthesise, however, the weak van der Waals forces between the hydrogen gas and the porous materials require cryogenic temperatures (77 K) and high pressures (20 bar) to achieve attractive storage capacities.

The above mentioned porous materials have a high affinity to hydrogen gas because they are micro and nano-scaled porous powders with a high surface area and micropore channels that are tunable. Integrating these porous powders into a hydrogen fuel cell vehicle is challenging because of their low packing densities and the possible contamination of pipelines during charge and discharge cycles. Therefore it is necessary for these porous powders to be shaped into monoliths, pellets and fibres via mechanical pressing, granulation and electrospinning respectively. Although some of the shaping techniques are complimentary to each other, electrospinning is the most versatile and easily up-scaled technique that can produce the necessary materials such as composite fibres so as to advance the research in this field.

Although the production of composite fibres is not a novel idea, this study produces composite fibres with porous materials (zeolite 13X, ZTCs, Cr MOF) that have not been studied before with the exception of Zr MOF and investigates these electrospun composite fibres that contain the abovementioned porous materials for their hydrogen adsorption capacity which has also never been done previously.

The next chapter entails the details about the materials and experimental procedures used to synthesis the materials for the study as well as the analytical methods used to characterise the synthesised materials.

Materials, Experimental and Analytical Methods

The focal point of this chapter is on the materials, experimental methods and analytical techniques utilised for the study. It begins with a flow diagram depicting the experimental route taken to achieve the different objectives set out. This is followed by a list of the materials and the electrospinning equipment used in the study. Thereafter a detailed explanation of the experimental methods used in the synthesis of pristine electrospun fibres, the porous powdered materials and composite fibres is provided. The chapter ends with a description of the characterisation techniques and the conditions under which the samples were characterised.

3.1 Experimental overview

Figure 3.1 presents a general schematic for the approach to the experimental work.
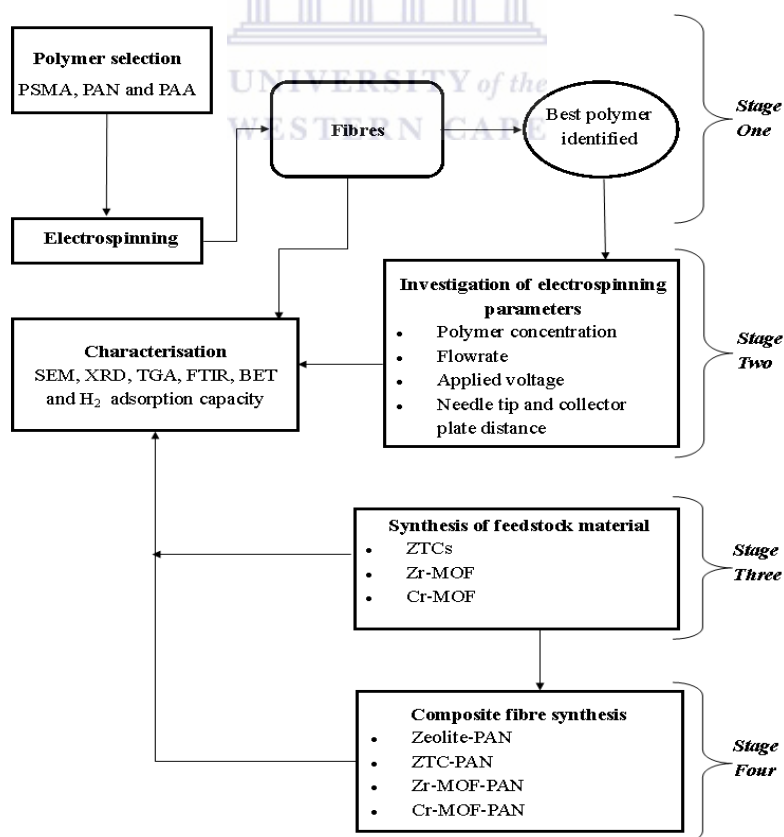
Figure 3.1: General schematic for experimental approach.

The experimental approach was divided into four stages. Firstly, three polymers were chosen from literature based on the physical properties of the resultant electrospun fibres. Once the polymers were electrospun and the fibres evaluated according to specific characteristics required (discussed in section 4.1) the most suitable polymer was selected. Thereafter the electrospinning parameters were optimised for the most suitable polymer in order to determine the range in which the fibres were non-defected (*i.e* beads not present) and the fibre diameter was between 300-500 nm (stage two). Stage three was the synthesis of the porous powdered materials followed by the encapsulation of the porous powdered materials into the polymer to synthesise composite fibres (stage four). At each stage the materials were characterised via various techniques.

3.2 Materials

This section lists (Table 3.1) all relevant information about the chemicals, materials and gasses utilised to synthesise the pristine polymer fibres, the porous powdered materials as well as the composite fibres.

Table 3.1: The chemicals, materials and gases utilised for the synthesis of the pristine polymer fibres, porous powdered materials and composite fibres.

Item name	Item abbreviation	Grade/Purity	Supplier
Polystyrene-alt-maleic anhydride	PSMA	M_w=109 000	Aldrich
Polyacrylic acid	PAA	M_w=250 000	Aldrich
Polyacrylonitrile	PAN	M_w=150 000	Aldrich
N,N-dimethylformamide	DMF	99.8%	Sigma-Aldrich
Acetone	-	Analytical grade	AB CHEM
Molecular sieves 13X	Zeolite 13X	Powder~2 μm	Sigma-Aldrich
Argon gas	Ar	99.9999% pure	Afrox gas
Furfuryl alcohol	FA	98%	Acros Organics
Hydrofluoric acid	HF	37% concentrated AR fuming	Labchem
Terephthalic acid	H_2BDC	98%	Sigma-Aldrich
Zirconium tetrachloride	$ZrCl_4$	99.5%,	Sigma-Aldrich
Formic acid	HCOOH	95%	Sigma-Aldrich
Chromium chloride hexahydrate	$CrCl_3 \cdot 6H_2O$	99.5%	Sigma-Aldrich
Nitrogen gas	N_2	99.9999% pure	Afrox gas
Hydrogen gas	H_2	99.9999% pure	Afrox gas

3.3 Electrospinning Equipment

This section presents the electrospinning set-up adopted to conduct the study. Since the electrospinning set up is composed of various components a photograph (Figure 3.2) along with a description of the function of the various components (Table 3.2) are highlighted.
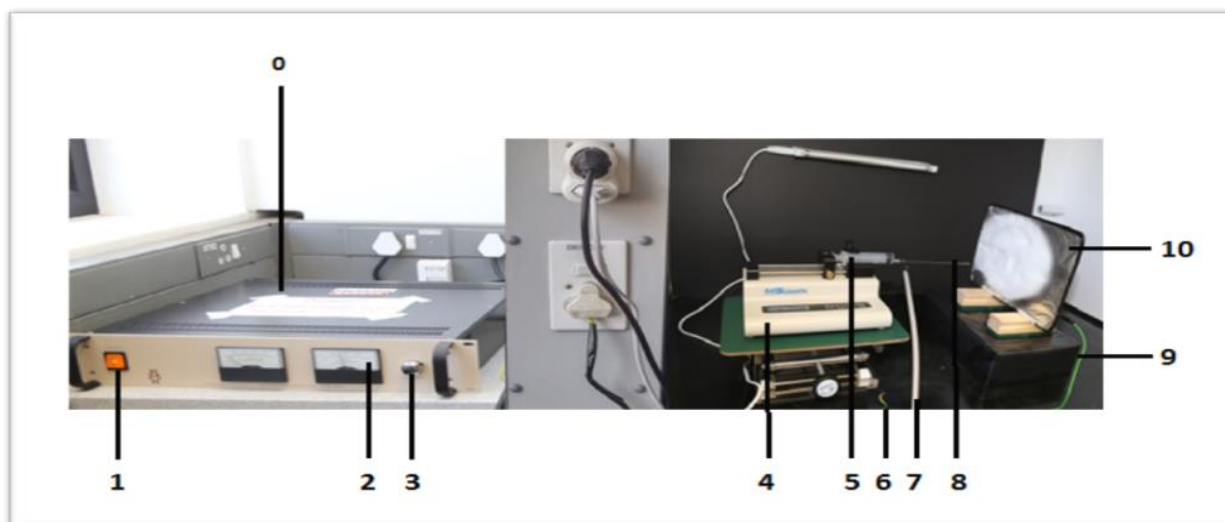
Figure 3.2: The bench top electrospinning set up adopted for the study

Table 3.2: Description of the function of the individual components for the electrospinning set-up illustrated in Figure 3.2.

Key	Name	Function
0	High voltage meter	Supplies voltage
1	Main switch	Used to switch high voltage meter unit on and off
2	Display screen	Displays the voltage that is being applied
3	Voltage control	Used to increase or decrease the applied voltage
4	Syringe pump	Used to automatically eject the polymer solution at a set rate
5	Syringe	Holds the polymer solution
6	Earth cord	Used to discharge the unit after use
7	Applied voltage clip	Supplies the voltage to the polymer solution present in the needle, for electrospinning to occur
8	Electrospinning needle	Ejects the polymer solution
9	High voltage cord	Attached to the collector plate in order to create an electric field in order for the fibres to be collected
10	Collector plate	Collector plate is covered in aluminium foil and is used to collect the fibres

Figure 3.3a and b presents a schematic as well as the actual electrospinning setup adopted in this study.
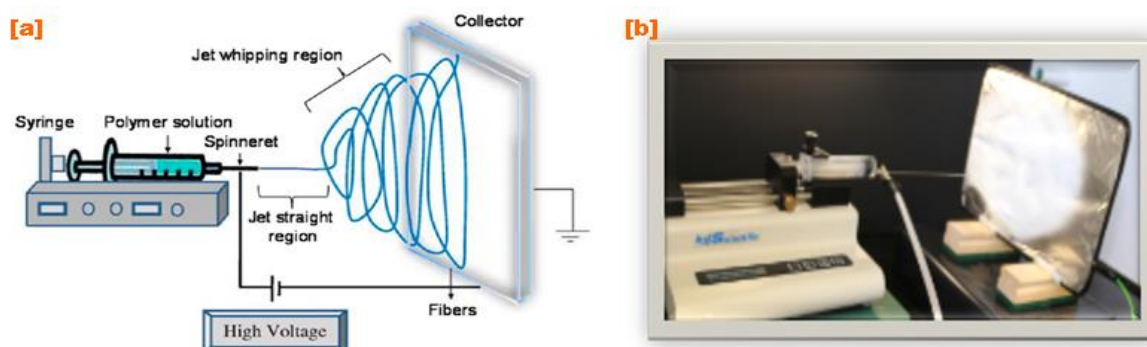
Figure 3.3: Schematic diagram of the horizontal electrospinning setup (a) illustrating the trajectory of the polymer stream resulting in fibres, adapted from (Richard-Lacroix & Pellerin, 2013) and a picture of the experimental set-up used for the study (b).

3.4 Experimental Methods

This section presents details of the experimental procedures undertaken to synthesise the materials for the study. It is divided into four subsections; the first part is on polymer selection, followed by optimising the parameters for electrospinning these selected polymers (part two). The third part deals with the synthesis of the porous powdered materials that will be incorporated into the polymer solution, and finally the fourth part details the procedure for the synthesis of the composite electrospun fibres.

3.4.1 Polymer selection

The aim of this section was to determine a suitable polymer to produce composite fibres. Three polymers along with the corresponding solvent systems in which the polymers dissolve were selected (illustrated in Table 3.3) from literature based on the physical characteristics of the resultant polymer fibres.

Table 3.3: Polymers and corresponding solvent systems to dissolve the polymers selected for the study

Polymer	Solvent system	References
PSMA	50:50 DMF:Acetone	(Cécile & Hsieh, 2009)
PAA	DMF	(Li & Hsieh, 2005)
PAN	DMF	(Arshad et al., 2011)

3.4.1.1   Calculation of polymer mass

This subsection presents the calculations of the mass of the polymers that was used for the preparations of the polymeric solutions. Optimisation of the parameters as well as the conditions under which the electrospinning process was carried out is also presented.

The process of determining the concentration (categorised as solution parameters explained in section 2.2.4.1) of the polymer solution was adopted from Leach and colleagues, whereby a range of polymer solutions with varying concentrations were prepared and subjectively assessed to find a polymer solution that forms a viscous flowing gel (Leach et al., 2011). Therefore calculations shown in this section are based on that specific concentration for each polymer. The calculation for PSMA concentration is based on Equation 1 because it is dissolved in a co-solvent system, the PAA and PAN concentrations will be based on Equation 2 since they are dissolved in a single solvent system. The definitions of the symbols for the equations are found in Table 3.4.

$$\text{wt\%}_p = \frac{P_m}{d_\alpha \times V_\alpha + d_\beta \times V_\beta + P_m}$$ Equation 1

$$P_m = \frac{\text{wt\%}_p \times d_s \times V_s}{1 - \text{wt\%}_p}$$ Equation 2

Table 3.4: Meaning of the symbols from Equation 1 and 2.

Symbol	Definition of symbol
$wt\%_p$	Concentration of polymer solution
d_α	Density of first solvent
d_β	Density of second solvent
V_α	Volume of first solution
V_β	Volume of second solution
d_s	Solution density
V_s	Solution volume

The mass of PSMA required for the preparation of a 25 wt% concentrated solution with DMF and acetone as the first and second solvent was calculated as follows:

$$0.25 = \frac{P_m}{0.944 \text{ g.mL}^{-1} \times 2.5 \text{ mL} + 0.79 \text{ g.mL}^{-1} \times 2.5 \text{ mL} + P_m}$$

$$0.25 = \frac{P_m}{4.6 + P_m}$$

$$1.15 + 0.25P_m = P_m$$

$$1.15 = 0.75 \, P_m$$

$$P_m = 1.5 \text{ g}$$

Since PAA utilises one solvent, Equation 2 was used to determine the mass of PAA required to prepare a 50 wt% solution.

$$P_m = \frac{0.50 \times 0.944 \text{ g. mL}^{-1} \times 10 \text{ mL}}{1 - 0.50}$$

$$P_m = 9.44 \text{ g}$$

The mass of PAN was calculated in the same way and is presented in Table 3.5

The calculation of the polymer mass for PSMA and PAA are given as examples of how the calculation was done, therefore all corresponding information necessary to prepare the polymeric solutions for the study is found in Table 3.5.

Table 3.5: Polymer mass and the corresponding solvent system volumes and ratios required to prepare the solutions with the optimal concentration (described in section 3.4.1.1).

Polymer	Polymer solution concentration (wt%)	Polymer mass (g)	Solvent system	Solvent volume (mL)
PSMA	25	1.50	50:50 DMF:Acetone	5
PAA	50	9.44	DMF	10
PAN	10	1.05	DMF	10

3.4.1.2   Preparation of polymeric solutions

The polymer solutions were prepared by adding the respective mass of polymer and volume of solvents (quantities found in Table 3.5) into a sealed vial to prevent evaporation of solvent. The solution was then mixed with a magnetic stirrer between 250-500 rpm until the polymer had dissolved. Thereafter the polymer solution was transferred to a syringe attached to needle with a diameter of 0.7 mm and was placed on the syringe pump. By using the various components of the electrospinning equipment set as illustrated in Figure 3.2, the polymer solution was electrospun.

3.4.1.3   Optimisation method of processing parameters

The parameters under which the aforementioned polymer solutions were electrospun are vital since they determine whether the resultant fibres are desired. Therefore the methodology utilised to optimise the processing parameters of the polymer solutions was adopted from Leach et al. (2011) and a general description of how the fibres were electrospun was highlighted in this section. First, the collector plate (aluminium foil on a wooden substrate) was set at a certain distance (measured with a ruler) from the needle tip to ensure there is adequate time for the solvent to evaporate so that the fibres were able to solidify and reach the collector plate. Thereafter the rate at which the polymer solution was pumped out of the syringe (commonly referred to as flowrate) was determined, by setting it to a low flow rate

and gradually increased while observing the ejected polymeric droplet. Once the first drop of polymer solution had appeared at the needle tip, it was wiped away and when another drop immediately replaced it then the flowrate was deemed to be optimised. The voltage was slowly increased until the droplet transformed into a steady stream (Figure 3.4). Once the steady stream was observed the collector plate was moved either towards or away from the needle tip so that the fibres reached the collector plate and thus rendering it optimised. The electrospinning process for all subsequent runs was done under ambient conditions and a digital monitor was utilised to record the temperature and humidity of the surrounding area.
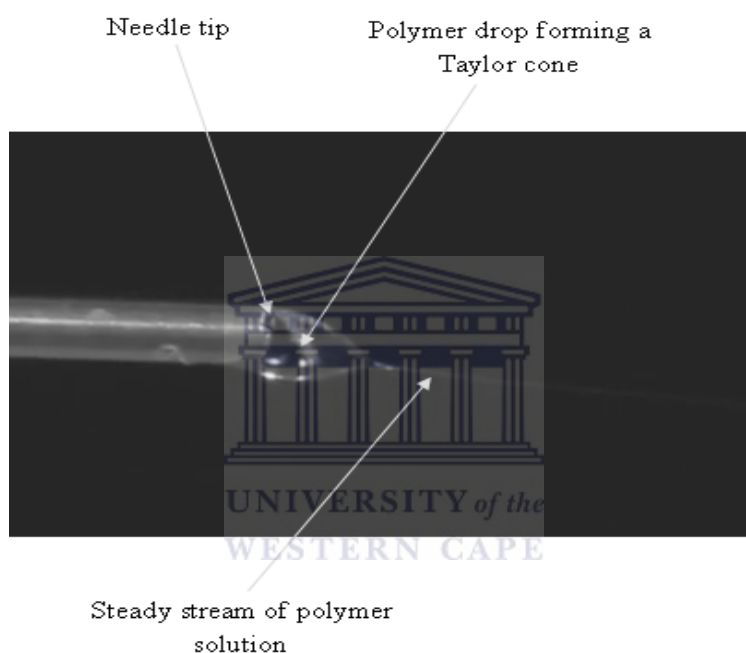
Figure 3.4: Illustration of the polymer drop at the needle tip forming a steady stream (Leach et al., 2011).

3.4.1.4   Optimisation of parameters for polymeric solutions

The method of optimising the solution and processing parameters was described in 3.4.1.1 and 3.4.1.3 respectively. The most important solution and processing parameters are polymer concentration, flowrate of the polymer solution, distance between the needle tip and collector plate, applied voltage, as well as the temperature and humidity. The parameters under which the polymeric solutions were electrospun are presented in Table 3.6.

Table 3.6: Electrospinning parameters for the polymeric solutions.

	PSMA	*PAA*	*PAN*
Concentration (wt%)	25	50	10
Flowrate (mL/h)	0.50	0.45-0.95	0.35
Distance (cm)	8	5	10
Applied voltage (kV)	9	9-11	7
Temperature (ºC)	26-27	21-25	23-24
Humidity (%)	36-40	36-57	54-62

After analysis of the PSMA, PAA and PAN fibres the most suitable polymer for the production of composite fibres was identified to be PAN (a full explanation of how it was determined will be presented in Chapter 4 section 4.1). Since the polymer had been selected the study progressed onto stage two of the experimental approach which was the investigation of the processing parameters of the PAN solution to achieve fibres with the desired characteristics (that is non-beaded fibres that possess a narrow diameter).

3.4.2 Optimisation of the processing parameters for PAN

This subsection deals with the investigation of electrospinning parameters to obtain smooth PAN fibres with a diameter range of 300-500 nm so the fibre is of adequate thickness to encapsulate the porous powdered materials into the composite fibres. The concentration of the PAN solution was 10 wt% (the method of determining the concentration is highlighted in section 3.4.1.1) since it formed a flowing gel with sufficient viscosity for electrospinning. The PAN solution was then electrospun via the method described in section 3.4.1.3. However, for this investigation there were both fixed and varied parameters. The rate at which the PAN solution was pumped was set and remained at 0.4 mL/h for the duration of all the experimental sets. The experiments for this investigation were done at ambient temperatures and humidity, which was recorded at 17 ºC and 41-42% respectively. The varying parameters were the applied voltage and the distance between the needle tip and collector plate. The applied voltage was ranged at three levels (approximately 5-6, 8-9 and greater than 12 kV), whereas the distance between the needle tip and collector plate was

varied at 5, 10 and 15 cm. The distance from the needle tip and applied voltage for each experimental set is shown in Table 3.7. The formation of beads and fibre diameter were the main response factors used to identify the optimal electrospinning conditions and SEM micrographs were used to determine these morphological variations.

Table 3.7: The distance from the needle tip to collector (denoted as distance) and the applied voltage for the parameter investigation for 10 wt% PAN solution pumped out at 0.4 mL/h and electrospun at 17 ºC and 41-42% humidity.

Experimental set code	Distance/ cm	Applied voltage/ kV
PI-1	5	5
PI-2	5	6-8
PI-3	5	12
PI-4	10	5-6
PI-5	10	8
PI-6	10	12
PI-7	15	5
PI-8	15	9
PI-9	15	12

3.4.3 Synthesis of porous powdered materials

Stage three of the experimental approach was the synthesis of the porous powder materials (which adsorbs hydrogen) used in the production of the composite fibres. The porous powdered materials used in the study were zeolites 13X, zeolite templated carbons (ZTCs) as well as chromium and zirconium based metal-organic frameworks (Zr and Cr MOFs). The commercial zeolite 13X (obtained from Sigma-Aldrich) was used without further processing. Sub-section 3.4.3.1 and 3.4.3.2 presents pertinent details of the procedure used to synthesise ZTCs and MOFs respectively.

3.4.3.1   ZTC synthesis

The commercial zeolite 13X was used as a template for the synthesis of ZTC. A general schematic highlighting the synthesis route for ZTC is presented in Figure 3.5.
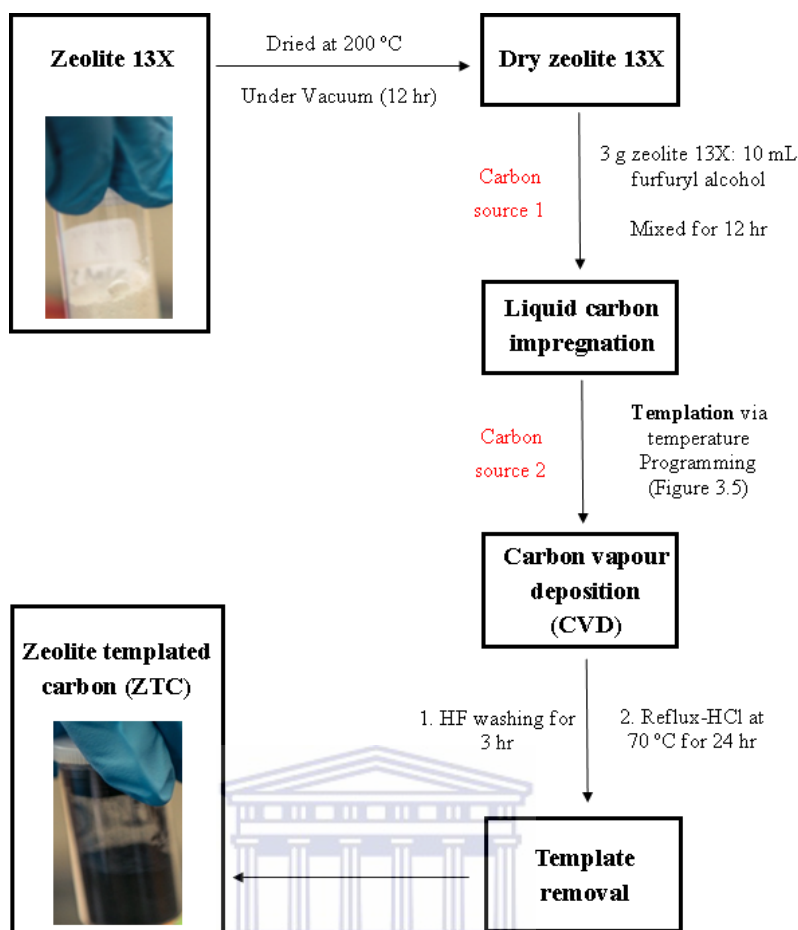
Figure 3.5: Schematic of ZTC synthesis route.

The procedure for the synthesis of ZTC is as follows; commercial zeolite 13X (17.24 g) was dried at 200 ℃ for 12 h in a vacuum oven and thereafter cooled under the flow of argon in a tube furnace to prevent the zeolites from reabsorbing atmospheric moisture. The dried zeolite was impregnated (ratio of 3 g zeolite: 10 mL furfural alcohol) with furfural alcohol (58 mL). After 24 h the impregnated sample was filtered, washed with ethanol (approximately 1 mL) and thereafter left to dry at room temperature for 3 h. The sample was then transferred to alumina combustion sample boats, placed in the tube furnace under argon gas (100 mL/min) for the chemical vapour deposition (CVD) process. The CVD process involved the use of a temperature program illustrated in Figure 3.6.
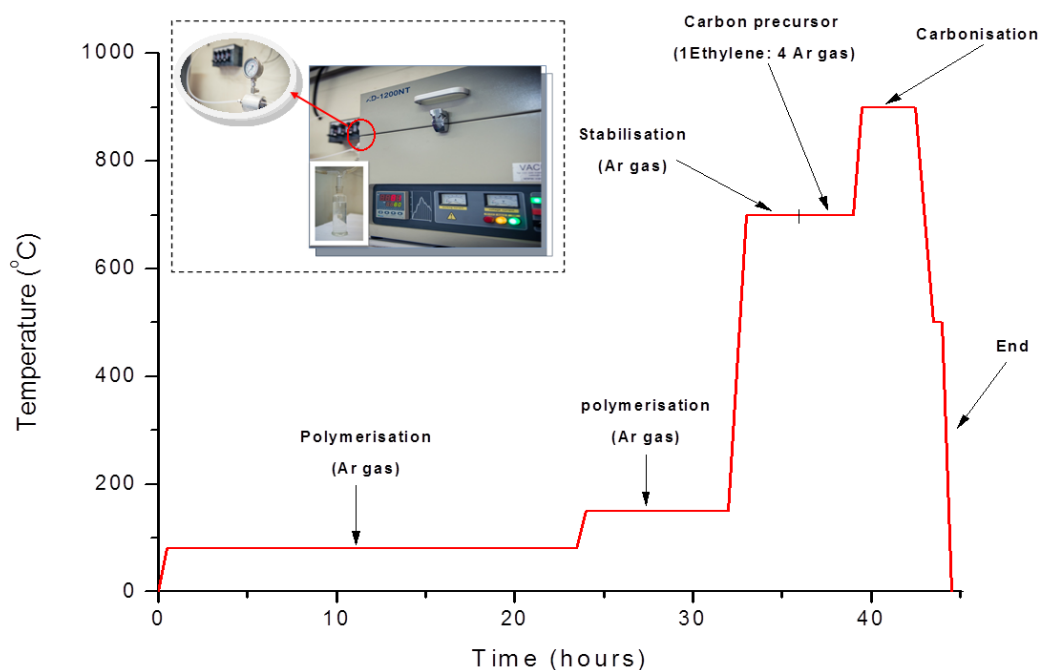
Figure 3.6: Graphical representation of the temperature programme utilised for the CVD process with picture of the tube furnace (magnified picture of the pressure guages and the bubbler inserted) used for the CVD process inserted.

Still under argon flow the temperature was ramped up from 0 to 80 ºC at which time polymerisation of the furfuryl alcohol impregnated zeolite 13X occurred for 24 h, thereafter polymerisation occurred for a further 8 h at 150 ºC. The temperature was then ramped up to 700 ºC for stabilisation of the impregnated zeolite 13X for 3 h still under argon gas. After which a mixture of ethylene/argon (100:400 mL/min carbon precursor) gas is passed through the tube. After 3 h the gas flow is switched back to argon only and the temperature was ramped up to 900 ºC where carbonisation of the chemical vapour deposited carbon took place for a further 3 h under argon gas. Thereafter the temperature was ramped down to 500 ºC and held there for 20 minutes and finally cooled down to 25 ºC which marked the completion of the CVD process.

The sample then underwent the detemplation process to remove silica via hydrofluoric acid (20 mL) washing for 3 h and thereafter diluted to 2 L with deionised water and filtered. The sample was then refluxed in 10% hydrochloric acid (200 mL) at 70 ºC for 24 h. Thereafter the ZTC was filtered and washed with deionised water (2 L) and dried in a conventional oven at 90 ºC.

3.4.3.2 MOF synthesis

The MOFs were synthesised via a modulated synthesis route (Ren et al., 2014a; Ren et al., 2014b). Although the reaction vessels did differ, a general schematic of the synthesis route undertaken for Zr and Cr based MOFs is illustrated in Figure 3.7 and a detailed explanation of the procedure is in section 3.4.3.2.1 and 3.4.3.2.2 respectively.
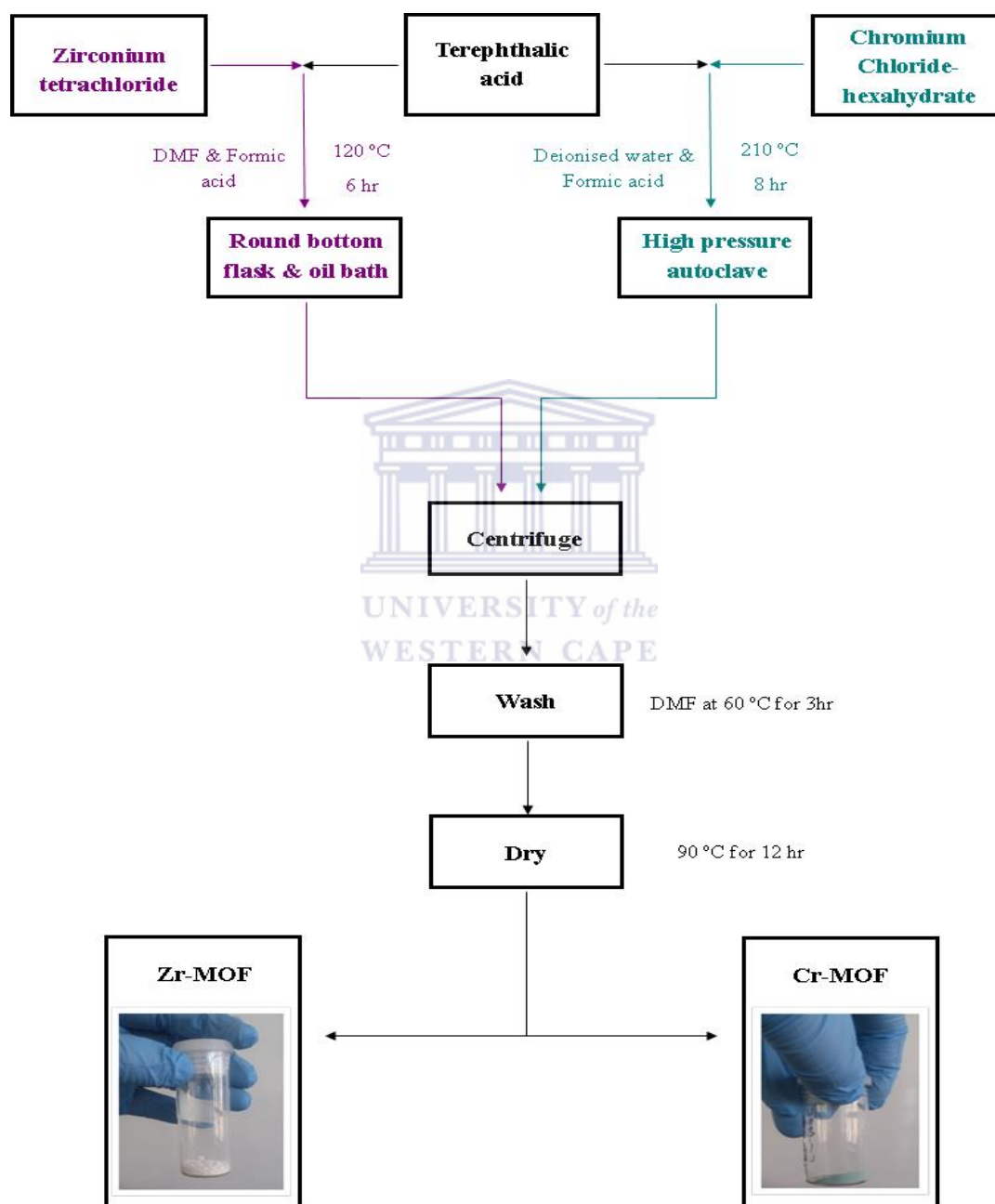
Figure 3.7: General schematic for the synthesis of Zr and Cr MOFs.

3.4.3.2.1 Zr MOF synthesis

Terephthalic acid (0.68 g) was dissolved in DMF (25 mL) and sonicated for 10 min and thereafter zirconium tetrachloride (1.06 g) was added and thoroughly mixed. The resulting solution was transferred to a round bottom flask. Formic acid (17.2 mL) was added to the round bottom flask and then placed in an oil bath and heated to 120 ℃ for 8 h. The Zr MOF crystals were then centrifuged and washed with DMF at 60 ℃ to remove unreacted terephthalic acid and dried at 90 ℃ in a conventional oven.

3.4.3.2.2 Cr MOF synthesis

Terephthalic acid (1.66 g) was dissolved in deionised water (45 mL) with the aid of a sonicator. Chromium chloride hexahydrate (2.66 g) was transferred along with 55 mL of deionised water to the high pressure autoclave reaction vessel (picture shown in Figure 3.8). Formic acid (30.2 mL) was added to the resulting solution and the mixture was heated to 210 ℃ and held at that temperature for 8 h. Once the reaction was done the autoclave was left to cool overnight and the Cr MOF crystals were removed, centrifuged and washed in DMF at 60 ℃ for 1 h and finally dried at 90 ℃ in a conventional oven.

Figure 3.8: Picture of the high pressure autoclave reactor used to synthesise Cr MOF.

3.4.4   Synthesis of electrospun composite fibres

The suitable polymer was selected in section 3.4.1 and the processing parameters (specifically distance between the needle tip and collector plate and applied voltage) were investigated to determine the range at which suitable polymer (PAN) fibres were defect free

and of a narrow diameter in section 3.4.2. Having optimised the conditions for electrospinning pristine PAN fibres, it was then possible to start the incorporation of the porous powdered materials into the polymeric solution in order to produce composite electrospun fibres, which was the final stage of the experimental approach. The route undertaken to synthesise the composite fibres is presented in Figure 3.9, with zeolite 13X-PAN composite fibres being the example.
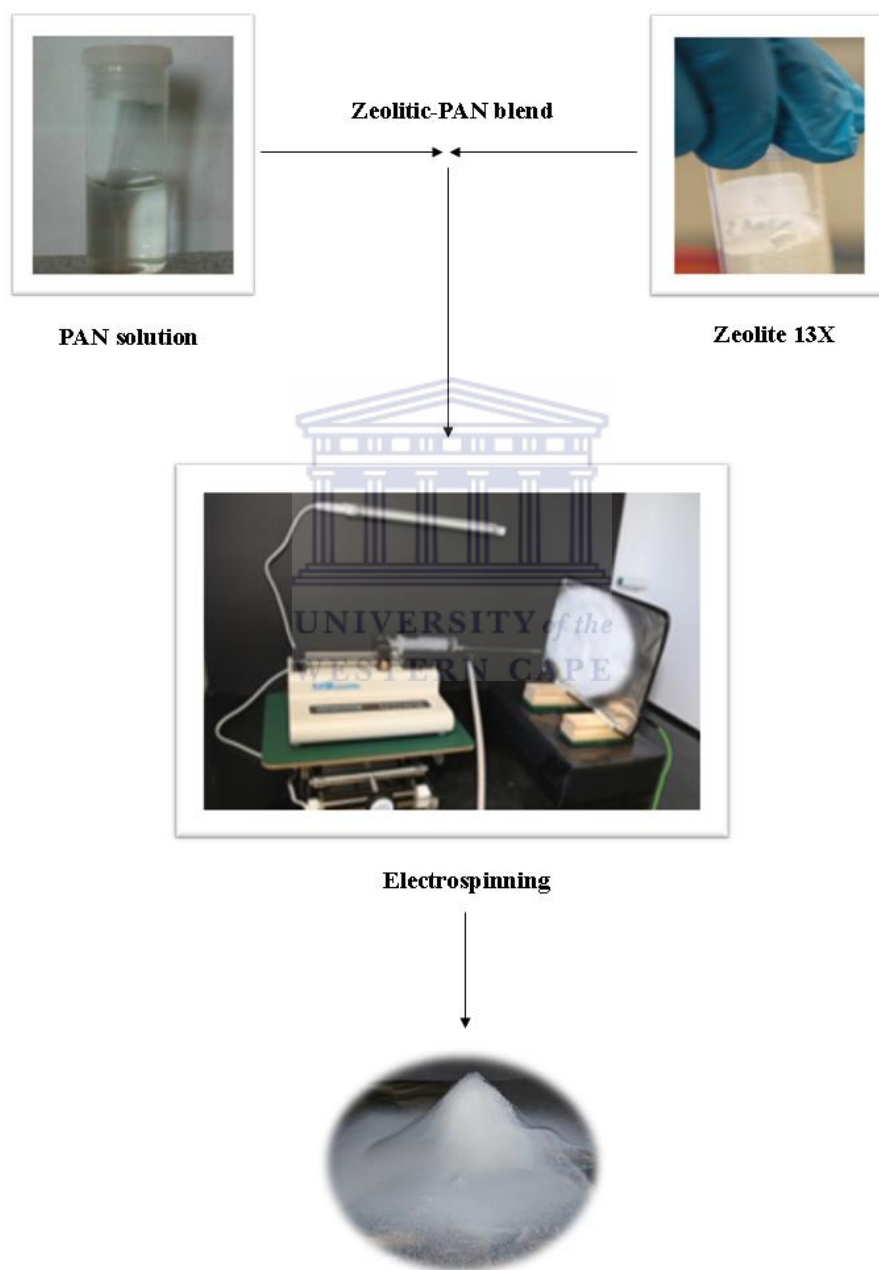
Figure 3.9: Schematic flow diagram of the synthesis route for zeolite 13X-PAN composite fibres.

Composite fibres were synthesised by incorporating the porous powdered materials into the PAN solution and then electrospun. The percentage of porous powdered materials incorporated into the fibres was based on observable viscosity as determined by the electrospinability of the resultant polymeric blend. A general description of the procedure for the synthesis of composite fibres is as follows; the mass of the vial, vial cap and magnetic stirrer bar was recorded and thereafter a PAN solution (10 wt%) was prepared as stated previously in section 3.4.1.1 and 3.4.1.2 in the weighed vial. Once the PAN was dissolved, the vial along with the PAN solution in it was weighed. The mass of the PAN solution was recorded and the thereafter the porous powdered material was added to achieve the desired weight percent loading. The polymeric blend (refers to the mixture of PAN solution and the porous powdered materials) was first mixed with a spatula, thereafter the vial was sealed and further mixed with a magnetic stirrer for approximately 60 min and sonicated for 10 min and then electrospun (like in section 3.4.1.3).

The amount of zeolite 13X encapsulated (referred to as loading weight percent (wt%)) in the PAN fibre ranged between 5-40 wt% since loadings higher than 40 wt% were too viscous to electrospin. The parameters under which the zeolitic-PAN blend was electrospun are found in Table 3.8. The loading weight percent for ZTC-PAN composite fibres ranged between 7.5 and 12.5 wt%. The parameters under which the various ZTC-PAN blends were electrospun are found in Table 3.9. The relevant information regarding the loading of the Zr and Cr-MOFs as well as their electrospinning parameters for the MOF-PAN blends is found in Table 3.10.

Table 3.8: Loading percentage and electrospinning conditions for zeolite-PAN composite fibres.

Sample code	*Loading (wt%)*	*Flowrate (mL/h)*	*Distance (cm)*	*Applied voltage (kV)*	*Temperature (ºC)*	*Humidity (%)*
Zeo-5	5	1.50-1.90	10	7-8	23-24	23-27
Zeo-10	10	2.00	10	7	25-26	30-36
Zeo-20	20	2.50-2.80	10	9	26-28	20-23
Zeo-40	40	2.80-3.00	10	8-10	19-25	40-60

Table 3.9: Loading percentage and electrospinning conditions for ZTC-PAN composite fibres

Sample code	Loading (wt%)	Flowrate (mL/h)	Distance (cm)	Applied voltage (kV)	Temperature (ºC)	Humidity (%)
ZTC-7.5	7.5	0.30-0.40	10	7-9	23-23	59-60
ZTC-10	10	0.35-0.60	10	6-8	18-19	52-56
ZTC-12.5	12.5	0.35	10	8-9	24-25	50-53

Table 3.10: Loading percentage and electrospinning conditions for MOF-PAN composite fibres.

Sample	Loading (wt%)	Flowrate (mL/h)	Distance (cm)	Applied voltage (kV)	Temperature (ºC)	Humidity (%)
Zr-MOF fibres	20	1.25-2.50	10	10	22-24	40-60
Cr-MOF fibres	20	0.34-0.50	10	8-9	26-28	30-35

3.5 Characterisation Methods

This section focuses on the technical aspect of characterising the samples. It will describe the techniques used and all relevant information regarding the characterisation of the samples.

3.5.1 Scanning Electron Microscopy (SEM)

The procedure for preparing samples for SEM analysis was as follows; double-sided sticky tape was mounted on the aluminium stubs, then either the porous powdered materials or electrospun fibres (or the composites) were transferred to the sticky tape and the excess removed and placed on a multiple stub stage. The samples were then coated with carbon to reduce charging effects during analysis and thereafter transferred to an Auriga Cobra Focused-Ion Beam Scanning Electron Microscope (FIB-SEM) for analysis of surface morphology measurement fibre diameters.

3.5.2 Powder X-Ray Diffraction (PXRD)

Samples for PXRD were prepared by either placing the porous powdered or electrospun fibres on to a disc, which was then transferred to a PANalytical X'Pert Pro powder diffractometer equipped with a Pixcel detector (Ni-filtered Cu-K$_{\alpha}$ radiation, 0.154 nm). The XRD patterns were acquired at room temperature, at a scanning rate of $0.1^{\circ} \cdot s^{-1}$ and 2θ ranging between $1–60^{\circ}$.

3.5.3 Thermal Gravimetric Analysis (TGA)

TGA was done by loading 9-10 mg of sample into a sample ceramic pan, placed in a Mettler, Toledo, TGA/SDTA 851^{e}, heated to 1000 ℃, temperature ramped up at $10 \, ^{\circ}C \cdot min^{-1,}$ under an air flow of $10 \, mL \cdot min^{-1}$.

3.5.4 Surface area and hydrogen adsorption measurements

First, the samples had to undergo a process known as degassing whereby 0.1-0.3 g of the samples were transferred to a sample tube, which was then transferred to the degassing port of a Micromeritics ASAP 2020 HD analyser. Degassing occurred between 200-280 ℃ under 10^{-7} bar vacuum for 6 h to remove any solvent from the samples. The temperature for degassing was determined from the results of the thermal gravimetric analysis. Then the sample tube was transferred to the analysis port of the Micromeritics ASAP 2020 HD analyser and degassed again under the same temperature and vacuum but for only 3 h to remove any atmospheric moisture and gas. The BET surface area was obtained from the nitrogen isotherms. The measurements were conducted at 77 K. Then the sample was degassed again while still on the analysis port under the aforementioned conditions to remove the nitrogen gas from the pores of the materials, and analysed for volumetric hydrogen adsorption at 77 K and pressures up to 1 bar.

3.5.5 Fourier Transform Infrared (FTIR) analysis

FTIR spectra were obtained from a Perkin Elmer spectrum 100 FT-IR spectrometer fitted with an ATR configuration. Approximately 15 mg of the solid sample was placed on the sample holder then analysed at 60 scans reducing the noise and range between 400-4000 wavenumbers.

Chapter summary

The experimental methods section of the chapter was structured in sequential manner whereby, first a suitable polymer was selected from three polymers chosen from literature based on the physical characteristics of the resultant electrospun fibres. An explanation of how the solution and processing parameters were optimised for electrospinning of PSMA, PAA and PAN solutions was also presented. Once the most suitable polymer (which in this case was PAN) was selected, its electrospinning parameters were investigated. To determine the range at which the electrospun fibres were not beaded and had a fibre diameter in the range of 300-500 nm, the investigation was done by keeping the concentration of the PAN solution and the flowrate constant, and varying the distance between the collector plate and needle tip as well as the voltage. The experiments were conducted under ambient temperature and humidity.

Commercial zeolite 13X and its templated carbon derivative as well as synthesised MOFs was utilised in the synthesis of composite fibres. The MOFs were synthesised via a modulated method whereas ZTC was produced from the combination of liquid carbon impregnation of the zeolite followed by CVD. Since the polymer had already been selected and the porous powdered materials synthesised, the next step involved the synthesis of the composite fibres by mixing the porous powdered materials with 10 wt% PAN solution and its resulting blend was electrospun. The amount of porous powdered materials incorporated (also known as loading weight percent) into the fibres was dependent on the observable viscosity and thereafter increased as determined by the electrospinability of the porous powdered material-polymeric blend. The loading weight percent for zeolite 13X, ZTCs and MOFs was 0-40, 7.5-12.5 and 20 wt%, respectively. All the samples from the study were characterised using SEM, PXRD, TGA, BET surface area, hydrogen adsorption measurements and FTIR analysis.

The next chapter presents and discusses the results of the suitable polymer selected for the study and optimised conditions under which it was electrospun. Morphological, structural and thermal analysis of the suitable as well as its surface area and hydrogen measurements will be presented in the following chapter.

Chapter Four

Polymer Selection and Optimisation

This chapter is divided into two sections; the first part discusses the results obtained when selecting the most suitable polymer for the synthesis of composite fibres and the second part presents the results for the optimisation of the processing parameters for the electrospinning of the suitable polymer to determine the optimum range in which the resultant fibres possess a medium fibre diameter and are not beaded.

4.1 Polymer selection

The first step for obtaining electrospun composite fibres with attractive hydrogen adsorption capacity involves identification of a polymer that has good electrospinability properties. In this regard the suitable polymer has to adhere to certain criteria such as; resulting in fibres that are not beaded, desirable fibre diameters and also its ability to incorporate the porous powders.

4.1.1 Analysis of PSMA fibres

Visual inspection was used to examine the fibres during electrospinning. Previous studies done on the formation of beads on electrospun fibres highlighted that beading results from the viscosity of the polymer solution as well from the unsteady stream of the ejected polymeric jet (Lee et al., 2003; Fong et al., 1999). Since lower concentrations (10 and 18 wt%) PSMA solutions did not yield fibres; the concentration was increased to 25 wt% resulting in a viscous flowing PSMA solution that yielded fibres. The parameters under which the PSMA fibres were electrospun are presented in Table 3.6.
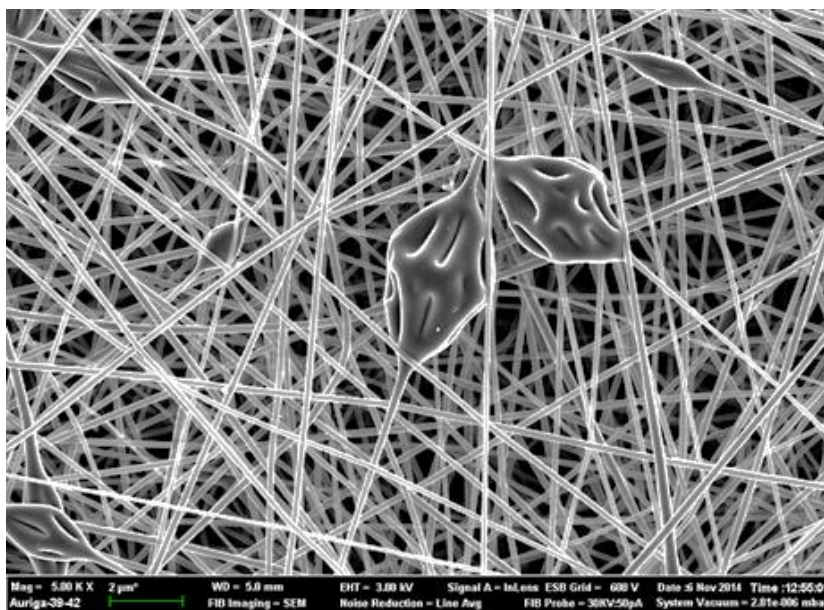
Figure 4.1: SEM micrograph of electrospun PSMA fibres.

Since the concentration of polymer solution is directly correlated to its viscosity, the formation of beads on the PSMA fibres as can be seen from the SEM micrograph in Figure 4.1 was related to the PSMA solution being too viscous. This observation was also reported by Cecile and Hsieh who studied the synthesis of electrospun PSMA fibres and reported that between 20 and 40 wt% there was formation of fibres with the presence of beads (Cécile & Hsieh, 2009). The rationale that the bead formation on the PSMA fibres were due to high concentration of the PSMA solution was also supported by Lee and colleagues who studied the morphology of the beads on the polystyrene (PS) moiety of PSMA (Lee et al., 2003). The diameter of the unbeaded part of the PSMA fibres was measured with the FIB-SEM when the SEM micrographs were taken. The PSMA fibre diameter ranged between 100-300 nm which can be described as narrow. Based on the criteria mentioned in the introductory section of this sub-section; PSMA polymer could be considered as unsuitable for this work since it failed to produce unbeaded fibres. Hence the study focused on a different polymer as discussed below.

4.1.2 Analysis of PAA fibres

For the study, PAA was received as an aqueous solution (35 wt% in water) which was too thick to electrospin, therefore it was diluted with DMF resulting in a 50 wt% PAA solution which possessed adequate viscosity for electrospinning (parameters can be found in Table 3.6). Adequate molecular chain entanglement is a characteristic determined by the polymer structure and concentration and is a necessary requirement for the formation of fibres (Chen

et al., 2008). Implying that if the polymer concentration is too low there is insufficient molecular entanglement resulting in droplets (Kim et al., 2005a; Li & Hsieh, 2005).
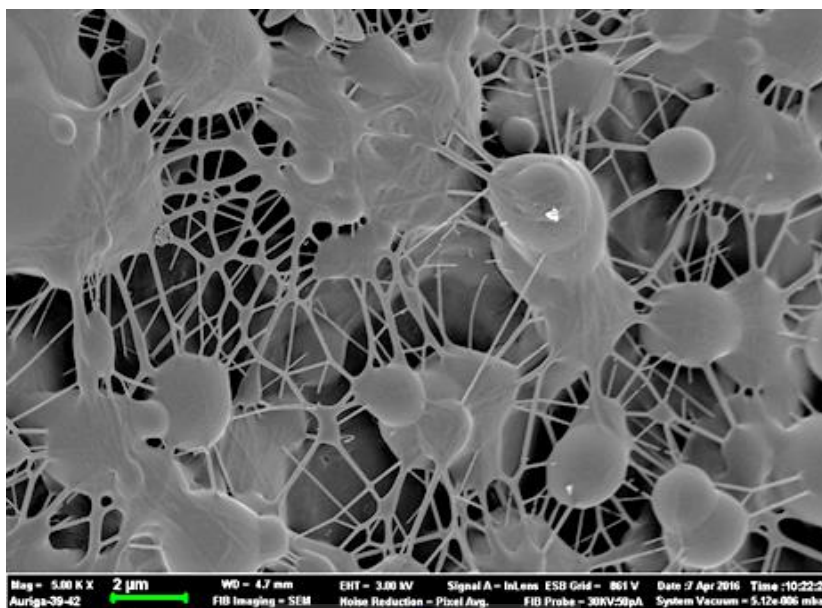
Figure 4.2: SEM micrograph of PAA fibres.

There was no visible formation of beads on the PAA fibres while electrospinning, however, the SEM micrograph (Figure 4.2) illustrated that the PAA fibres were beaded which was not visible to the naked eye due to the fine nature of the fibres. This coupled with the fibre diameter of 100-200 nm renders PAA not suitable to encapsulate the porous powdered materials.

4.1.3 Analysis of PAN fibres

The morphological analysis obtained following the employment of the electrospinning parameters shown in Table 3.6 is illustrated in the SEM micrograph presented in Figure 4.3.
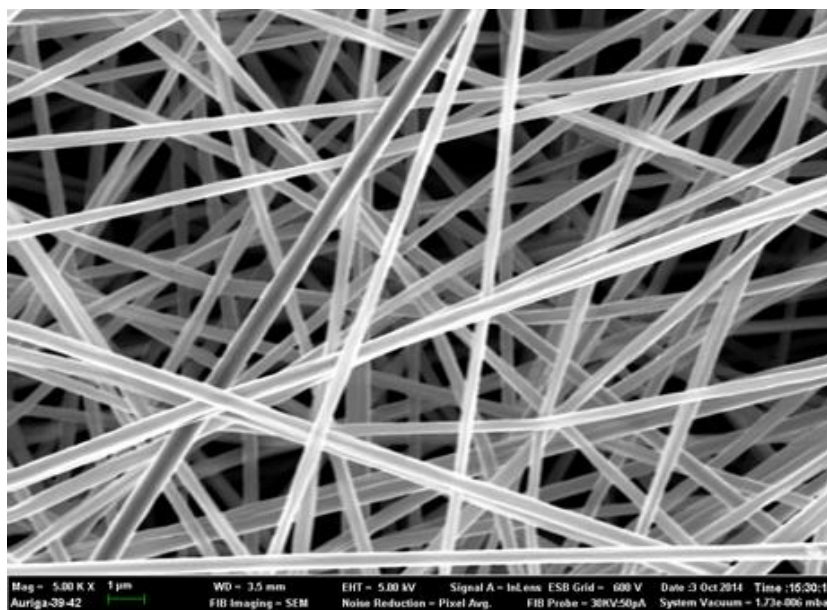
Figure 4.3: SEM micrograph of electrospun PAN fibres.

During electrospinning of PAN solution there was no visible formation of beads, which was confirmed by SEM micrograph (figure 4.3) and the fibres appeared to be thicker as compared to the PSMA and PAN fibres. This observation was confirmed by the relatively thick diameter of the PAN fibres of 300-600 nm. Li and Wang noted that the fibre diameter is dependent on the distance between the needle tip and the collector plate, however, this distance was kept constant for the electrospinning of all three polymers therefore it can be deduced that the large fibre diameter is attributed to the high viscosity of the PAN solution (Li & Wang , 2013), this deduction was corroborated by (Gu et al., 2005). For purposes of the study, an adequate fibre diameter would be between 300-500 nm since the fibre will be thick enough to encapsulate the powders but still allow the hydrogen gas molecules to access the pores of the porous powdered materials. As mentioned in section 3.4.1.1 the polymer solutions were selected via Leach et al. (2011) method that is preparing polymer solutions of varying concentrations and selecting the solution that is a viscous flowing gel. From the results presented in this section, it can be deduced that PAN was the most suitable polymer for the production of composite fibres because it formed bead free fibres as compared to PSMA and PAA which had beads. However, the fibre diameter of the PAN was a drawback because it was thicker than the diameters of PSMA and PAA. Fibre diameters are varied by changing the parameters they are electrospun under thus initiating the next section.

4.2 Optimisation of electrospinning parameters for PAN

Since the general consensus amongst scientists is that the morphology and diameter of fibres are controlled by the electrospinning parameters, this section will focus on determining their effects of the PAN fibres (Jacobs et al., 2010; Li & Wang, 2013; Chowdhury & Stylios, 2010). Having optimised the concentration of the PAN solution (10 wt%) in section 3.4.1 for electrospinning which yielded bead free fibres shown in Figure 4.3. The flowrate of the PAN solution was kept constant at 0.4 mL/h throughout the investigation as well as the temperature at 17 ℃ and the humidity ranged between 41-42% since the investigation was done during the day and took a few hours to perform. Therefore it was necessary for the applied voltage and distance between the needle tip and the collector plate to be investigated and optimised in this section. It was also important to note the range in which beaded and unbeaded fibres resulted. The investigation was done by varying the applied voltage and distance between the needle tip and collector plate which was set at 5, 10 and 15 cm. The ranges for the applied voltage was subjective, the first range occurs at the first occurrence of a steady stream and thereafter increased consisting of the second and third range. This investigation yielded fibres from nine experimental sets (presented in Table 3.7) which underwent morphological analysis with the aid of SEM micrographs presented in Figure 4.4. The response factors were beaded or unbeaded fibres and the diameter size of the fibres found in Table 4.1.

Table 4.1: The experimental code corresponding SEM micrographs (Figure 4.5) along with the diameter range of the fibres for parameter investigation of 10 wt% PAN solution.

Experimental set code	*SEM micrograph*	*Fibre morphology*	*Fibre diameter range/nm*
PI-1	-	No fibres	-
PI-2	[a]	Beaded	451-521
PI-3	[b]	Beaded	451-622
PI-4	[c]	Beaded	496-624
PI-5	[d]	Not beaded	487-507
PI-6	[e]	Beaded	488-523
PI-7	[f]	Beaded	542-577
PI-8	[g]	Beaded	401-459
PI-9	[h]	Beaded	397-413
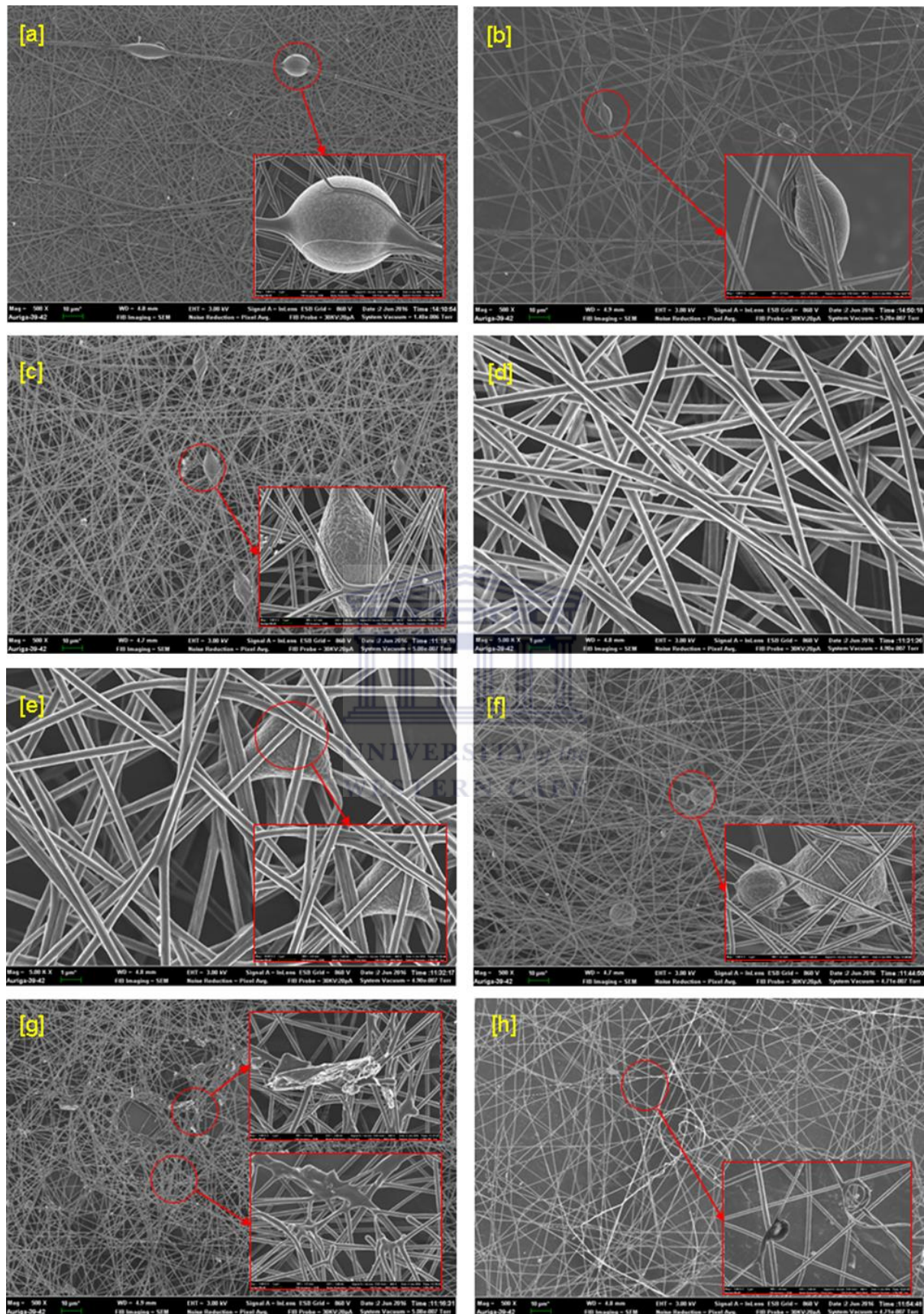
Figure 4.4: SEM micrographs from the parameter investigation. Experimental set codes PI-2 to PI-9 are correlated to SEM micrograph [a] to [h].

It can be seen from the SEM micrographs in Figure 4.4a, b, c, e and f that beaded fibres occurred with the exception of Figure 4.4d which yielded smooth fibres which is synonymous with the steady stream that was observed during electrospinning. Rather interesting are the structures in Figure 4.4g and h, these structures were observed while electrospinning when the applied voltage was increased and the steady stream of PAN solution split up. However, these structures were also seen in previous studies (Han et al., 2005; Zhang et al., 2014) due to the residual solvent that causes the intersecting fibres to coagulate. This reasoning contradicted the observation from the current study because these structures were observed for a needle tip to collector distance of 15 cm which had enough time for the solvent to evaporate (Chowdhury & Stylios, 2010). The diameters for all experimental sets were similar but thinner diameters were seen for fibres in Figure 4.4h when the distance was 15 cm and the applied voltage was 12 kV. The thick fibres seen in Figure 4.4b occurred when the distance was 5 cm and the voltage was 12 kV confirming that distance between the needle tip and collector was a determining factor. The optimal parameters for electrospinning unbeaded PAN fibres with a diameter of 300-500 nm was concluded from this investigation as follows; a 10 wt% concentrated PAN solution ejected from the needle tip at a flowrate of 0.4 mL/h. The optimal distance from the needle tip to the collector plate and applied voltage was 10 cm and 8 kV respectively.

4.3 Further characterisation of optimised PAN fibres

Characterisation of the optimised electrospun PAN fibres was vital for the aim of the study. Previous studies have illustrated that there is an increase in the tensile strength of the PAN fibres when it undergoes carbonisation via thermal treatment (Bai et al., 2011). Therefore the PAN fibres synthesised in this study (as described in section 3.4.1 and 3.4.2) underwent thermal treatment. Carbonisation is a two stage process; the first is stabilisation which occurs between 200 and 300 ^{o}C and then carbonisation which occurs at temperatures over 900 ^{o}C (Lee et al., 2012). For the current study, thermal treatment was employed to stabilise the electrospun PAN fibres at 280 ^{o}C under vacuum only and was not advanced to the carbonisation stage because the high temperatures would decompose the porous powdered materials used to produce the composite fibres. The stabilisation temperature for the PAN fibres were adopted from the work done by Cho and colleagues (2007) who reported that complete stabilisation occurred at 280 ºC.

4.3.1 Morphological, Structural and Physical analysis

Since thermal treatment was employed to improve tensile strength of the PAN fibres it was important to determine its effect on the morphology and structure which was analysed with the aid of SEM micrographs (Figure 4.5b) and PXRD pattern (Figure 4.5c).
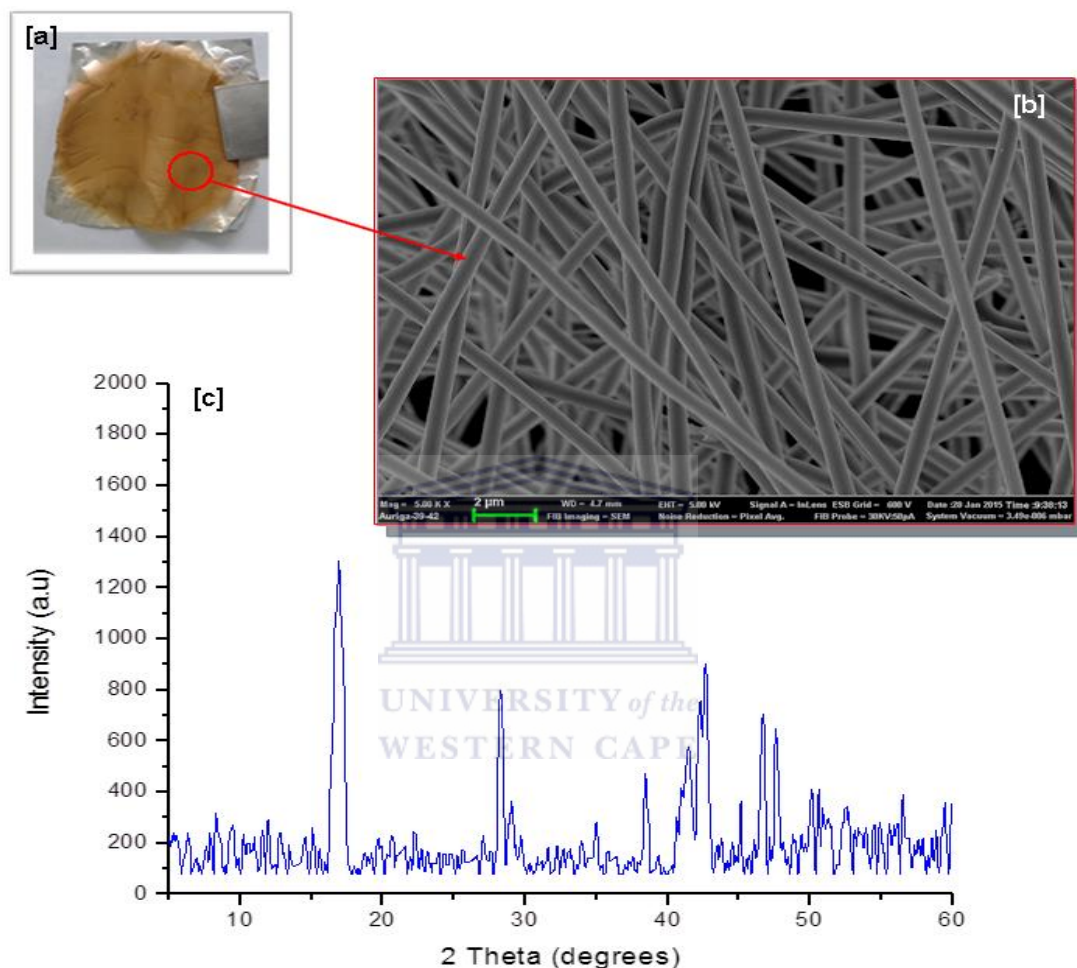
Figure 4.5: Picture (a), SEM micrograph (b) and PXRD patterns (c) of PAN fibres that underwent thermal treatment.

Morphological analysis of the PAN fibres pre (Figure 4.3) and post (Figure 4.5b) thermal treatment illustrate that the PAN fibres did not decompose during thermal treatment. However, there was a chemical change evident from the difference in colour from white (Figure 3.3b) to orange-brown (Figure 4.5a). The diffraction pattern of the PAN fibres presented in Figure 4.5c shows weak peaks at $2\theta = 17°$, $28°$, $41–43°$, $47°$ and $48°$ that are as a result of pre-oxidation, aromatization and stabilization of the fibres as they were thermally

treated. Earlier studies by Lee et al. (2012) reported that the diffraction peaks at 2θ = 17° and 29° corresponds with the (100) and (101) crystal planes of the PAN fibres.

The difference in colour due to chemical transformations can be explained by FTIR analysis (Figure 4.6).
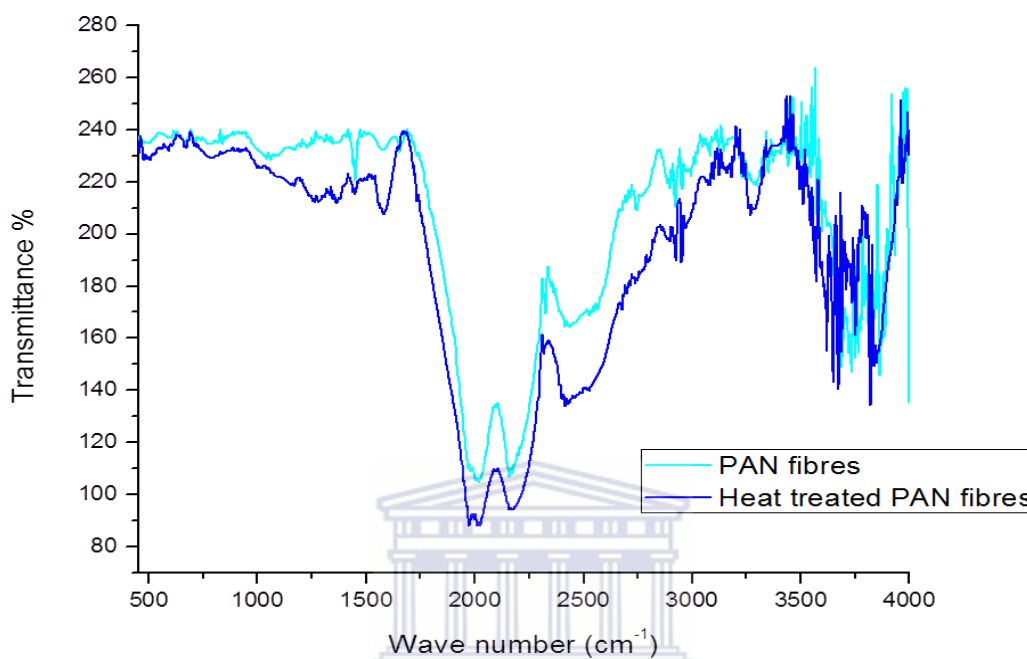
Figure 4.6: FTIR spectra for PAN fibres pre- and post-thermal treatment.

The PAN fibres showed peaks at ˷1500, ˷1650, ˷2200 and ˷2700 cm^{-1}, attributed to –C–H, –C=C, –C≡N, and –C–H respectively (Cho et al., 2007). A weak stretching band that developed at ˷1500 cm^{-1} after thermal treatment is due to –C=C and –C=N, indicating cyclisation (reaction seen in Figure 4.7) and dehydrogenation which occurs in inert and atmospheric conditions (Ouyang et al., 2008).
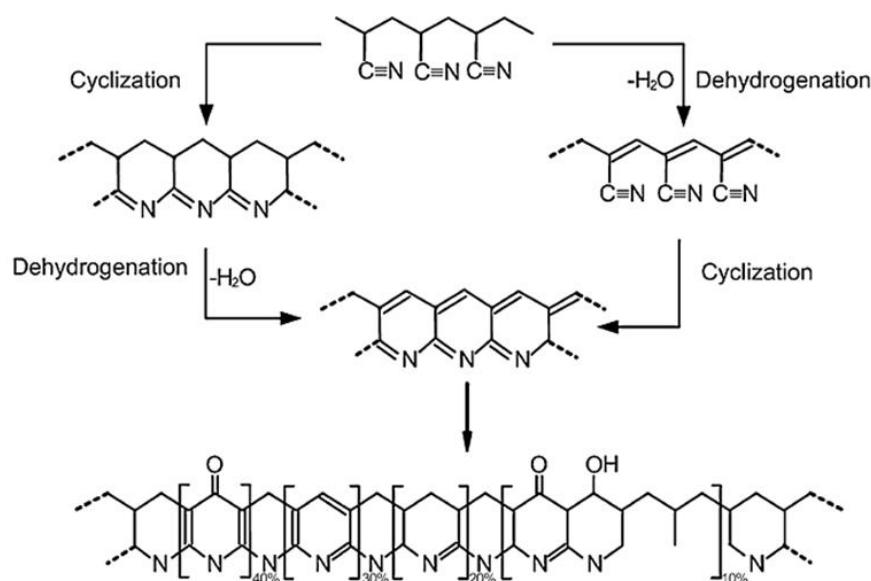
Figure 4.7: Cyclisation of the nitrile groups present in PAN and dehydrogenation process that occurs during the stabilisation of PAN adapted from (Rahaman et al., 2007).

Although literature states that tensile strength increases after the PAN fibres are stabilised, it was not the case in the study because after thermally treating the PAN fibres at 280 ºC under vacuum (referred to as degassing) for six hours the fibres became brittle. This observation could be due to the oxidation part of the stabilisation which does not occur because of the inert conditions (Rahaman et al., 2007).

The reason for not stabilising the PAN fibres before subjecting them to vacuum was that the residual solvent from the electrospun PAN fibres would be removed under vacuum conditions thus creating porosity which was an important aspect for hydrogen uptake when producing the composite fibres. If the fibres were to firstly undergo thermal treatment, the solvent would dry up, and hence the creation of porosity would not occur. Therefore the PAN fibres were subjected to thermal treatment and vacuum (at 10^{-7} bar) simultaneously. For this reason, it was hypothesised that the removal of the residual solvent in the pristine electrospun PAN fibres under a high vacuum during degassing would result in the creation of porosity. Evidence to support or reject this hypothesis is presented in Figure 4.8, which are SEM micrographs of electrospun 10 wt% PAN fibres before and after the degassing process.
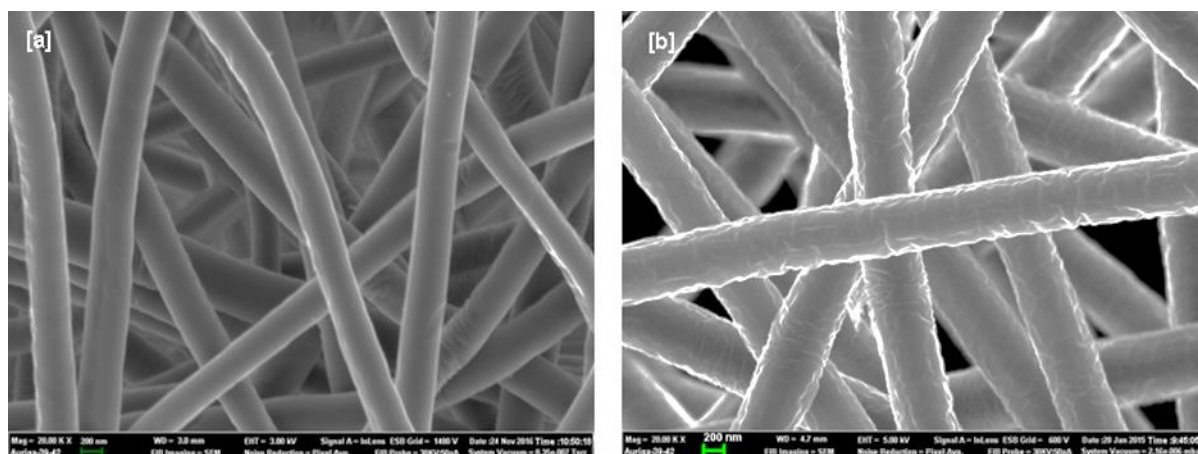
Figure 4.8: SEM micrographs of the electrospun 10 wt% PAN fibres pre (a) and post (b) degassing at 280 ℃ under 10^{-7} bar vacuum for six hours.

A smooth surface morphology was observed for the pristine electrospun PAN fibres (Figure 4.8a) prior to the degassing process. However, after the pristine electrospun PAN fibres were subjected to the degassing process (that is thermal treatment at 280 ℃ under 10^{-7} vacuum) the surface morphology became rough (Figure 4.8b) implying that there was removal of residual solvent. Although, there was no porosity (Figure 4.8b) observed after degassing which could be due to insufficient residual solvent in the PAN fibres. Therefore the aforementioned hypothesis that degassing would create porosity on the electrospun PAN fibres was not accepted.

4.3.2 Thermal analysis

Thermal gravimetric analysis shown in Figure 4.9 was done on the PAN fibres pre and post heat treatment to determine whether thermal treatment made the PAN fibres more resistant to thermal decomposition.
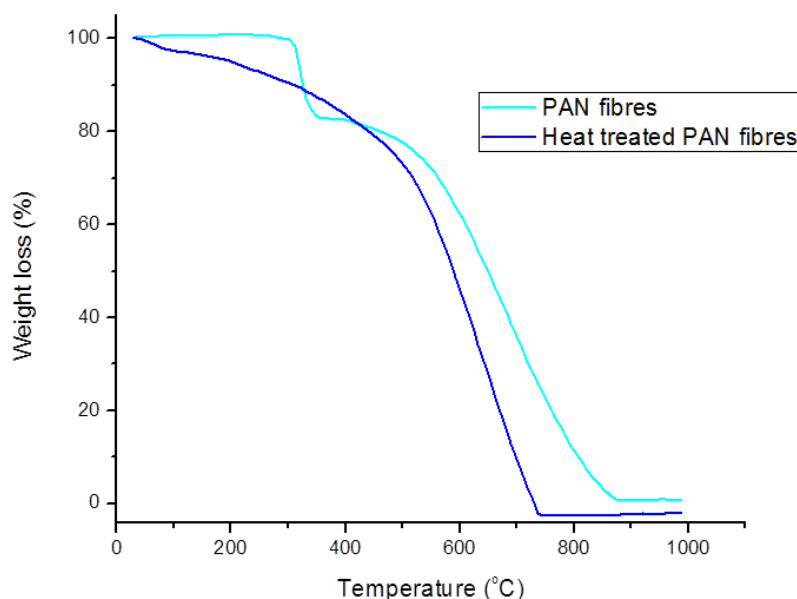
Figure 4.9: TGA plot of PAN fibres pre and post thermal treatment.

The pristine PAN fibres before thermal treatment showed a sharp decrease in the weight percent of approximately 20% at 370 ℃ due to loss of residual DMF and then a gradual weight loss making it stable until approximately 500 ℃. The thermal treated PAN fibres showed a gentle reduction in weight loss since they were free of any DMF and were relatively stable up to 400 ℃. Implying that the thermal treatment of PAN fibres reduced the temperature at which the fibres are thermally stable by 100 ℃, confirming the previous observation that thermal treatment did not improve the tensile strength of the fibres.

4.3.3 Surface area and Hydrogen adsorption measurements

Previous studies have reported that PAN fibres can adsorb hydrogen gas, although the adsorption capacity was low (ranging in 0.16-0.5 wt%) (Kim et al., 2005b), however, these studies were done on carbonised PAN fibres which were not adopted for this study (reasons for which is explained in the introduction of section 4.3). Therefore it was essential that surface area and hydrogen adsorption measurements be performed on these pristine thermally treated PAN fibres because they would assist in determining whether the PAN fibres contribute towards the surface area and hydrogen adsorption for the composite fibres. Degassing enables the removal of residual solvent which affects the surface area and hydrogen adsorption measurements. Therefore the pristine electrospun PAN fibres were degassed at 200 ℃ for six hours under 10^{-7} bar vacuum which was the same temperature used

for the degassing of the porous powdered materials used in the synthesis of the composite fibres (which can be found in chapter six). The nitrogen isotherm in Figure 4.10a was used to determine the BET surface area of the thermal treated PAN fibres and corresponding hydrogen adsorption isotherm is presented in Figure 4.10b.
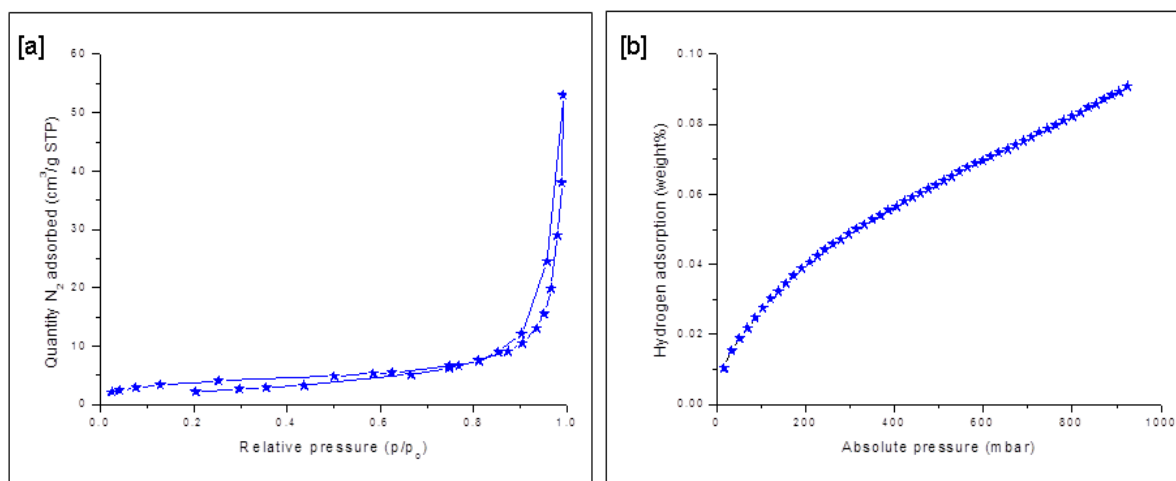
Figure 4.10: Nitrogen sorption isotherm (a) and hydrogen adsorption capacity (b) for pristine electrospun PAN fibres that was degassed at 200 ºC for six hours under 10^{-7} bar vacuum and measured at 77 K and 1bar.

The nitrogen isotherm in Figure 4.10a is of Type II isotherm implying that an identifiable monolayer has not formed and that there is a very weak interaction between the nitrogen gas molecules and the degassed PAN fibres. The BET surface area was recorded to be a negligible 13 cm^3/g. The hydrogen adsorption capacity for the thermally treated PAN fibres was recorded at 0.05 wt% (Figure 4.10b).

Chapter summary

The chapter presented the results and discussion of the first aspect of the study that was the selection of a suitable polymer for the production of composite fibres. After electrospinning three polymers, PAN was selected as the most suitable polymer because it yielded bead free fibres. However, the diameter of the PAN fibres was large/thick which prompted the investigation aimed to determine whether the distance from the needle tip to the collector plate and the applied voltage would affect the fibre diameters while the optimised PAN concentration (10 wt%) and flowrate were held constant. The experiments were done under ambient temperatures and humidity. It was found that a distance and voltage of 10 cm and 8

kV respectively, yielded smooth unbeaded fibres with diameter of 480-510 nm which is within the desired range of 300-500 nm.

Following the optimisation of the solution and processing parameters under which PAN was electrospun, the resultant PAN fibres underwent thermal treatment intending to improve its tensile strength. Due to previous studies reporting an increase in tensile strength during the first stage (that is stabilisation) of carbonisation of the PAN fibres. Therefore for this study, the optimised PAN fibres were stabilised via thermal treatment (between 200-300 ℃) under vacuum and did not progress to the carbonisation stage. This is due to carbonisation occurring at temperatures greater than 900 ℃ which will result in the destruction of the porous powdered materials (that adsorb hydrogen gas) utilised to synthesise the composite fibres.

The results from the morphological analysis illustrated that the PAN fibres did not decompose after thermal treatment, although there was a colour change from white to orange-brown implying a chemical transformation. Phase crystallinity analysis showed peaks at $2\theta =17°$, 28°, 41–43°, 47° and 48° due to pre-oxidation, aromatization and stabilization of the PAN fibres during thermal treatment. The cyclisation and dehydrogenation of the nitrile groups present in PAN fibres were confirmed by the weak stretching band at 1500 cm^{-1} seen in the FTIR spectrum. Although literature reports an increase in tensile strength of the PAN fibres after stabilisation, this was not corroborated by this study due to the embrittlement of the thermally treated PAN fibres. This observation is probably due to oxidation not occurring since thermal treatment was performed under vacuum conditions. The embrittlement of the PAN fibres was corroborated by thermal stability tests which illustrated that the pre-thermal treated PAN fibres were stable up to 500 ℃ and the post thermal treated PAN fibres were only stable up to 400 ℃. However, the pristine electrospun PAN fibres had to undergo degassing (at 200 ℃ under 10^{-7} bar vacuum for six hours) to remove residual solvent from the fibres. Since BET surface area and hydrogen adsorption capacity is gravimetric measurements (dependent of the mass of the fibres), the degassing temperature was reduced to 200 ℃ which was suitable for the residual solvent to be removed.

The next chapter presents the results and discussion from the analysis of the porous powdered materials that make up the composite fibres that is commercial zeolite 13X, its templated carbon derivative (ZTCs) and the Zr and Cr metal organic frameworks (MOFs).

Chapter Five

Analysis of Pristine Porous Materials

Since the focus of the study was to analyse the electrospun composite fibres for hydrogen storage applications, it was necessary to first analyse its constituents that is the optimised electrospun PAN fibres (presented in chapter four) and the pristine porous powdered materials. Therefore this chapter will provide an explanation of the results from the analysis of the porous powdered materials specifically commercial zeolite 13X, its synthesised templated carbon derivative (ZTC) and metal organic frameworks (Zr and Cr based MOFs). The results for the porous powdered materials are categorised according to morphological and phase crystallinity analysis, followed by the thermal analysis and finally the surface area and hydrogen adsorption analysis.

5.1 Zeolite 13X and ZTC

Commercial zeolite 13X in Na-form was selected for the study since it is thermally stable, possesses good pore size distribution and furthermore is an excellent templating agent for the synthesis of ZTC (Li et al., 2012; Masika & Mokaya, 2013). ZTC is advantageous over most carbons because the zeolite template creates ordered microporous network structure which is beneficial for the storage of gas (Chen et al., 2007).

The synthesis of ZTC in the study was a three stage process, whereby the zeolite 13X was templated by first impregnating the zeolite channels with furfuryl alcohol (a liquid carbon source), thereafter the impregnated zeolite underwent polymerisation and carbonisation (with the second carbon source being ethylene gas) via a temperature programmed chemical vapour deposition (CVD). The third stage involved the removal of the zeolite template, which was obtained by washing with hydrofluoric (HF) acid. A full description of the ZTC synthesis process can be seen in section 3.4.3.1.

A comparative analysis of the zeolite 13X and its ZTC derivative will be presented in this section.

5.1.1 Morphological and Phase Crystallinity analysis

The surface morphology and crystallinity of the zeolite and ZTC were assessed with the aid of SEM micrographs (Figure 5.1a-b respectively) and PXRD patterns (Figure 5.1c-d respectively). Photographs of the zeolite 13X and synthesised ZTC powders can be seen in Figure 5.1e and f respectively.
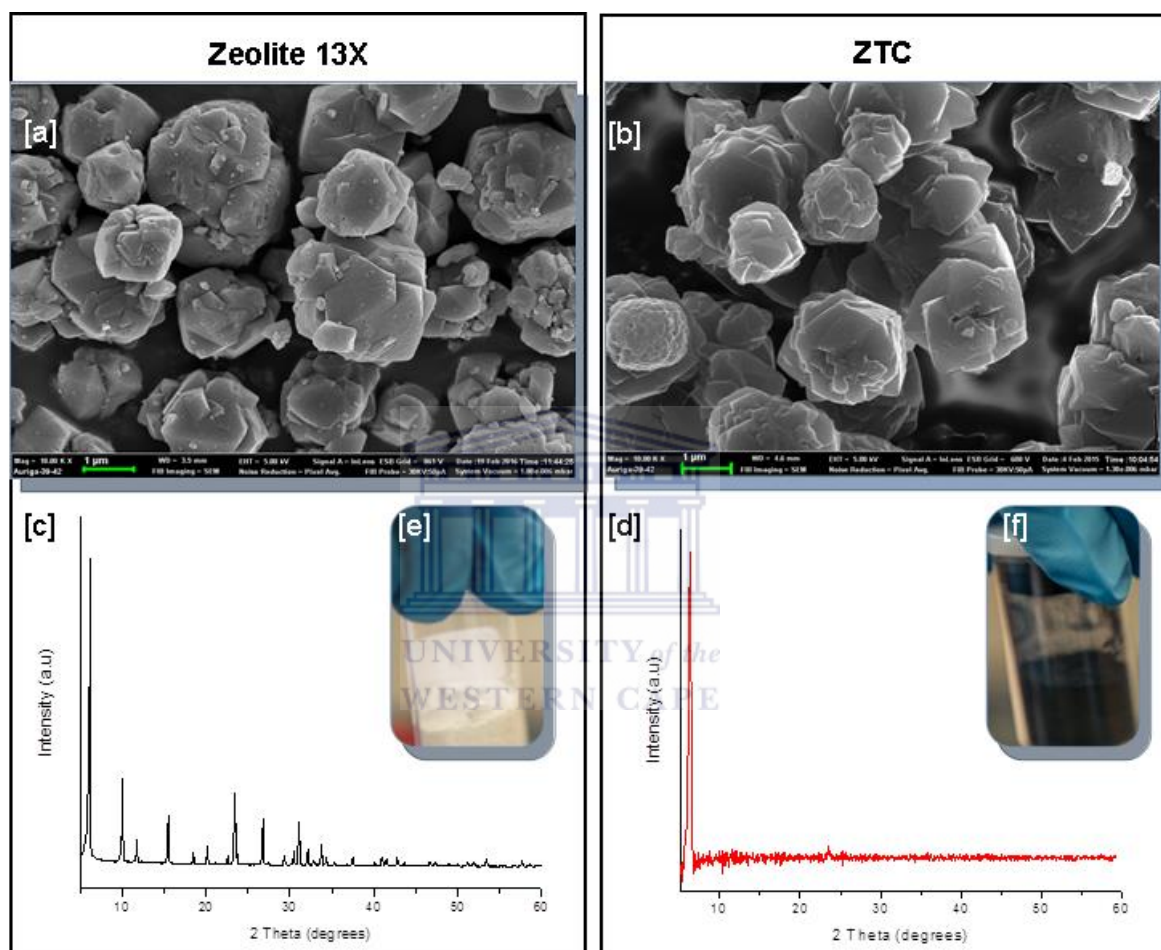
Figure 5.1: SEM micrographs (a-b), PXRD patterns (c-d) and pictures (e-f) of zeolite 13X and ZTC powders.

Well defined octahedral particles that are 2 µm can be seen from the SEM micrographs for both the commercial zeolite and the ZTC. The crystallinity of the zeolite particles was corroborated by numerous sharp peaks of the XRD pattern presented in Figure 5.1c which corresponds to the simulated powder XRD patterns for zeolite 13X reported by Treacy & Higgins, (2007). The observed sharp peaks present for the zeolite XRD pattern were absent in the XRD pattern for the ZTC implying that the ZTC was amorphous because the scattering of the phase contrast was reduced due to the filling of the pores (Masika & Mokaya, 2013;

Musyoka et al., 2015). The prominent peak that appears at approximately 2θ=7° in both Figure 5.1c and d implies that the pore structure of the ZTC was an inverse of the zeolite pores and regular pores formed which possessed a d-spacing of 1.4 nm (Masika & Mokaya, 2013; Yang et al., 2005). Since the prominent peak for the ZTC in Figure 5.1d is sharp and intense, it implies that the method utilised to fill the carbon into the pores (liquid impregnation and CVD method) of the zeolite was the most successful method for FAU structured zeolites such as in the case of zeolite 13X (Kyotani et al., 2003). According to literature the weak peak at around 2θ=26° and 2θ=43° which are a result of graphitic and turbostatic carbon (Yang et al., 2005; Masika et al., 2013). However, these aforementioned peaks were not present in the PXRD pattern (Figure 5.1d) of the ZTC synthesised in this study.

5.1.2 Thermal analysis

Determination of the temperature at which materials decompose especially when they are to be integrated into a hydrogen storage system is of vital importance. Therefore thermal gravimetric analysis (TGA) was done on the zeolite and its templated carbon derivative under air flow and the results are presented in Figure 5.2.
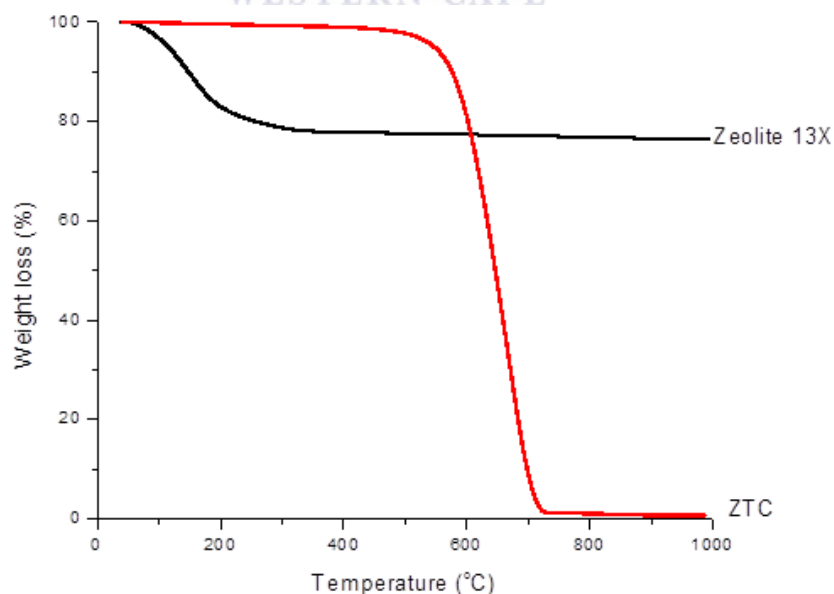
Figure 5.2: TGA plots for commercial zeolite 13X and its ZTC derivative.

From the TGA plot of zeolite 13X (Figure 5.2) an initial decrease in mass of approximately 20% was observed between 100-350 ℃ zeolite 13X which can be attributed to the evaporation of atmospheric moisture that the zeolite had adsorbed during sample preparation. After 350 ^{o}C there was no weight loss implying that the zeolites was stable up to high temperatures (1000 ^{o}C) which can be corroborated by previous studies (Li et al., 2012). Thermal analysis of ZTC show that it was thermally stable up to 550 ^{o}C after which a sharp loss in weight was observed to occur between 600-710 ^{o}C. This drastic weight loss can be ascribed to carbon combustion in air or burn-off. Since the ZTC was completely combusted leaving no residual material behind indicates that the silica had been completely dissolved by the HF treatment (Musyoka et al., 2015).

5.1.3 Surface area and Hydrogen adsorption

The BET surface area of the porous zeolite 13X and ZTC materials is a vital characteristic and is obtained from the nitrogen isotherm presented in Figure 5.3. The hydrogen adsorption isotherm for zeolite and ZTC was determined via the gravimetric method detailed in section 3.5.4 and the results of hydrogen adsorption capacity can be found in Figure 5.4. A summary of the physical characteristics and hydrogen adsorption capacity for zeolite and ZTC is found in Table 5.1.
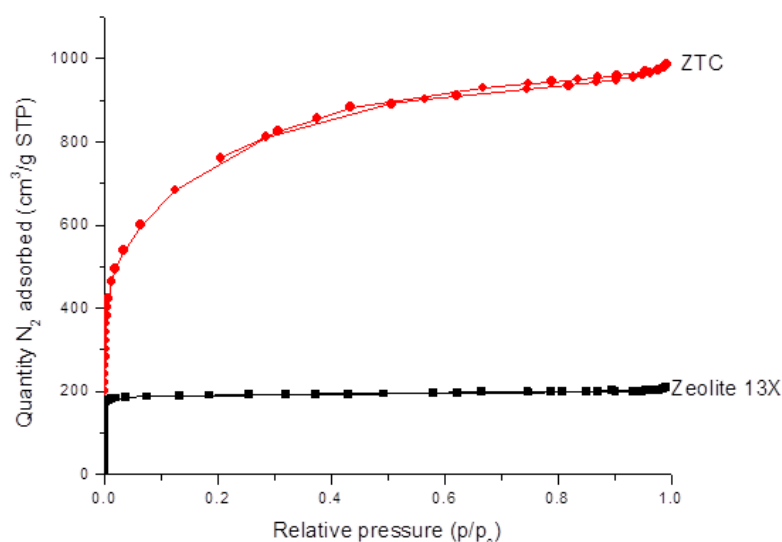
Figure 5.3: Nitrogen sorption isotherms for zeolite 13X and its ZTC derivative measured at 77 K and 1 bar.
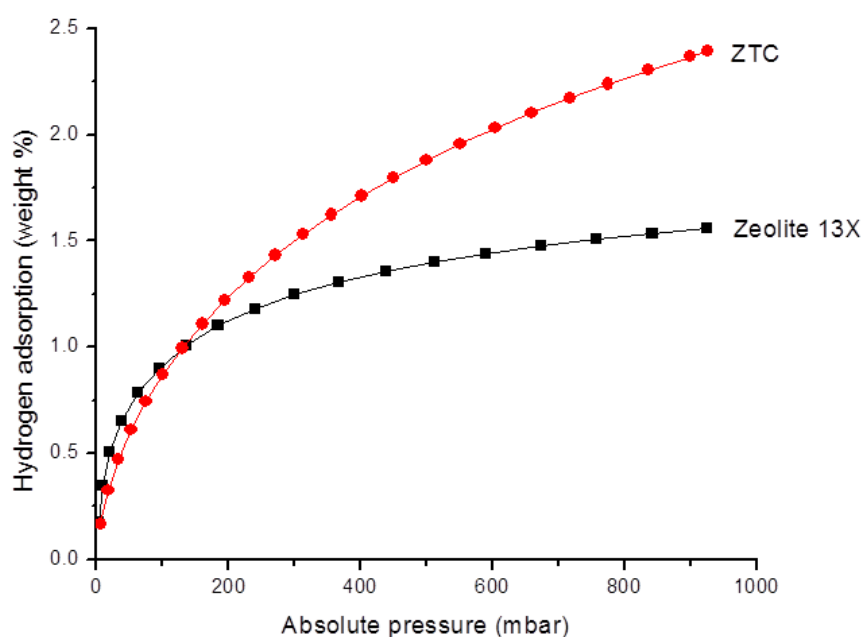
Figure 5.4: Hydrogen adsorption isotherm for zeolite 13X and its ZTC derivative measured at 77 K and 1 bar.

Table 5.1: Physical properties and hydrogen adsorption capacities of zeolite 13X and ZTC porous powdered materials.

Sample	*Particle Size[a]*	*S_{BET} (m^2/g)[b]*	*Pore volume (cm^3/g)[c]*	*H_2 adsorption ($wt\%$)[d]*
Zeolite 13X	2 μm	730	0.35	1.6
ZTC	2 μm	2717	1.44	2.4

[a] Estimated from SEM images. [b] BET surface area. [c] From H-K analysis. [d] Adsorbed at 77K and 1 bar.

The S-shaped N_2 sorption isotherms for zeolites and ZTCs (Figure 5.3) are of Type I classification which depicts well-defined micropores because the nitrogen fills most of the pores at approximately 0.05 P/P_0 and thereafter reached a plateau (Thommes et al., 2015) (Lowell et al., 2012). The BET surface area for zeolite 13X and ZTC was 730 and 2717 m^2/g respectively. A pore volume of 0.35 and 1.44 cm^3/g was observed for zeolite 13X and ZTC

respectively. It is evident from the higher surface area and pore volume of the ZTC that the structural ordering of the zeolite framework was effective in the templation process when compared to other carbons (Musyoka et al., 2015). The trend of physical properties improving after the carbonisation of the zeolitic template was also observed for the hydrogen adsorption capacity seen in Figure 5.4 which had increased by 67% after the silica was removed (detemplation). These trends were corroborated by previous studies (Masika & Mokaya, 2013; Alam & Mokaya, 2011). From Figure 5.4 it is also observed that the hydrogen adsorption isotherm did not reach a plateau implying that ZTC pores were not saturated with hydrogen gas. This observation suggests that the hydrogen adsorption capacity will increase at higher pressures (Musyoka et al., 2015).

5.2 Zr and Cr based MOFs

As a result of the attractive hydrogen adsorption properties of MOFs, great emphasis has been placed on determining MOFs for hydrogen storage over recent years, however, MOFs developed initially (Zn based MOFs) presented moisture instability (Kaye et al., 2007; Nguyen & Cohen, 2010). This moisture instability has been a limiting factor in the synthesis and processing of MOFs for hydrogen storage, this prompted the development of more stable MOFs such as Zr and Cr MOFs which were selected for this study (Cavka et al., 2008; Ferey et al., 2005).

It is important to note that synthesis conditions play a vital role in determining the topology and physical properties of the Zr and Cr based MOFs therefore synthetic conditions were optimised previously by the HySA infrastructure research group and can be found in Ren et al., (2014a) and Ren et al., (2014b) respectively. Consequently, this section will only present the analysis of the MOFs synthesised under the optimised conditions as specified in section 3.4.3.2.

5.2.1 Morphological and Phase Crystallinity analysis

Scanning Electron Microscopy and powder X-ray analysis techniques were employed to assess the morphology and the phase crystallinity of the Zr and Cr based MOFs and the results can be found in Figure 5.5 and 5.8 respectively.
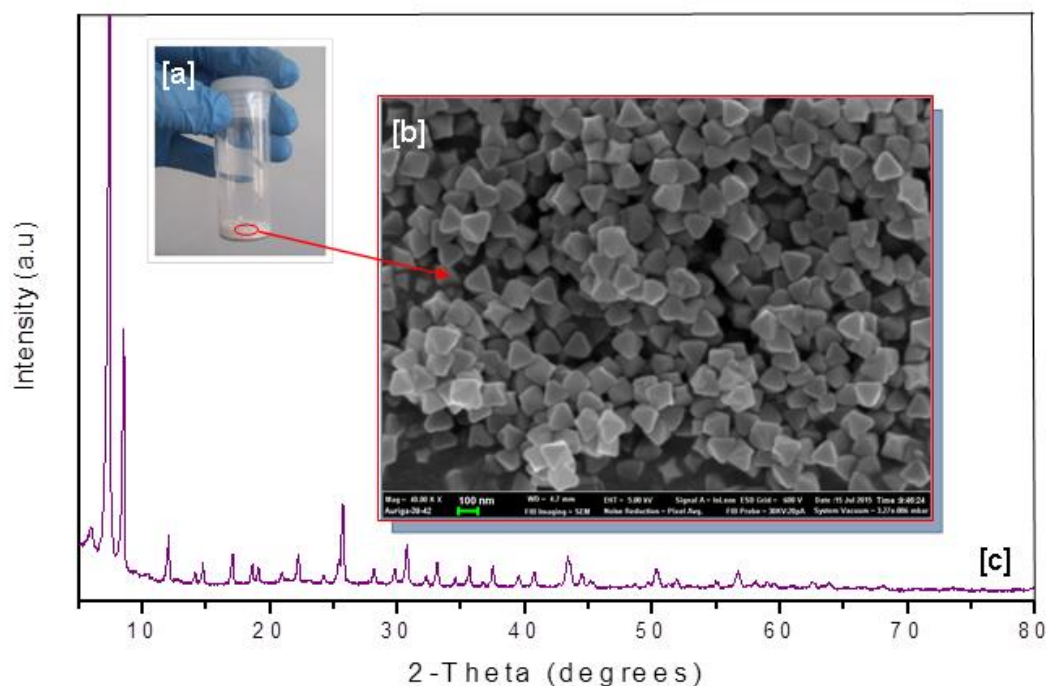
Figure 5.5: Zr MOF powder; Picture (a) SEM micrograph (b) PXRD spectrum (c).

The PXRD pattern (Figure 5.5c) illustrate peaks at 2Θ= 7.4, 8.5, 14.1, 14.7, 17, 18.6 and 19.1º that are typical of the simulated PXRD pattern of Zr MOF which can be found in Zhao et al., (2013) thus confirming the synthesis of Zr MOF. Since the peak at 2Θ = 7.4º has a relatively higher intensity than the peak at 2Θ = 8.5º and both peaks are sharp, it can be deduced that the phase crystallinity of close packed cubic Zr MOF is high (Hafizovic et al., 2007). Evidence of crystalline Zr MOF was corroborated by the SEM micrographs (Figure 5.5b), which illustrates well-defined 100 nm octahedral shaped crystals. The modulated synthesis route utilised for Zr MOF is the reason for the highly crystalline Zr MOFs during which the $Zr_6O_4(OH)_4(O_2C)_{12}$ secondary building units are generated when there is sufficient water and oxygen for the $ZrCl_4$ (precursor) hydrolysis. The reaction of N,N-dimethylformamide (DMF) with water is illustrated in Figure 5.6 below (Ren et al., 2014; Schaate et al., 2011; Wißmann et al, 2012).
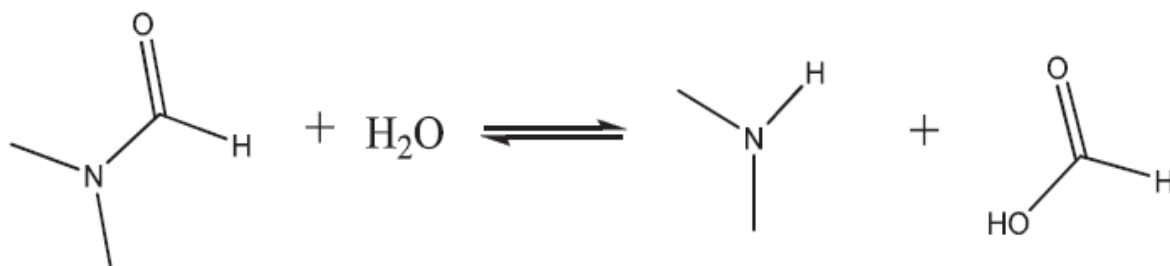
Figure 5.6: The hydration and decomposition reaction of DMF (Ren et al., 2014).

The equilibrium of the hydration and decomposition reaction in Figure 5.6 shifts to the left upon the addition of formic acid (modulator) resulting in the availability of excess water for the $ZrCl_4$ hydrolysis (Ren et al., 2014).

Since HF was not ideal for the synthesis of Cr MOF because it is highly toxic and corrosive, alternative synthetic routes which involved the modulated solvothermal method utilising formic acid (the modulator) was followed to synthesise Cr MOF (Zhao et al., 2015; Ren et al., 2014; Zhang et al., 2011; Zhao et al., 2011). The XRD pattern and SEM micrographs for Cr MOF can be found in Figure 5.7.
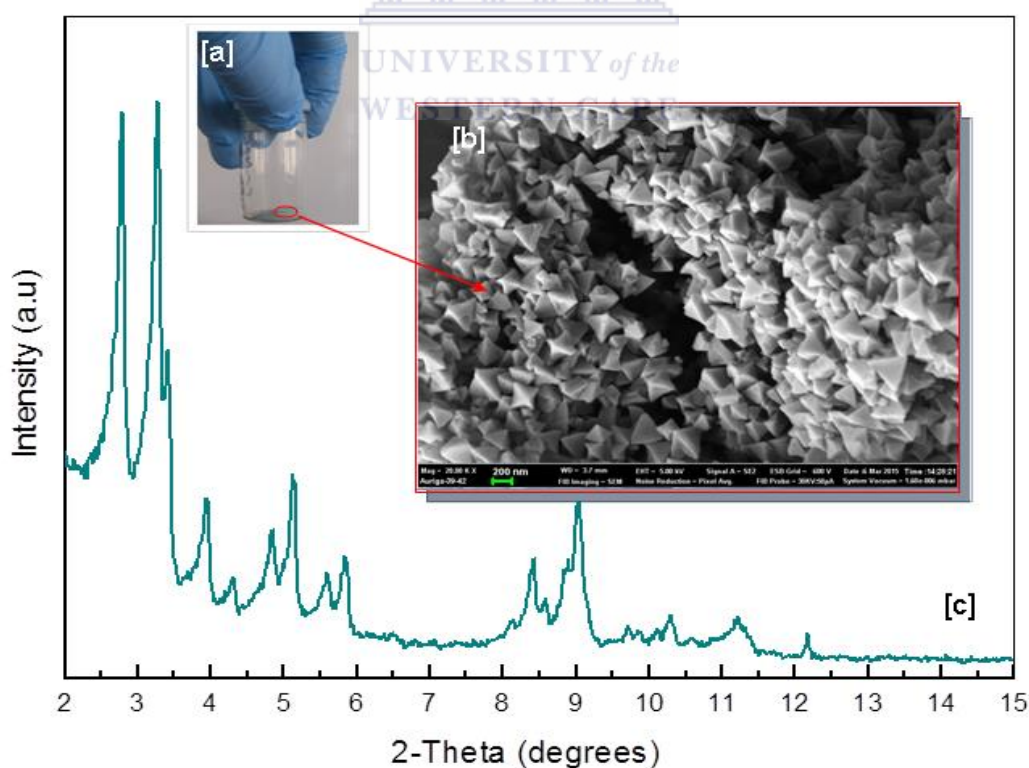
Figure 5.7: Cr MOF powder; Picture (a) SEM micrograph (b) PXRD spectrum (c).

The synthesis of Cr MOF was confirmed by the PXRD pattern illustrated in Figure 5.7c which contained peaks at 2Θ = 2.8, 3.3, 3.9, 4.3, 4.8, 5.6,5.8, 8.4, 9.0 and 10.3º that are typical of the simulated PXRD pattern found in (Yang &Yan, 2011). The Cr MOF crystals were crystalline due to the modulator which was confirmed by the SEM micrograph (Figure 5.7b) showing small but defined 200 nm octahedral agglomerated crystals resulting in broad peaks in the PXRD pattern. The synthesised Cr MOF was greenish is colour as shown in Figure 5.7a.

5.2.2 Thermal analysis

Figure 5.8 presents the thermal gravimetric plots of Zr and Cr based MOFs that was utilised to assess the thermal stability and decomposition of the MOF crystals.
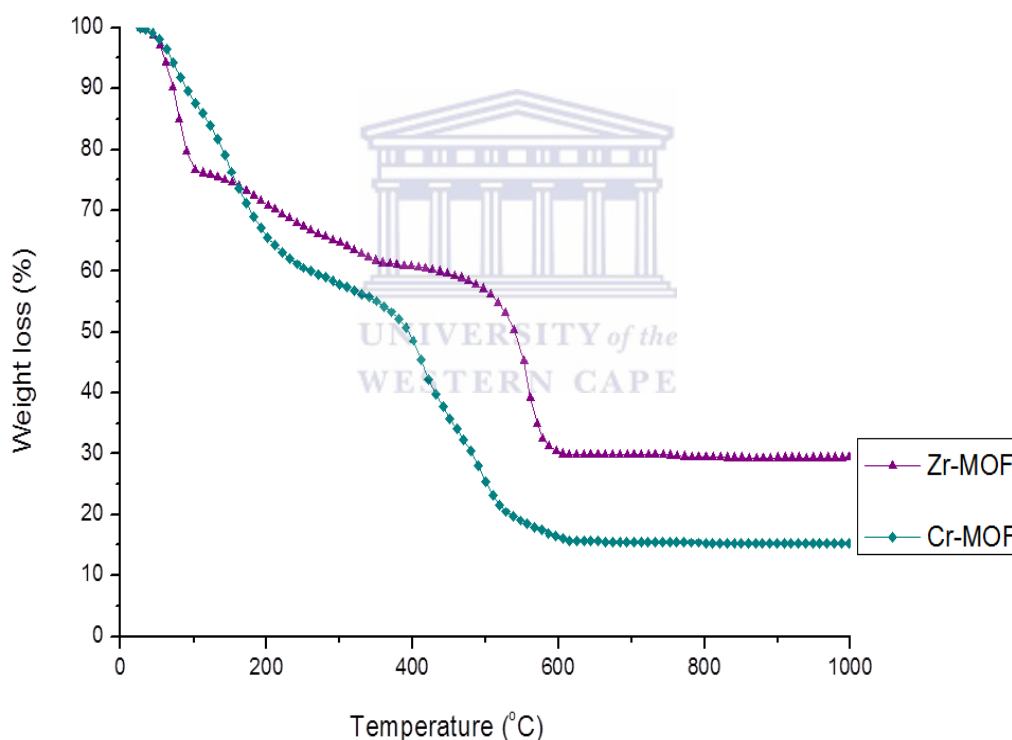
Figure 5.8: TGA plots of Zr and Cr based MOF powders.

From Figure 5.8, the Zr MOF was observed to have a weight loss of approximately 25% at about 100 ºC which can be attributed to the loss of adsorbed water molecules, thereafter there was gradual decomposition happening between 100 and 390 ºC due to loss of residual DMF molecules (Ren et al., 2014). From approximately 400-600 ºC a drastic weight loss of 30% was observed rendering Zr MOF thermally stable up to about 500 ºC. Above 600 ºC the

organic ligand is broken down and Zr MOF is decomposed to ZrO_2 (Zhao et al., 2013). The TGA plot for Cr MOF shows a gradual decrease of approximately 35% below 200 ºC due to water and DMF molecules, followed by a drastic loss in weight which resulted from the decomposition of the linker molecule that occurred between 400-600 ºC making Cr MOF nanocrystals stable up to 350 ºC (Solomon & Banerjee, 2006; Ren et al., 2014).

5.2.3 Surface area and Hydrogen adsorption

The BET surface area was assessed with the aid of nitrogen isotherms found in Figures 5.9 a and c, the hydrogen adsorption isotherms are presented in Figures 5.9 b and d for MOF nanocrystals. A summary of the resulting physical properties and hydrogen adsorption capacities for the MOF nanocrystals are found in Table 5.2.
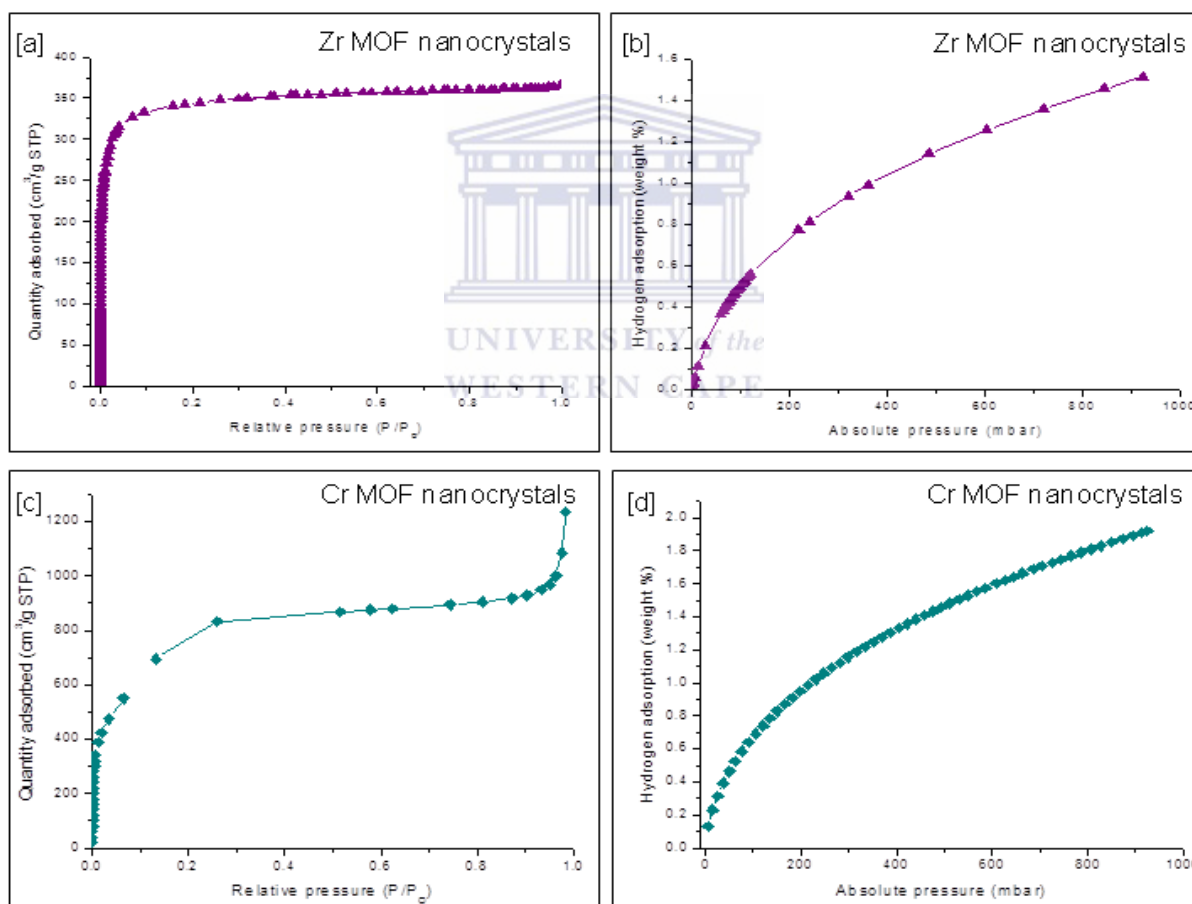
Figure 5.9: Nitrogen sorption isotherms (a and c) and hydrogen adsorption isotherms (b and d) for Zr and Cr MOF nanocrystals measured at 77 K and 1bar.

Table 5.2: Physical properties and H_2 uptake capacities of the MOF nanocrystals

Sample	Particle Size[a]	S_{BET} (m^2/g)[b]	Pore volume (cm^3/g)[c]	H_2 adsorption $(wt\%)$[d]
Zr-MOF	100 nm	1186	0.56	1.5
Cr-MOF	200 nm	2618	1.29	1.9

[a] Estimated from SEM images. [b] BET surface area. [c] From H-K analysis. [d] Adsorbed at 77K and 1 bar.

The nitrogen isotherm for Zr MOF nanocrystals was Type I (Figure 5.9a) indicating the presence of micropores and the Zr MOF possessed a BET surface area of 1186 cm^3/g with a micropore volume of 0.56 cm^3/g. The excellent interaction between the nitrogen gas molecules and the Zr MOF micropores is the reason for the steep region of the curve at relative pressures lower than 0.1 p/p$_o$ seen in Figure 5.10a (Thommes et al., 2015). Cr MOF nanocrystals nitrogen isotherm was Type IV in nature indicative of some presence of mesopores (Thommes et al., 2015). The BET surface area and pore volume for Cr MOF nanocrystals was 2618 m^2/g and 1.29 cm^3/g respectively. The hydrogen adsorption was 1.5 and 1.9 wt% for Zr and Cr MOF respectively at 77 K and 1 bar, however, there was no plateaus present for both MOFs indicative of incomplete saturation. Therefore at higher pressures the hydrogen storage capacity can be expected to increase.

Chapter summary

The morphological phase crystallinity, thermal, surface area and hydrogen adsorption results of the pristine porous powdered materials that are zeolite 13X, ZTC and MOFs were discussed in this chapter.

Due to the many advantages zeolite 13X presents such as high thermal stability and good pore size distribution, commercial zeolite 13X was selected for the study. Furthermore zeolite 13X is excellent for the synthesis of templated carbons (referred to as ZTC) via the liquid impregnation coupled with CVD approach followed by silica removal. Analysis of the morphology and phase crystallinity illustrated that preparing the carbon inverse of the zeolite

13X was successful since the pore ordering structure of the zeolite was retained for the ZTC. However, ZTC was more armorphic in nature illustrated by phase crystallinity analysis. This was due to the presence of the peak at 2Θ=7º on the PXRD spectrum for the ZTC synthesised in this study and the absence of the typical peaks ascribed to graphitic and turbostatic carbon reported in literature. TGA illustrated that zeolite 13X was thermally stable at temperatures up to about 1000 ºC; however, its ZTC counterpart was only stable up to   550 ºC. The BET surface area was assessed with the aid of nitrogen sorption isotherms, both zeolite 13X and ZTC isotherms were classified as a Type I isotherm indicating the presence of micropores and with reduced external surfaces. The BET surface area for zeolite 13X and ZTC was 730 m^2/g and 2717 m^2/g respectively. The pore volume was also found to be   0.35 cm^3/g and 1.44 cm^3/g respectively. The excellent interaction between the nitrogen gas molecules and the ZTC micropores is the reason for the precipitous section of the curve at relative pressures lower than 0.1 p/p_o. The inverse carbon microporous material prepared with the zeolites illustrated an increase of hydrogen adsorption from 1.6 wt% (for zeolite) to 2.4 wt% (for ZTC).

With increasing development of moisture and thermal stability and due to their attractive hydrogen adsorption properties, Zr and Cr MOFs were selected for the study. A comparison of the as-synthesised MOFs and their simulated PXRD patterns confirmed the synthesis of Zr and Cr MOFs. The synthesised MOFs were defined, crystalline octahedral crystals due to the modulated synthetic route undertaken. Thermal analysis illustrated Zr and Cr MOF was stable up to 500 and 350 ºC respectively. Zr MOF had a BET surface area and pore volume of 1186 cm^3/g and 0.56 cm^3/g respectively. The BET surface area and pore volume for Cr MOF was 2618 m^2/g and 1.29 cm^3/g respectively. The hydrogen adsorption capacity was 1.5 and 1.9 wt% for Zr and Cr MOF respectively at 77 K and 1 bar. The hydrogen adsorption isotherms of ZTC and both MOFs with the exception of zeolite 13X illustrated incomplete saturation since no plateaus were present indicating that the hydrogen storage capacity should increase with higher pressures.

The next chapter will present and discuss the results obtained for the electrospun composite PAN fibres containing the porous powdered materials.

Chapter Six

Analysis of the Electrospun Composite Fibres

Previous chapters presented the analysis of the individual constituents of the composite fibres, namely pristine electrospun PAN fibres and porous powdered materials that adsorbed hydrogen in chapter four and five respectively. The results from the analysis of the zeolite, ZTC and MOF electrospun composite nanofibres which are the main focus of the study will be presented and discussed in this chapter.

The composite electrospun fibres were synthesised by first identifying the loading percentage range of the porous powdered materials by incorporating varying masses of the porous powders into the PAN solution resulting in a polymeric blend. Since the addition of the porous powders resulted in a more viscous polymeric, the loading percentage was incremented until the blend was too viscous to be electrospun. A full description of the synthesis and electrospinning conditions for the composite fibres can be found in section 3.4.4.

It is important to note that the hydrogen adsorption capacity and surface area measurements for the composite fibres was determined by the amount of porous powdered materials incorporated into fibres because pristine PAN nanofibers have a negligible hydrogen adsorption capacity and surface area (presented in section 4.3.3). The composite fibres underwent degassing which involves the subjecting composite fibres to thermal treatment at 200 ℃ under 10^{-7} bar vacuum for six hours (reasons for which are presented in section 4.3). Degassing of the composite fibres enables the removal of residual solvent which affects their gravimetric surface area and hydrogen adsorption capacity.

6.1 Zeolite-PAN composite fibres

Zeolite-PAN composite fibres were synthesised by incorporating a loading weight percent range of 5-40 wt% of commercial zeolite 13X into the PAN solution which resulted in a zeolitic-PAN blend that was then electrospun. The experimental protocol for the synthesis of zeolite-PAN composite fibres is presented in section 3.4.4.

6.1.1 Morphological and Phase Crystallinity analysis

The loading weight percentage range for the zeolite-PAN composite fibres was 5, 10, 20 and 40 wt% which can be seen in the SEM micrographs in Figure 6.1.
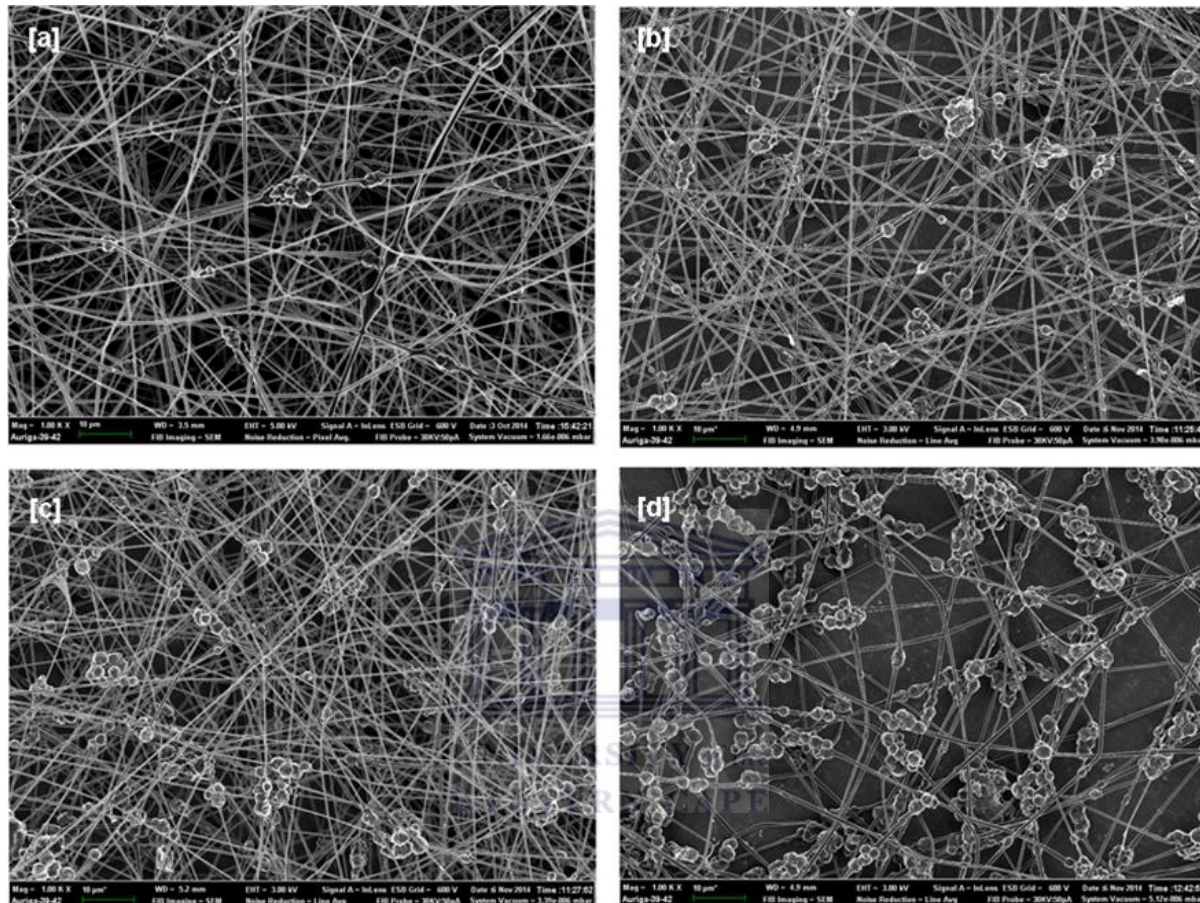
Figure 6.1: SEM micrographs of 5 (a), 10 (b), 20 (c) and 40 wt% (d) zeolite-PAN composite fibres

From Figure 6.1, it is evident that the zeolite 13X crystals are too big to be incorporated into the PAN nanofibers therefore it can be said that the zeolite 13X crystals are adhered to the PAN nanofibers. As the loading percentage of zeolite 13X is increased a more uniform distribution of zeolite 13X crystals on the PAN fibres can be observed in Figure 6.1d for the 40 wt% loading. The loading weight percent greater than 40 wt% was not possible because the polymeric blend had become too viscous to electrospin. After identifying 40 wt% to be the highest possible loading for the zeolite-PAN composite fibres, vacuum degassing was conducted to improve the accessibility of the gas into the micropores of the zeolite. The effect of vacuum degassing can be seen on the SEM micrographs of the zeolite-PAN composite fibres pre- and post-vacuum degassing presented in Figure 6.2a and b respectively. X-ray

diffraction analysis technique was employed to assess the phase crystallinity of the zeolite-PAN composite fibre and is presented in Figure 6.2c.
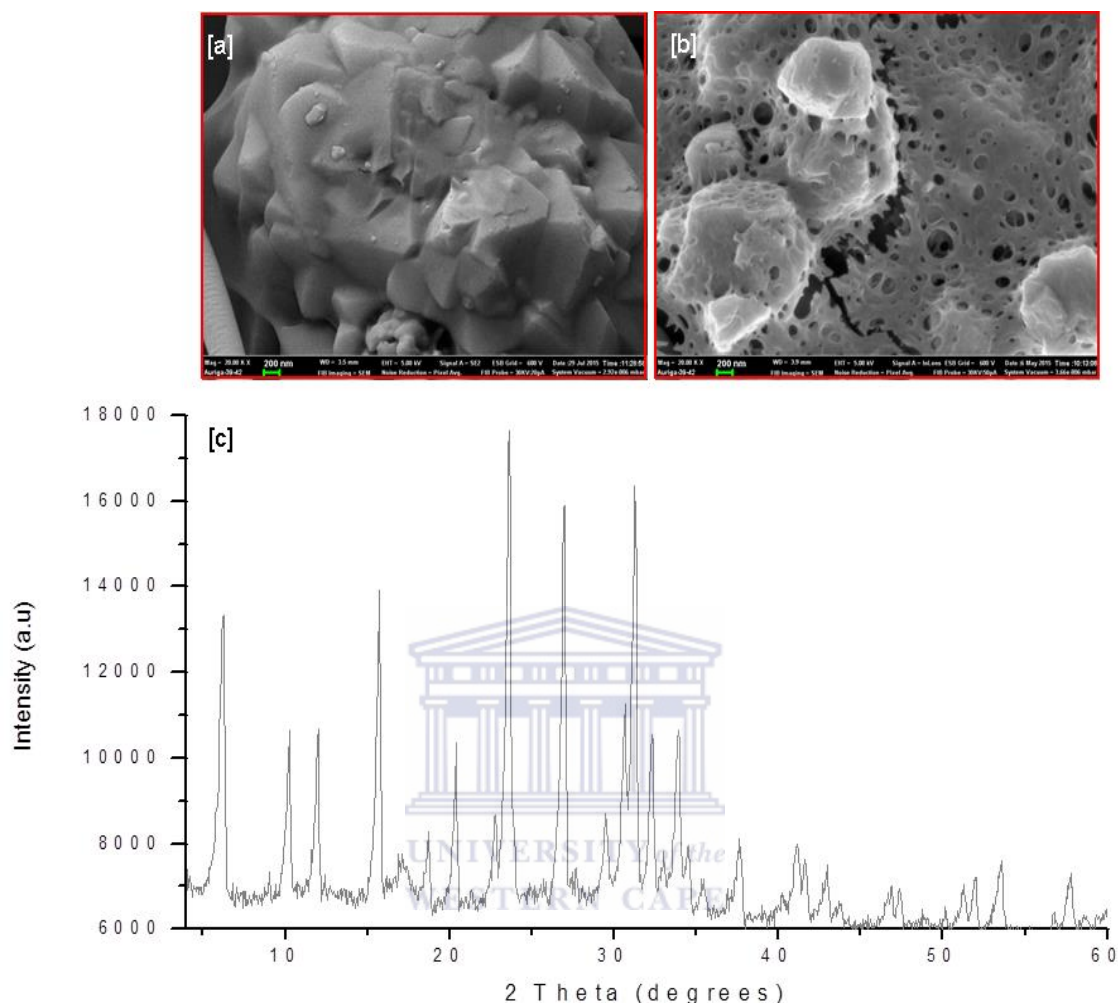
Figure 6.2: SEM micrographs of zeolite-PAN composite fibres before (a) and after (b) vacuum degassing with the PXRD pattern (c).

From Figure 6.2a and b it can be observed that the degassing process has created pores on the PAN fibres adhering the zeolite 13X crystals, thus allowing the nitrogen and hydrogen gas to access the micropores of the zeolite 13X crystals. It can also be seen that the morphology of the zeolite 13X crystals was conserved during the electrospinning process. Evidence of structural conservation of zeolites in the electrospun composite can be illustrated by the PXRD pattern shown Figure 6.2c. The low signal-to-noise of the zeolite-PAN fibres is due to the influence of the incorporation of zeolites on to the fibres. Since the optimised loading of zeolite 13X was 40 wt% into the PAN solution, therefore 40 wt% zeolite-PAN composite fibres is the focus for the thermal, surface area and hydrogen adsorption analysis which will be presented and discussed in this section.

6.1.2 Thermal analysis

Thermal gravimetric analysis of zeolite 13X, thermal treated PAN fibres and zeolite-PAN composite fibres can be seen from the TGA plot presented in Figure 6.3.
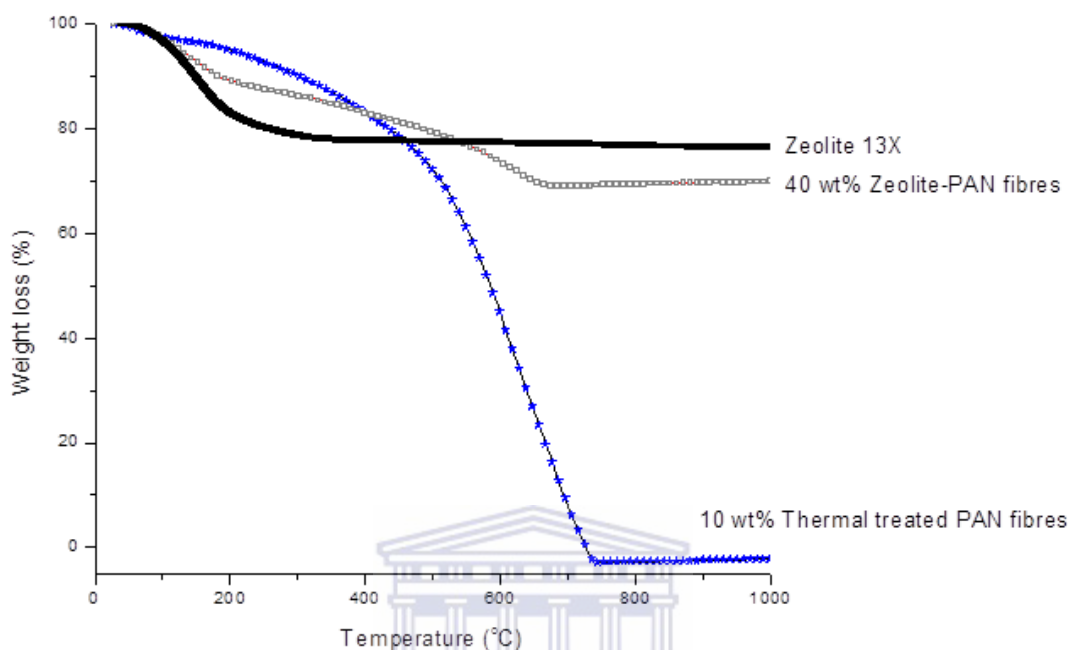
Figure 6.3: TGA plot of zeolite 13X, thermal treated (degassed) PAN fibres and zeolite-PAN composite fibres.

A 10% weight loss can be seen around 100 ºC for the zeolite-PAN composite fibres which can be attributed to the loss of water molecules adsorbed. Thereafter a weight loss of approximately 20 wt% was seen between 180–680 ºC due to the decomposition of the PAN polymeric fibres. Thermal analysis of the thermally treated (degassed) PAN fibres (presented in section 4.3.2) showed it was stable up to 400 ºC. After 720 ºC no further loss in weight occurred, this can be attributed to the presence of the zeolite 13X because zeolites have a high thermal stability up to 1000 ºC as explained in section 5.1.2.

6.1.3 Surface area and Hydrogen adsorption

The BET surface area for the zeolite 13X crystals, thermal treated PAN fibres and zeolite-PAN composite fibres was assessed with the aid of nitrogen isotherms presented in Figure 6.4a and its hydrogen adsorption capacity (Figure 6.4b) were both measured at 77 K and 1 bar.
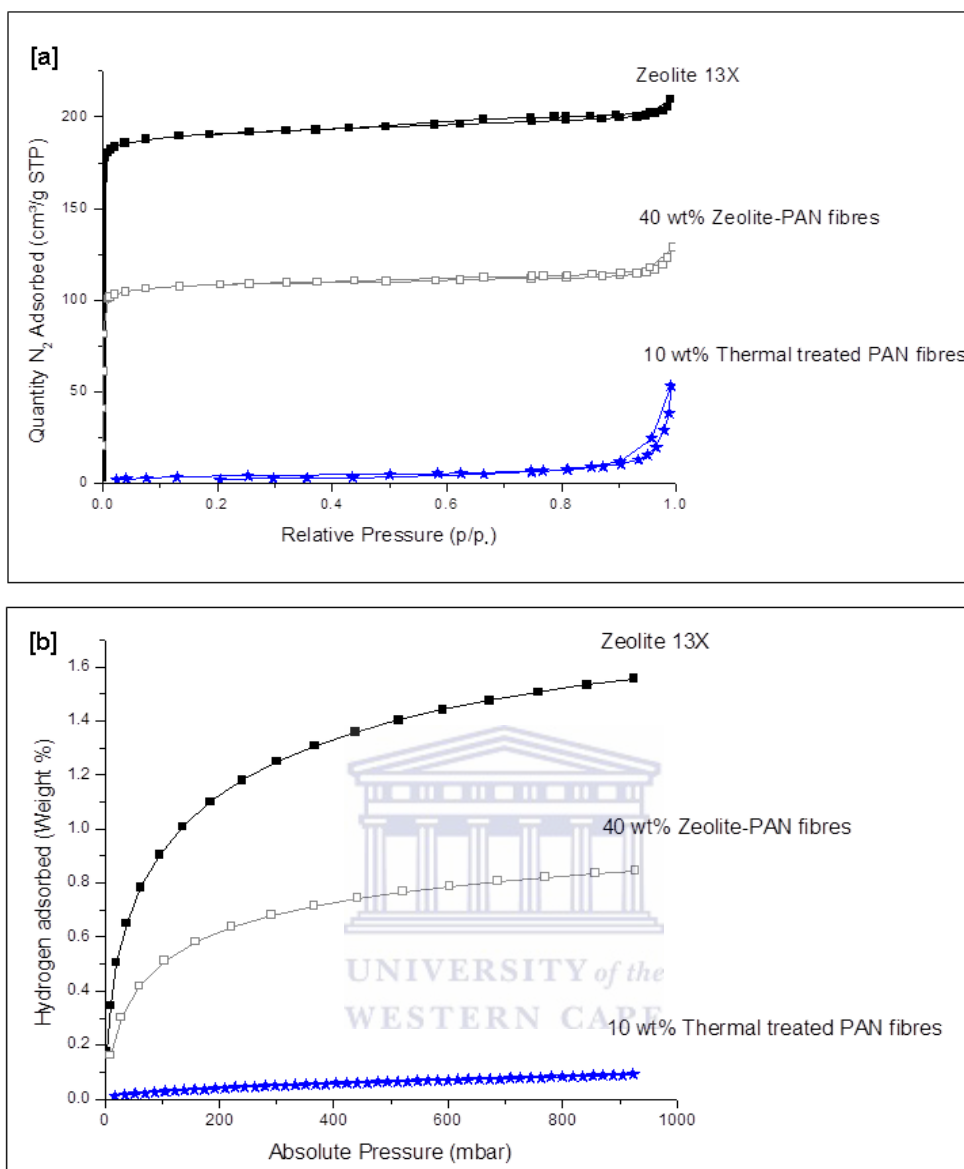
Figure 6.4: Nitrogen isotherm (a) and hydrogen adsorption isotherm (b) of zeolite 13X, thermal treated (degassed) PAN fibres and zeolite-PAN composite fibres measured at 77 K and 1 bar.

The S-shaped N_2 adsorption isotherm is of a Type 1V classification which depicts well-defined micropores because the nitrogen fills most of the pores at approximately 0.05 P/P_0 and thereafter reached a plateau. The BET surface area of the 40 wt% zeolite-PAN composite fibres (440 $m^2 \cdot g^{-1}$) was lower than that of the pristine zeolite 13X (730 $m^2 \cdot g^{-1}$). This observation could be attributed to the limited amount of zeolite adhered by the PAN nanofibres since loading percentage greater than 40 wt% resulted in the viscous polymeric blend being unable to be electrospun. Furthermore, Ostermann et al., (2011) reported the decrease in surface area could be due to the layer of polymer formed over the zeolite

obstructing the nitrogen gas from adsorbing onto the pore walls, even though porosity was evident (in section 6.1.1) from the vacuum degassing of the composite fibres used in this study. Since surface area measurements can be correlated to hydrogen measurements (Weitkamp et al., 1995), a comparison of the H_2 isotherms (Figure 5.4b) of the zeolite 13X crystals on their own indicates that the hydrogen capacity for the 40 wt% zeolite-PAN composite fibres (0.85 wt%) is over 50% of that of the pristine zeolite13X crystals (1.6 wt%).

6.2 ZTC-PAN composite fibres

Since ZTC is a result of the carbon infilling of zeolite pores it would be expected that the weight loading percent range would be similar to that of zeolites. However, the loading weight percent range of ZTC was 7.5, 10 and 12.5 wt%. The density of carbon based ZTC is 1.5 Kg/m^3 (Musyoka et al., 2015) making it less dense than silica based zeolite with a density of 1.9 Kg/m^3 (Masika & Mokaya, 2013). This section will present the discussed results for 7.5, 10 and 12.5 wt% ZTC-PAN composite fibres.

6.2.1 Morphological analysis

The SEM micrographs of 7.5, 10 and 12.5 wt% loading of ZTC into ZTC-PAN composite fibres are illustrated in Figure 6.5.
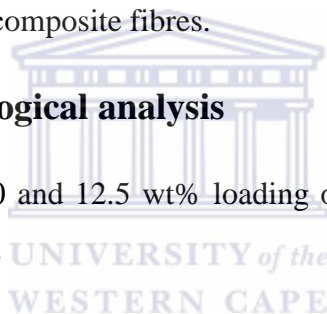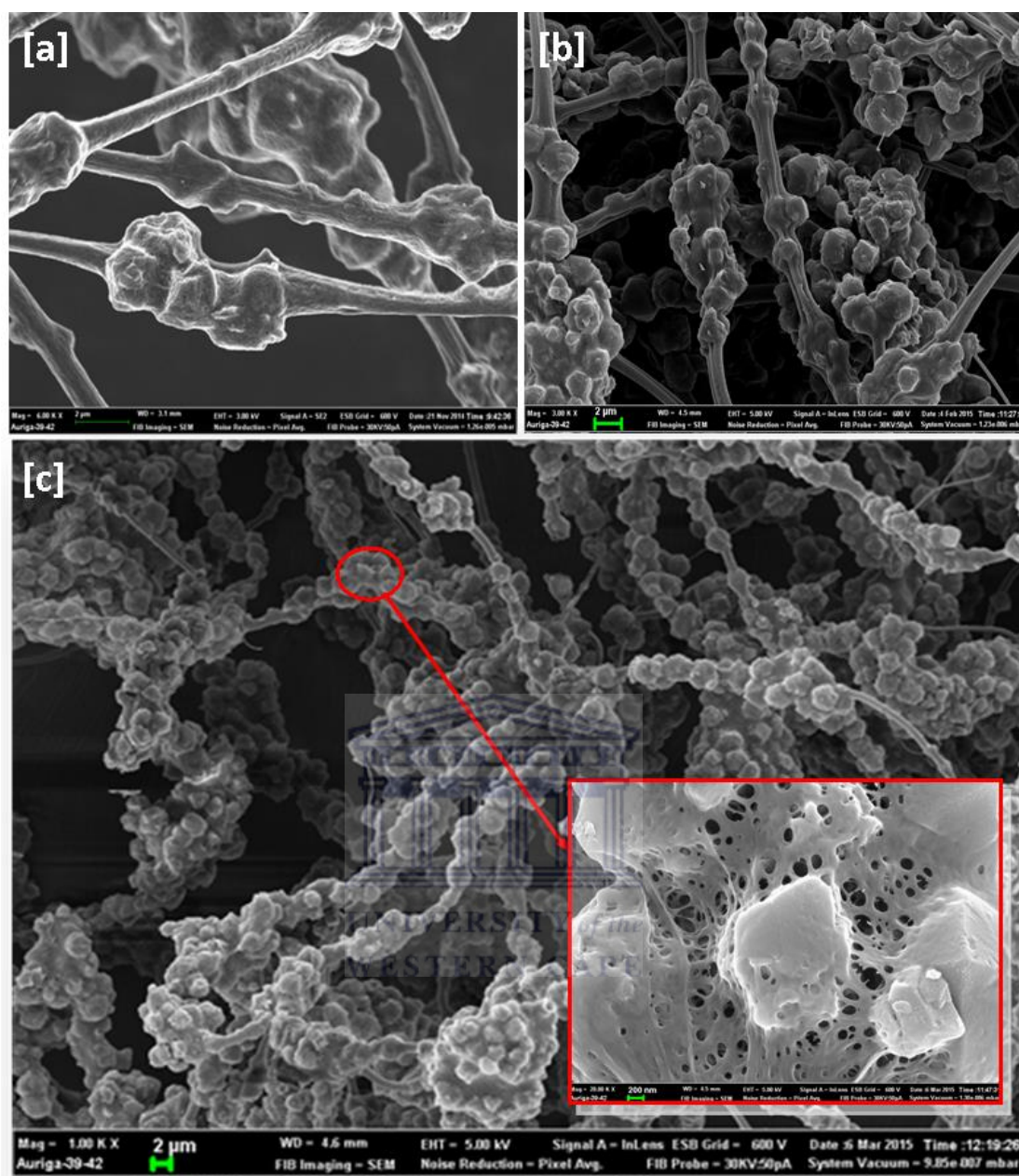
Figure 6.5: SEM micrographs of 7.5 (a), 10 (b) and 12.5 wt% (c) loadings of ZTC into the ZTC-PAN composite fibres.

Comparison of the SEM micrographs of the pristine ZTC powders (Figure 5.1b) with that of the ZTC-PAN composite fibres (Figure 6.5), it is evident that the ZTC had retained the octahedral pyramidal shape after being electrospun. Figure 6.5 also shows that ZTC had adhered well to the PAN fibres. It was also noted that as the loading weight percent of the ZTC was increased, the ZTC-PAN blend became more viscous resulting in coagulated ZTC composite fibres. Therefore a higher weight percent loading (greater than 12.5 wt%) would make the ZTC-PAN polymeric blend too thick to be electrospun. Thus rendering 12.5 wt%

loading of ZTC as the optimised loading weight percentage of ZTC into the polymeric blend that was electrospun resulting in ZTC-PAN composite fibres was characterised further in the study.

6.2.2 Thermal analysis

Thermal gravimetric analysis for the ZTC powders, thermal treated (degassed) PAN fibres and 12.5 wt% ZTC-PAN composite fibres is presented in Figure 6.6. The experimental procedure is found in section 3.5.3.
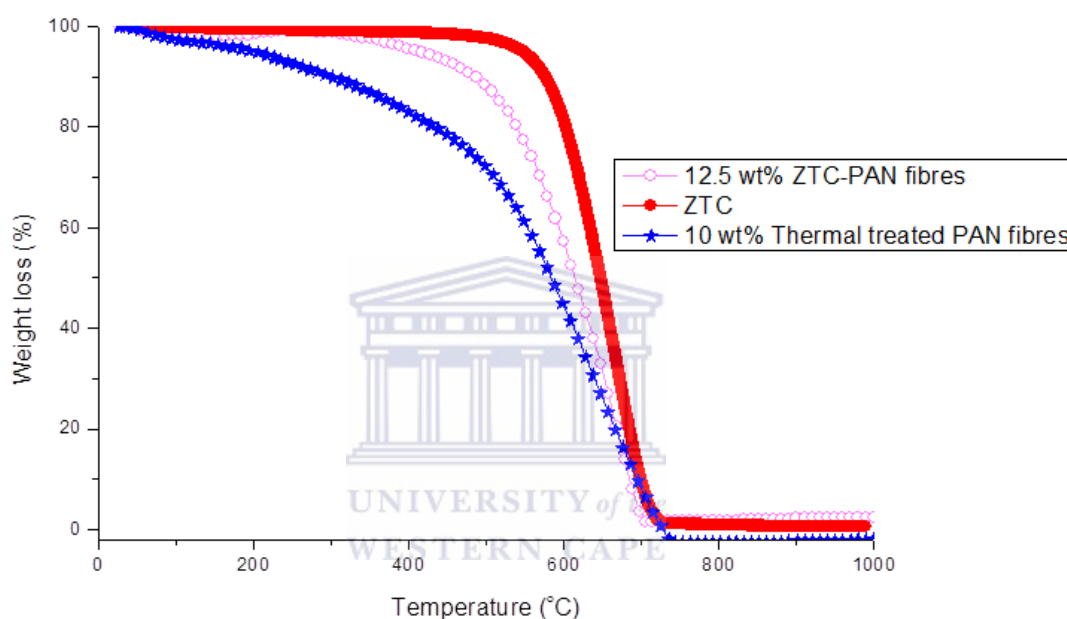
Figure 6.6: TGA plot for the ZTC powders, thermal treated (degassed) PAN fibres and 12.5 wt% ZTC-PAN composite fibres.

The TGA plot (Figure 6.6) shows that the 12.5 wt% ZTC-PAN composite fibres were stable up to about 500 ºC, after which a gradual weight loss was observed until its complete combustion by 700 ºC. It was observed that the TGA plots for the thermally treated (degassed) PAN fibres and the pristine ZTC were similar in shape when compared to the ZTC-PAN composite fibres. However, thermally treated (degassed) PAN fibres and pristine ZTC powders were stable up to 400 and 550 ºC respectively. The gradual weight loss observed between 0-550 ºC for the ZTC-PAN composite fibres can be due to the constituents of the composite fibres being burnt off followed by the complete combustion at approximately 700 ºC due to the carbonisation process. The ZTC-PAN composite fibres were

less thermally stable compared to the ZTC powders and this could be ascribed to the PAN which was less thermally stable.

6.2.3 Surface area and hydrogen adsorption analysis

Since it was hypothesised that the hydrogen adsorption capacity would increase as the amount of porous powdered materials adhered by the PAN nanofibres increased, evidence to support or reject this hypothesis is presented in this section. Figure 6.7a presents the nitrogen sorption isotherms for ZTC powder, thermally treated (degassed) PAN fibres and 7.5, 10 and 12.5 wt% loadings of ZTC into ZTC-PAN composite fibres and hydrogen adsorption isotherms presented in Figure 6.7b. The experimental protocol is detailed in section 3.5.4.
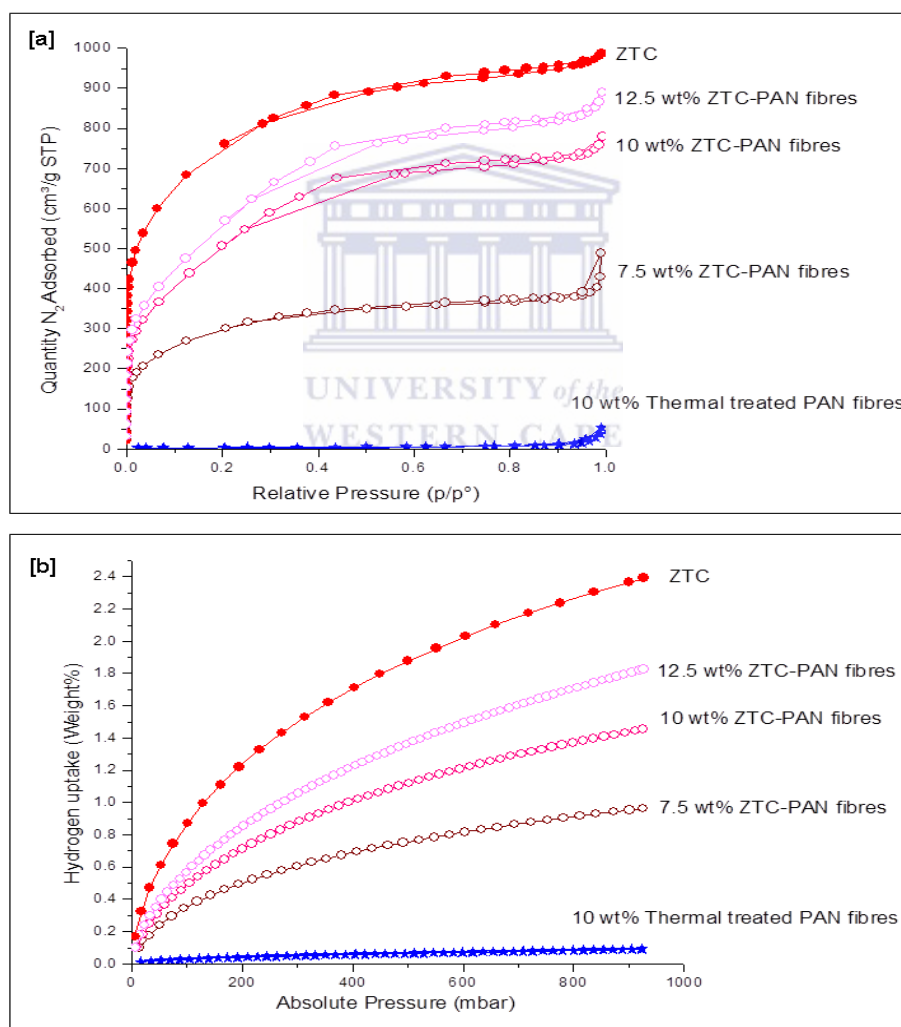

Figure 6.7: Nitrogen isotherm (a) and hydrogen adsorption isotherm (b) for ZTC powders, thermal treated (degassed) PAN fibres and 7.5, 10 and 12.5 wt% loadings of ZTC into ZTC-PAN composite fibres measured at 77 K and 1 bar.

According to the shape of the ZTC-PAN nitrogen isotherms presented in Figure 6.7, they can be classified as type IV isotherms which are attributed to the presence of both micropores and mesopores due to the hysteresis loop. PAN was not classified since the surface area was too low. Since PAN and powder ZTC had a surface area of 13 and 2717 m^2/g respectively, the enhanced surface area observed for the ZTC-PAN composite fibres can be attributed to the presence of ZTC in the composite. The trend observed correlated positively with the variation of the weight percent of the ZTC adhered by the PAN nanofibres and shows an increase in surface area of 1018, 1663 and 1787 m^2/g for 7.5, 10 and 12.5 wt% ZTC-PAN composite fibres respectively. This trend was also observed for the hydrogen adsorption capacities for the different loadings of ZTC into the ZTC-PAN fibres presented in Figure 6.7b. Therefore the hypothesis (section 1.4) that hydrogen adsorption would increase with increased amounts of porous powdered materials incorporated was accepted.

A reduction in surface area when compared to pristine ZTC powders was to be expected since the PAN would block nitrogen gas from accessing the pores of the ZTC. Moreover the surface area depended upon the percentage of ZTC powders incorporated into the PAN fibres. These observations were supported by findings presented by Ostermann et al., (2011). The reduction in surface area when comparing the pristine ZTC powders to 12.5 wt% ZTC-PAN composite fibres amounts to approximately 66%. Since the addition of ZTC greater than 12.5 wt% results in a viscous polymeric blend that was unable to be electrospun therefore higher surface areas and hydrogen adsorption capacities could not be achieved. It can be debated that if the concentration of the PAN is decreased the weight percentage of the ZTC could be increased. However, reducing the PAN concentration makes the composite fibres susceptible to the formation of beads which would lead to a decrease of the surface area. Furthermore, the concentration of the ZTC-PAN blend needs to possess sufficient molecular entanglement to ensure that electrospinning takes place (Cécile & Hsieh, 2009).

6.3 MOF-PAN composite fibres

A single loading of 20 wt% was used for both Zr and Cr MOFs to prepare the MOF-PAN composite fibres. The loading percentage of MOFs (20 wt%) achieved was due to the nanosize of the MOF crystals. The experimental protocol detailing the synthesis of the MOF-PAN composite fibres are presented in section 3.4.4.

6.3.1 Morphological and Phase Crystallinity analysis

The morphology and phase crystallinity of the 20 wt% Zr and Cr MOF-PAN composite fibres were assessed by SEM micrographs (a and c) and PXRD patterns (b and d) presented in Figure 6.8.
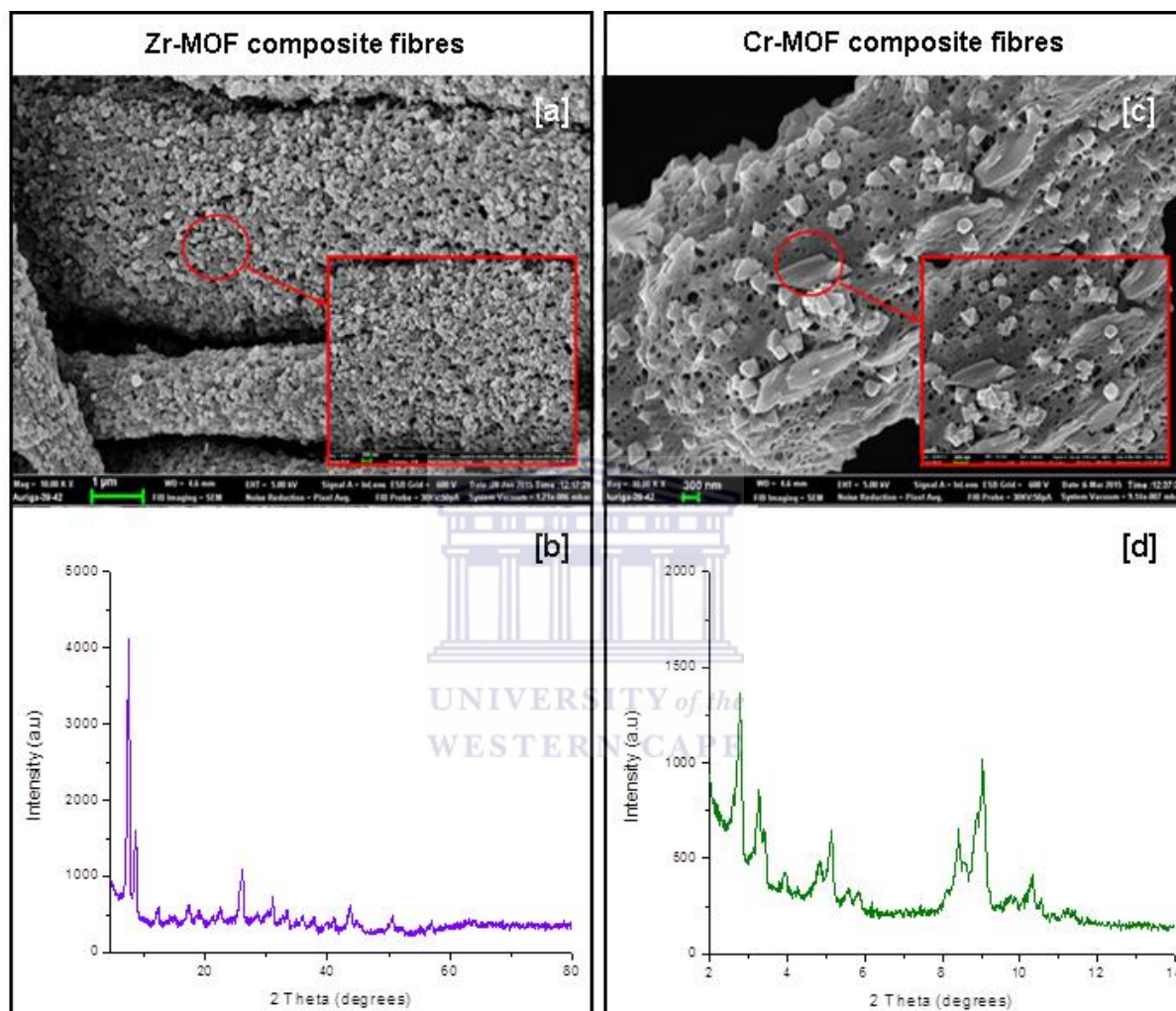
Figure 6.8: SEM micrographs (a and c) and PXRD patterns (b and d) for Zr and Cr MOF-PAN composite fibres.

From Figure 6.8 a and c, it can be observed from the examination of the SEM micrographs that the octahedral shape of the Zr- and Cr- based MOFs was conserved after electrospinning which can also be confirmed from the XRD patterns since the peaks of the powdered MOFs correspond to the peaks shown for the pristine MOF materials (see Figure 5.5 and 5.7 respectively). However, the signal to noise ratio seen in the PXRD peaks of the MOF composite fibres is due to the amorphous PAN (Ren et al., 2015). The Zr and Cr MOFs used

in the study was fully characterised in section 5.3, and particle sizes were 100-200 nm making them smaller and less dense than the zeolites or ZTC therefore these MOF nanocrystals were embedded into the PAN fibres whereas the zeolite and the ZTC particles were just adhered together by the PAN (see Figure 6.1 and 6.5 respectively).

6.3.2 Thermal analysis

Thermal analysis for both MOF composite fibres and their pristine constituents are presented in Figure 6.9. The experimental protocol for TGA is presented in section 3.5.3.
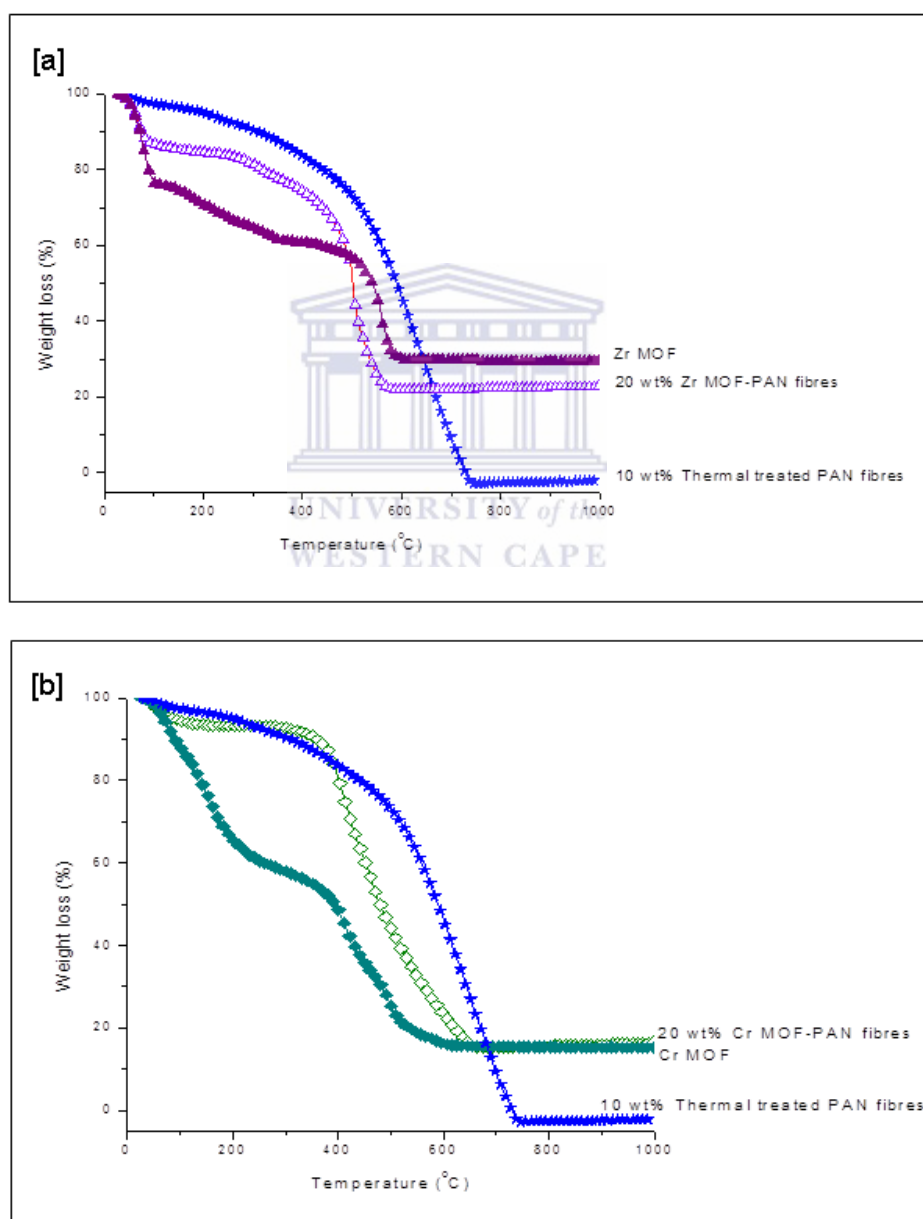
Figure 6.9: TGA plots for MOF powders, thermal treated (degassed) PAN fibres and the MOF composite fibres.

From the thermal gravimetric analysis of the MOF nanocrystals, thermal treated (degassed) PAN fibres and the MOF composite fibres presented in Figure 6.9, showed an initial weight loss of approximately 20% was observed for the MOF nanocrystals around 100 ℃. Whereas at the same temperature a 10% weight loss was observed for the MOF composite fibres. This weight loss is attributed to the loss of moisture as the MOF nanocrystals adsorbed more moisture than the MOF composite fibres because fewer MOF crystals per unit mass were used in the case of the composite. From Figure 6.9, Zr and Cr MOF composite fibres show a gradual weight loss up to 500 and 400 ℃ respectively, due to the nitrile groups in the PAN undergoing cyclisation (Ren et al., 2015). Thereafter a drastic weight loss followed by the partial or complete combustion of the composite fibres between 550 and 650 ℃ respectively. The Zr MOF composite fibres was stable up to 500 ℃ (Figure 6.9a) showing that the Zr MOF nanocrystals was stable (up to 500 ℃) even when PAN fibres was combusted implying that the PAN fibres had protected the Zr MOF nanocrystals. The residue remaining above 600 ℃ in the TGA plot presented in Figure 6.9a is as a result of the organic ligand being broken down and Zr MOF is decomposed to ZrO_2 (Zhao et al., 2013). From Figure 6.9b a residue was observed due to the decomposition of the linker molecule that occurred between 400-600 ℃ making Cr MOF nanocrystals stable up to 350 ℃ (Solomon & Banerjee, 2006; Ren et al., 2014).

6.3.3 Surface area and hydrogen adsorption analysis

The BET surface areas for the pristine MOF powders, thermal treated (degassed) PAN fibres and the MOF-PAN composite fibres were obtained from the nitrogen isotherms presented in Figure 6.10. The hydrogen adsorption isotherms are presented in Figure 6.11 and the physical properties of the MOF composite fibres are shown in Table 6.1. The experimental protocol for the surface area and hydrogen adsorption analysis of the samples are presented in section 3.5.4.
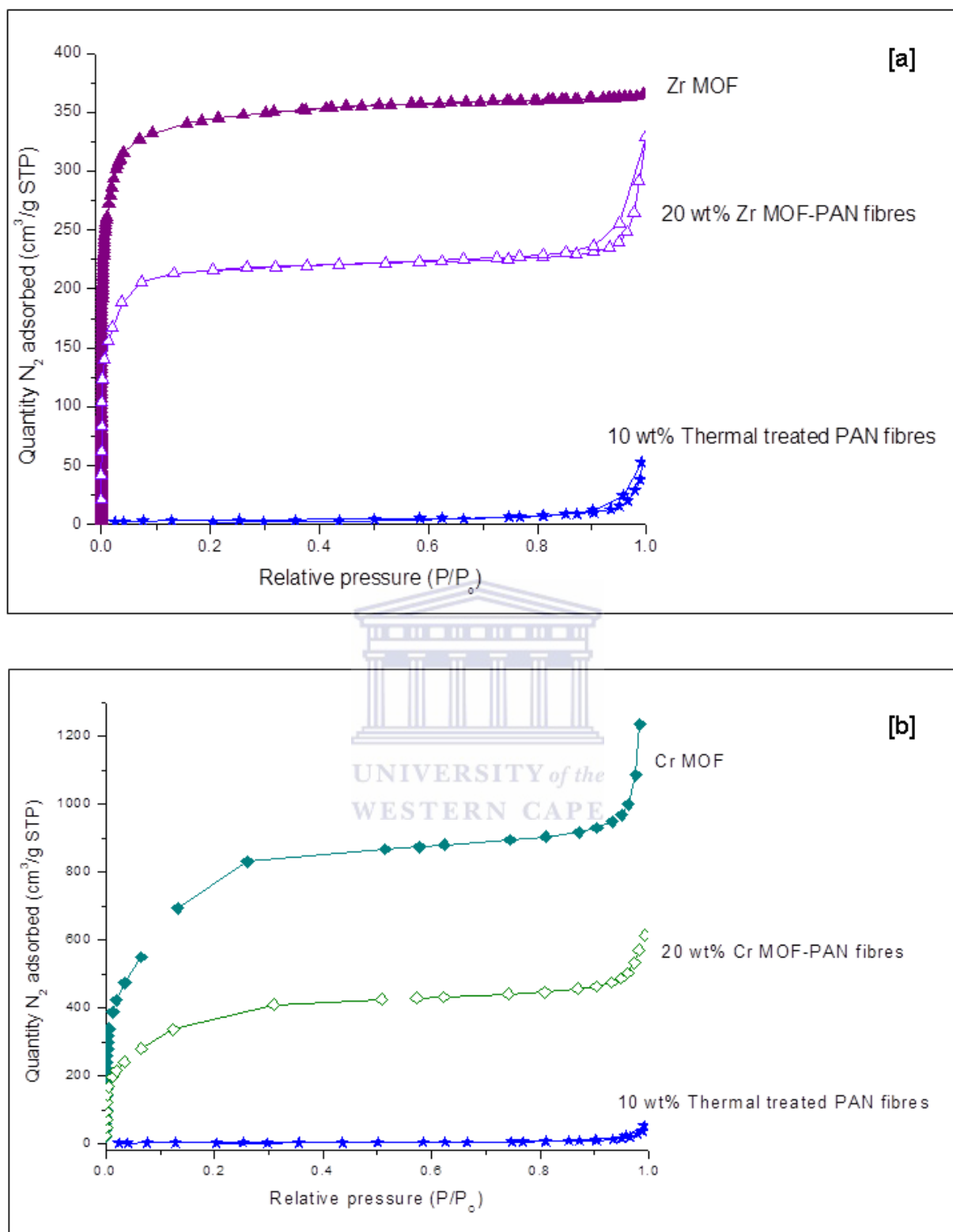
Figure 6.10: Nitrogen isotherms for Zr (a) and Cr (b) pristine MOF powders, thermal treated (degassed) PAN fibres and MOF composite fibres measured at 77 K and 1 bar.
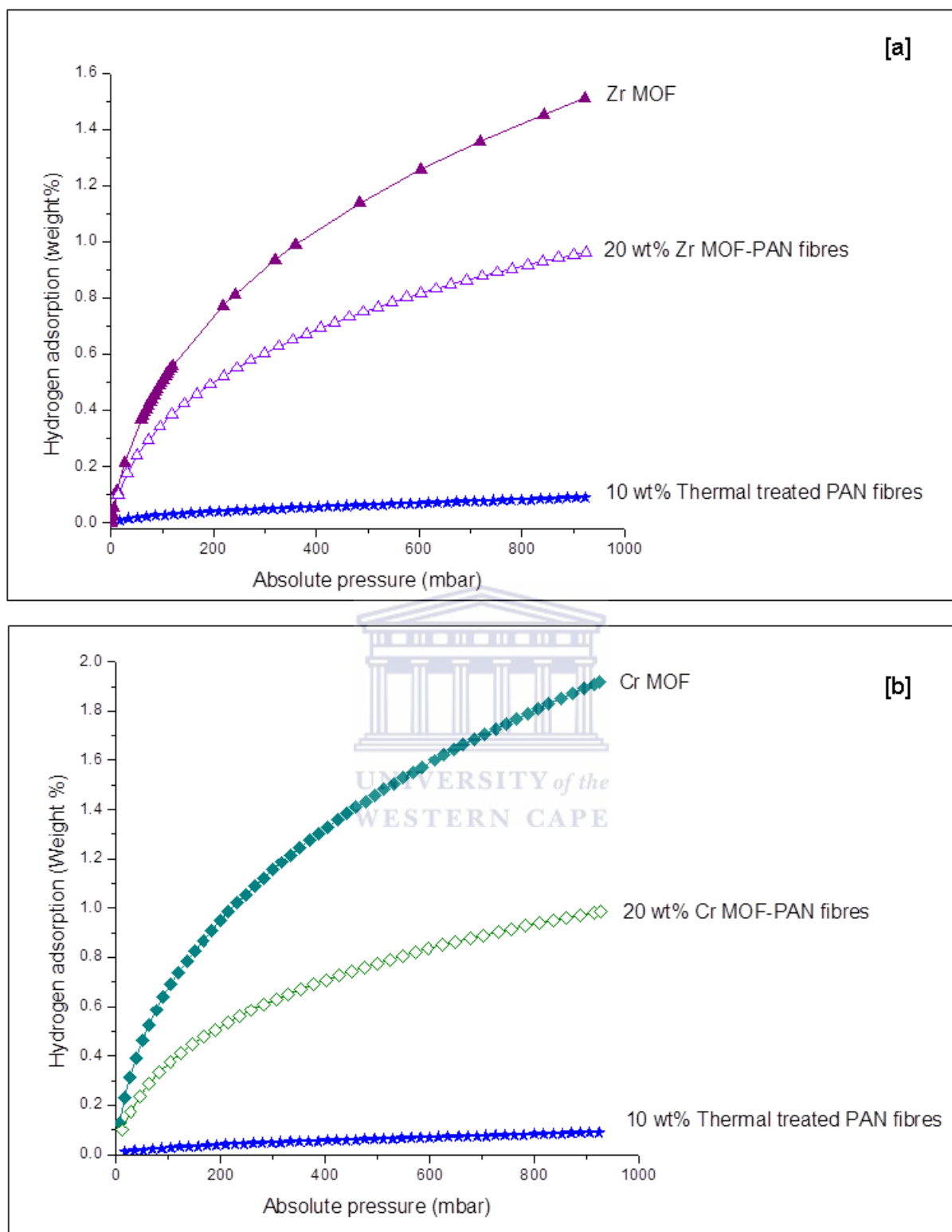
Figure 6.11: Hydrogen adsorption isotherms for Zr (a) and Cr (b) pristine MOF powders, thermal treated (degassed) PAN fibres and MOF composite fibres measured at 77 K and 1 bar.

It was observed from the Nitrogen isotherms in Figure 6.10 for the pristine MOF powders and MOF composite fibres that the pores were sharply filled below 0.1 P/P_o indicating high microporosity. Pristine MOFs depicted the type I classification of the isotherms whereas MOF-PAN composite fibres had a type IV isotherm (Thommes et al., 2015). The physical properties and hydrogen uptake capacities of the MOF composite fibres are presented in Table 6.1.

Table 6.1: Physical properties and H_2 uptake capacities of MOF composite fibres.

Sample	*Size[a]*	*$S_{BET} (m^2/g)$[b]*	*Pore volume (cm^3/g)[c]*	*H_2 adsorption $(wt\%)$[d]*
Zr-MOF (20 wt.%) PAN fibre	1-2 μm	815	0.70	0.9
Cr-MOF (20 wt.%) PAN fibre	1-2 μm	1134	0.43	1.1

[a] Estimated from SEM images. [b] BET surface area. [c] From H-K analysis. [d] Adsorbed at 77K and 1 bar.

From Table 6.1the Zr and Cr MOF composite fibres had a BET surface area of 815 m^2/g and 1134 m^2/g respectively. When compared to the BET surface area of the Zr and Cr MOF nanocrystals (of 1186 and 2618 m^2/g respectively) a surface area reduction of 31% and 57% respectively were observed once the MOF powders were incorporated into the PAN fibres. The hydrogen adsorption for Zr and Cr MOF composite fibres (Figure 6.11) were 0.9 and 1.1 wt% as compared to that of the Zr and Cr MOF nanocrystals (Figure 5.9) which was 1.5 wt% and 1.9 wt% respectively. The hydrogen adsorption capacity was reduced by 60% and 73% for Zr and Cr MOF nanocrystals respectively after they were electrospun into composite fibres.

It is important to note that the reduction in surface area and hydrogen adsorption capacities of after the incorporation of pristine MOF powders into the PAN fibres was due to low weight percent loading of the MOF powders. In this case only 20 wt% of the MOF nanocrystals was used to synthesise the MOF composite fibres. Due to the density and size of the MOFs it was thought that by incorporating more than 20 wt% of the MOF crystals the hydrogen adsorption would increase however, the incorporation of 30 wt% MOF crystals into the PAN solution resulted in the MOF-PAN blends being too thick to be electrospun. Therefore 20 wt% MOFs was the optimised loading percentage for the MOF composite fibres. Furthermore, the

reduction in surface area and hydrogen adsorption capacities can also be due to the PAN layer blocking the nitrogen and hydrogen gases from filling the pores embedded into the fibres. Therefore the MOF composite fibres underwent vacuum degassing which removes residual solvent after electrospinning thus creating porosity which is evident from the SEM micrographs presented in Figure 6.8a and c. The porosity created by vacuum degassing of the MOF composite fibres aids in nitrogen and hydrogen gas accessing the pores of the MOF nanocrystals embedded within the fibres.

Since there was no plateau presented in hydrogen adsorption capacities for the MOF nanocrystals and MOF composite fibres (Figure 6.11), meaning saturation had not been reached therefore a higher hydrogen adsorption can be expected at higher pressures (Ren et al. 2015).

Chapter summary

The chapter began with the analysis of the zeolite-PAN composite fibres then progressed to the ZTC-PAN composite fibres and finally concluded with the analysis of the Zr and Cr MOF composite fibres. Morphological analysis illustrated that the porous powdered materials were successfully supported by or encapsulated within the PAN fibres forming composite fibres and that the shapes of the porous powdered materials were conserved in the composite fibres. The amount of powdered materials supported by or encapsulated within the PAN fibres were determined by the size and density of the powdered materials which affects the viscosity of the powdered-polymeric blend and in turn its ability to be electrospun. Although the hydrogen adsorption capacity is directly correlated to the weight percentage of powdered materials supported by or encapsulated within the PAN fibre there is an optimised weight percent implying that once this amount is surpassed the powdered-polymeric blend was unable to be electrospun. The optimised weight percent for zeolites, ZTC and MOFs composite fibres were 40, 12.5 and 20 wt% respectively.

The optimised weight percent loaded composite fibres showed similar thermal stability to that of its constituents that is the pristine PAN fibres and the porous powdered materials. The thermal gravimetric analysis of the zeolite-PAN composite fibres illustrate no weight loss after 680 ℃ due to the high thermal stability of zeolites (up to 1000 ℃), however the PAN fibres decomposed between 180-700 ℃. ZTC-, Zr MOF- and Cr MOF-PAN composite fibres were thermally stable up to 500, 500 and 400 ℃ respectively. This information was then

utilised to determine the temperatures at which degassing (that is the removal any gasses or moisture adsorbed onto the composite fibres) occurred.

The BET surface area of the 40 wt% zeolite-PAN composite fibres (440 m^2/g) was lower than that of the pristine zeolite 13X (730 m^2/g). As the weight percent of the ZTC adhered to the fibres was incremented, an increase in surface area of 1018, 1663 and 1787 m^2/g was observed for 7.5, 10 and 12.5 wt% ZTC-PAN composite fibres respectively. However, these surface area measurements were lower than that of the surface area of the pristine ZTC (2717 m^2/g). The BET surface of Zr and Cr MOF composite fibres were 815 and 1134 m^2/g respectively which had reduced by 31% and 57% respectively when the pristine Zr MOF (1186 m^2/g) and Cr MOF (2618 m^2/g) powders were incorporated into the PAN fibres.

The hydrogen capacity for the 40 wt% zeolite-PAN composite fibres (0.8 wt%) is over 50% to the pristine zeolite powders (1.6 wt%). On the other hand the trend of increasing hydrogen adsorption capacities were observed as the loadings of ZTC into the ZTC-PAN fibres was increased. The hydrogen adsorption capacities for 7.5, 10 and 12.5 wt% ZTC composite fibres were 0.9, 1.5 and 1.8 wt% respectively. However, the hydrogen adsorption capacity of the ZTC-PAN composite fibre was lower than that of the pristine ZTC powder of 2.4 wt%. The hydrogen adsorption for Zr and Cr MOF composite fibres were 0.9 and 1.1 wt% as compared to that of the Zr and Cr MOF nanocrystals which were 1.5 wt% and 1.9 wt% respectively. A comparison of the hydrogen adsorption capacities for the pristine porous materials and the electrospun composite fibres are summarised in Table 6.2.

Table 6.2: A comparison of the hydrogen adsorption capacities for the pristine porous powdered materials and their corresponding electrospun composite fibres.

Pristine powdered material	*H_2 adsorption capacity (wt%)*	*Electrospun composite fibres*	*H_2 adsorption capacity (wt%)*
Zeolite 13X	1.6	40 wt% Zeolite-PAN	0.8
ZTC	2.4	12.5 wt% ZTC-PAN	1.8
Zr MOF	1.5	20 wt% Zr MOF-PAN	0.9
Cr MOF	1.9	20 wt% Cr MOF-PAN	1.1

When comparing the hydrogen adsorption capacities of the electrospun composite fibres, it was deduced that ZTC-PAN composite fibres had the highest hydrogen adsorption capacity followed by Cr MOF-PAN composite fibres. Zr MOF-PAN composite fibres had the third highest hydrogen adsorption capacity. Zeolite-PAN fibres had the lowest hydrogen adsorption capacity even though it had the highest loading percentage of (40 wt%) zeolite 13X adhered by the PAN fibres.

The reduction in surface area and hydrogen adsorption capacities after the porous powdered materials were electrospun into composite fibres is mainly due to the low amounts of porous powdered materials supported by or incorporated within the PAN fibres. Since it is the porous powdered materials that adsorb the nitrogen and hydrogen gases not the PAN fibres. Another contributing factor to this reduction is the PAN layer blocking the nitrogen and hydrogen gases from filling the pores. Therefore the composite fibres underwent vacuum degassing which removes residual solvent after electrospinning thus creating porosity observed from the SEM micrographs. This aided in nitrogen and hydrogen gas accessing the pores of the porous powdered materials.

The following chapter will conclude the findings from the study and give recommendations for future work.

Chapter Seven
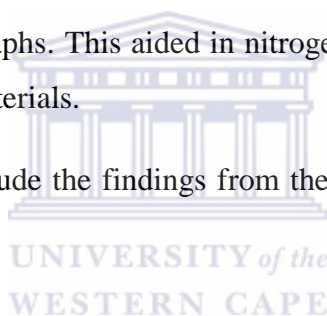
Conclusions and Recommendations

The transition from synthesising powdered materials that adsorb hydrogen gas in the laboratory to integrating them in a storage system necessitates the adoption of a versatile shaping technique such as electrospinning.

The first aspect of the study was the selection of a suitable polymer for the production of composite fibres. After electrospinning three polymers polyacrylonitrile (PAN) was selected as the most suitable polymer because it yielded bead free electrospun fibres. However, the diameter of the PAN fibres was large/thick which prompted further optimisation of the electrospinning parameters. This was aimed at determining whether the distance from the needle tip to the collector plate and the applied voltage would affect the fibre diameters. It was thereafter found that a PAN concentration of 10 wt%, a flow rate of 0.4 mL/h, a distance of 10 cm between the needle tip and collector plate and an applied voltage of 8 kV yielded smooth fibres (unbeaded) with nanofiber diameter of 480-510 nm which is within the desired range of 300-500 nm. Fibres of this diameter range are desirable since they are expected to be thick enough to enable incorporation of the porous powdered materials.

Since literature reports an increase in tensile strength during the stabilisation stage (that occurs between 200-300 ºC) of the carbonisation process for the PAN fibres, this study subjected the optimised electrospun PAN fibres to thermal treatment (stabilisation) and accessed its effects. It was observed that although thermal treatment did not decompose the PAN fibres, however it was observed to lead to brittle fibres. This observation could be due to the bypass of the oxidation stage since it was done under inert conditions. Stabilisation of the PAN fibres was done under vacuum conditions because; it was hypothesised that the residual solvent in the electrospun PAN fibres would be removed under the high vacuum thus creating porosity. However, from the results this hypothesis was not accepted.

The study then progressed on to the synthesis and characterisation of the pristine porous powdered materials which were commercial zeolite 13X, its synthesised zeolite templated carbon derivative (ZTC) and Zr (UiO-66) and Cr (MIL-101) based metal organic frameworks (MOFs). ZTC was synthesised via a liquid impregnation coupled with chemical vapour deposition (CVD) approach and the MOFs were synthesised by a modulated solvothermal

method. Analysis of the ZTCs morphology and phase crystallinity show that the carbon derivative of zeolite 13X was successful but ZTC was mainly amorphous in nature compared to crystalline zeolites. It was observed from the thermal gravimetric tests that zeolite 13X was more thermally stable (up to 1000 ℃) when compared to its ZTC derivative which was stable up to 550 ℃. The BET surface area was assessed with the aid of nitrogen sorption isotherms, for both zeolite 13X and ZTC which were 730 and 2717 m^2/g respectively. The pore volume was 0.35 and 1.44 cm^3/g for zeolite 13X and ZTC respectively. The hydrogen adsorption capacity for zeolite 13X was 1.6 wt% and increased to 2.4 wt% for the carbon derivative. The successful synthesis of defined, crystalline MOF nanocrystals was evident from X-ray diffraction and morphological analysis. The Zr and Cr MOFs were thermally stable up to 500 and 350 ℃ respectively. The BET surface area and pore volume for Zr MOF were 1186 m^2/g and 0.56 cm^3/g respectively. Cr MOF had a BET surface area of 2618 m^2/g and a pore volume of 1.29 cm^3/g. Zr and Cr MOF had a hydrogen adsorption capacity of 1.5 and 1.9 wt% respectively at 77 K and 1 bar. Since there were no plateaus observed for the hydrogen adsorption isotherms for ZTC and both MOFs, the hydrogen adsorption capacities for these samples are expected to increase at higher pressures.

The main focus and fourth aspect of the study was to synthesise electrospun composite nanofibres that can adsorb hydrogen gas. This was achieved by incorporating the porous powdered materials into the PAN resulting in a polymeric blend that was electrospun. Morphological analysis illustrated that the porous powdered materials were successfully supported by or encapsulated within the PAN fibres forming composite fibres. The achieved weight percent loading range of porous powdered materials into the PAN solution was based on the observable viscosity of the powdered-polymeric blends as determined by its electrospinability (based on the ability of the powdered-polymeric blend to flow through the needle tip).

The composite fibres showed similar thermal gravimetric stability to that of the pristine parent materials. Zeolite-PAN composite fibres showed no weight loss after 720 ℃ due to the high thermal stability of zeolites (up to 1000 ℃), however the PAN fibres decomposed between 180-700 ℃. ZTC-PAN, Zr MOF-PAN and Cr MOF-PAN composite fibres were thermally stable up to 500, 500 and 400 ℃ respectively.

The BET surface area of the 40 wt% zeolite-PAN and 12.5 wt% ZTC-PAN composite fibres were 440 and 1787 $m^2 \cdot g^{-1}$ respectively. Zr and Cr MOF composite fibres had a BET surface

area of 815 and 1134 m^2/g respectively. The BET surface area had reduced by 40, 34, 31 and 57% for zeolite 13X, ZTC, Zr and Cr MOFs respectively after these pristine porous powdered materials were electrospun into composite fibres. This reduction in surface area is primarily due the amount of porous powdered materials supported by or incorporated within the PAN fibres since only 40 wt% of zeolite 13X, 12.5 wt% of ZTC and 20 wt% of the MOFs were loaded into the PAN solution (resulting in a powdered-polymeric blend) prior to electrospinning of the composite fibres. Incorporating greater amounts of pristine porous materials resulted in a viscous powdered-polymeric blend that could not be electrospun. Another possible reason for the lower surface areas measured could be that the PAN layer blocked the nitrogen gas from entering the pores of the incorporated porous powdered materials. Therefore the composite fibres were subjected to vacuum degassing to remove residual solvent after electrospinning, which created porosity on the composite fibres but not on the pristine electrospun PAN fibres. The porosity on the composite fibres assisted the nitrogen gas in accessing the pores of the porous powdered materials. Similar trend would have been expected for the MOF-PAN composite fibres

It had been hypothesised that an increase in hydrogen adsorption capacity would be observed as the loading weight percent of the porous powdered materials was increased, since PAN fibres had a negligible hydrogen adsorption capacity. This hypothesis was accepted after the hydrogen adsorption capacities for 7.5, 10 and 12.5 wt% loadings of ZTC into the ZTC-PAN composite fibres showed an increase of 0.9, 1.5 and 1.8 wt% respectively. However, the hydrogen adsorption capacity of the ZTC-PAN composite fibre was lower than that of the pristine ZTC powder of 2.4 wt%. The hydrogen adsorption for Zr and Cr MOF composite fibres were 0.9 and 1.1 wt% as compared to that of the Zr and Cr MOF nanocrystals which were 1.5 wt% and 1.8 wt% respectively. Similar trend would have been expected for the MOF-PAN composite fibres. When comparing the hydrogen adsorption capacities of the electrospun composite fibres, it was deduced that ZTC-PAN composite fibres had the highest hydrogen adsorption capacity followed by Cr MOF-PAN composite fibres. Zr MOF-PAN composite fibres had the third highest hydrogen adsorption capacity. Zeolite-PAN fibres had the lowest hydrogen adsorption capacity even though it had the highest loading percentage of (40 wt%) zeolite 13X adhered by the PAN fibres.

Even though it has been shown in this study that zeolite-PAN, ZTC-PAN and MOF-PAN composite fibres had a lesser hydrogen adsorption capacity compared to that of their pristine porous powdered materials (zeolite, ZTC, Zr MOF and Cr MOF), the electrospinning

approach has been demonstrated to be a powerful tool for entrapping these loose powders. It can be anticipated that the use of a polymer with hydrogen adsorption properties would lead to enhanced hydrogen adsorption that could even surpass those of the porous powdered materials. Future work should thus form on the selection of polymers that could guarantee this improvement. These polymers can be polyaniline (PANi) or polymers with intrinsic microporosity (PIMs).

References

Abid, H.R., Tian, H., Ang, H., Tade, M.O., Buckley, C.E. and Wang, S. (2012). Nanosize Zr-metal organic framework (UiO-66) for hydrogen and carbon dioxide storage. *Chemical Engineering Journal,* **187**, pp. 415-420.

Aceves, S.M., Espinosa-Loza, F., Ledesma-Orozco, E., Ross, T.O., Weisberg, A.H., Brunner, T.C. and Kircher, O. (2010). High-density automotive hydrogen storage with cryogenic capable pressure vessels. *International Journal of Hydrogen Energy,* **35**(3), pp. 1219-1226.

Aceves, S., Martinez-Frias, J. and Garcia-Villazana, O. (2000). Analytical and experimental evaluation of insulated pressure vessels for cryogenic hydrogen storage. *International Journal of Hydrogen Energy,* **25**(11), pp. 1075-1085.

Agbossou, K., Chahine, R., Hamelin, J., Laurencelle, F., Anouar, A., St-Arnaud, J. and Bose, T. (2001). Renewable energy systems based on hydrogen for remote applications. *Journal of Power Sources,* **96**(1), pp. 168-172.

Ahluwalia, R., Hua, T., Peng, J., Lasher, S., Mckenney, K., Sinha, J. and Gardiner, M. (2010). Technical assessment of cryo-compressed hydrogen storage tank systems for automotive applications. *International Journal Of Hydrogen Energy,* **35**(9), pp. 4171-4184.

Akhtar, F., Andersson, L., Ogunwumi, S., Hedin, N. and Bergström, L. (2014). Structuring adsorbents and catalysts by processing of porous powders. *Journal Of The European Ceramic Society,* **34**(7), pp. 1643-1666.

Alam, N. and Mokaya, R. (2011). The effect of Al content of zeolite template on the properties and hydrogen storage capacity of zeolite templated carbons. *Microporous And Mesoporous Materials,* **144**(1), pp. 140-147.

Alam, N. and Mokaya, R. (2010). Evolution of optimal porosity for improved hydrogen storage in templated zeolite-like carbons. *Energy & Environmental Science,* **3**(11), pp. 1773-1781.

Almuhamed, S., Khenoussi, N., Bonne, M., Schacher, L., Lebeau, B., Adolphe, D. and Brendlé, J. (2014). Electrospinning of PAN nanofibers incorporating SBA-15-type ordered mesoporous silica particles. *European Polymer Journal,* **54**, pp. 71-78.

Ardelean, O., Blanita, G., Borodi, G., Lazar, M.D., Misan, I., Coldea, I. and Lupu, D. (2013). Volumetric hydrogen adsorption capacity of densified MIL-101 monoliths. *International Journal Of Hydrogen Energy,* **38**(17), pp. 7046-7055.

Armaroli, N. and Balzani, V. (2007). The future of energy supply: challenges and opportunities. *Angewandte Chemie International Edition,* **46**(1-2), pp. 52-66.

Armstrong, M.R., Arredondo, K.Y.Y., Liu, C., Stevens, J.E., Mayhob, A., Shan, B., Senthilnathan, S., Balzer, C.J. and Mu, B. (2015). UiO-66 MOF and poly (vinyl cinnamate) nanofiber composite membranes synthesized by a facile three-stage process. *Industrial & Engineering Chemistry Research,* **54**(49), pp. 12386-12392.

Arshad, S.N., Naraghi, M. and Chasiotis, I. (2011). Strong carbon nanofibers from electrospun polyacrylonitrile. *Carbon,* **49**(5), pp. 1710-1719.

Bai, B.C., Kim, J.G., Im Ji, S. and Lee, Y. (2011). The hydrogen storage capacity of metal-containing polyacrylonitrile-based electrospun carbon nanofibers. *Carbon Letters,* **12**(3), pp. 171-176.

Barthélémy, H., Weber, M. and Barbier, F. (2016). Hydrogen storage: recent improvements and industrial perspectives. *International Journal Of Hydrogen Energy,*), http://dx.doi.org/10.1016/j.ijhydene.2016.03.178.pp.1-9.

Berry, G.D. and Aceves, S.M. (1998). Onboard storage alternatives for hydrogen vehicles. *Energy & Fuels,* **12**(1), pp. 49-55.

Bhardwaj, N. and Kundu, S.C. (2010). Electrospinning: a fascinating fiber fabrication technique. *Biotechnology Advances,* **28**(3), pp. 325-347.

Bimbo, N., Ting, V.P., Sharpe, J.E. and Mays, T.J. (2013). Analysis of optimal conditions for adsorptive hydrogen storage in microporous solids. *Colloids And Surfaces A: Physicochemical And Engineering Aspects,* **437**, pp. 113-119.

Carnell, L.S., Siochi, E.J., Holloway, N.M., Stephens, R.M., Rhim, C., Niklason, L.E. and Clark, R.L. (2008). Aligned mats from electrospun single fibers. *Macromolecules,* **41**(14), pp. 5345-5349.

Cavaliere, S., Subianto, S., Savych, I., Jones, D.J. and Rozière, J. (2011). Electrospinning: designed architectures for energy conversion and storage devices. *Energy & Environmental Science,* **4**(12), pp. 4761-4785.

Cavka, J.H., Jakobsen, S., Olsbye, U., Guillou, N., Lamberti, C., Bordiga, S. and Lillerud, K.P. (2008). A new zirconium inorganic building brick forming metal organic frameworks with exceptional stability. *Journal Of The American Chemical Society,* **130**(42), pp. 13850-13851.

Cécile, C. and Hsieh, Y. (2009). Synthesis of ultrafine poly (styrene-maleic anhydride) and polystyrene fibers by electrospinning. *Journal Of Applied Polymer Science,* **113**(4), pp. 2709-2718.

Chan, B.C. (2007). The state of the art of electric, hybrid, and fuel cell vehicles. *Proceedings Of The Ieee,* **95**(4), pp. 704-718.

Chen, H., Snyder, J.D. and Elabd, Y.A. (2008). Electrospinning and solution properties of nafion and poly (acrylic acid). *Macromolecules,* **41**(1), pp. 128-135.

Chen, L., Singh, R.K. and Webley, P. (2007). Synthesis, characterization and hydrogen storage properties of microporous carbons templated by cation exchanged forms of zeolite Y with propylene and butylene as carbon precursors. *Microporous And Mesoporous Materials,* **102**(1), pp. 159-170.

Cho, C.W., Cho, D., Ko, Y. and Kwon, O.H. (2007). Stabilization, carbonization, and characterization of PAN precursor webs processed by electrospinning technique. *Carbon Letters,* **8**(4), pp. 313-320.

Chowdhury, M. and Stylios, G. (2010). Effect of experimental parameters on the morphology of electrospun nylon 6 fibres. *International Journal Of Basic & Applied Sciences,* **10**(06), pp. 116-131.

Chung, G., Jo, S. and Kim, B. (2005). Properties of carbon nanofibers prepared from electrospun polyimide. *Journal Of Applied Polymer Science,* **97**(1), pp. 165-170.

Conte, M., Iacobazzi, A., Ronchetti, M. and Vellone, R. (2001). Hydrogen economy for a sustainable development: state-of-the-art and technological perspectives. *Journal Of Power Sources,* **100**(1), pp. 171-187.

David, E. (2005). An overview of advanced materials for hydrogen storage. *Journal Of Materials Processing Technology,* **162**, pp. 169-177.

De Schoenmaker, B., Van Der Schueren, L., Zugle, R., Goethals, A., Westbroek, P., Kiekens, P., Nyokong, T. and De Clerck, K. (2013). Effect of the relative humidity on the fibre morphology of polyamide 4.6 and polyamide 6.9 nanofibres. *Journal Of Materials Science,* **48**(4), pp. 1746-1754.

Demirdoven, N. and Deutch, J. (2004). Hybrid cars now, fuel cell cars later. *Science (New York, N.Y.),* **305**(5686), pp. 974-976.

Di, J., Chen, H., Wang, X., Zhao, Y., Jiang, L., Yu, J. and Xu, R. (2008). Fabrication of zeolite hollow fibers by coaxial electrospinning. *Chemistry Of Materials,* **20**(11), pp. 3543-3545.

Dincer, I. (2000). Renewable energy and sustainable development: a crucial review. *Renewable And Sustainable Energy Reviews,* **4**(2), pp. 157-175.

Ding, B., Kim, H., Lee, S., Shao, C., Lee, D., Park, S., Kwag, G. and Choi, K. (2002). Preparation and characterization of a nanoscale poly (vinyl alcohol) fiber aggregate produced by an electrospinning method. *Journal Of Polymer Science Part B: Polymer Physics,* **40**(13), pp. 1261-1268.

Elahi, M.F., Lu, W., Guoping, G. and Khan, F. (2013). Core-shell fibers for biomedical applications-a review. *Journal Of Bioengineer & Biomedical Sci,* **3**(1), pp. 1-14.

Evans, A., Strezov, V. and Evans, T.J. (2009). Assessment of sustainability indicators for renewable energy technologies. *Renewable And Sustainable Energy Reviews,* **13**(5), pp. 1082-1088.

Ewald, R. (1998). Requirements for advanced mobile storage systems. *International Journal Of Hydrogen Energy,* **23**(9), pp. 803-814.

Ferey, G., Mellot-Draznieks, C., Serre, C., Millange, F., Dutour, J., Surble, S. and Margiolaki, I. (2005). A chromium terephthalate-based solid with unusually large pore volumes and surface area. *Science (New York, N.Y.),* **309**(5743), pp. 2040-2042.

Fong, H., Chun, I. and Reneker, D. (1999). Beaded nanofibers formed during electrospinning. *Polymer,* **40**(16), pp. 4585-4592.

Fu, R., Li, Z., Liang, Y., Feng, L., Fei, X. and Wu, D. (2011). Hierarchical porous carbons: design, preparation, and performance in energy storage. *New Carbon Materials,* **26**(3), pp. 171-179.

Gibson, P., Schreuder-Gibson, H. and Rivin, D. (2001). Transport properties of porous membranes based on electrospun nanofibers. *Colloids And Surfaces A: Physicochemical And Engineering Aspects,* **187**, pp. 469-481.

Gu, S., Ren, J. and Vancso, G. (2005). Process optimization and empirical modeling for electrospun polyacrylonitrile (PAN) nanofiber precursor of carbon nanofibers. *European Polymer Journal,* **41**(11), pp. 2559-2568.

Gupta, P., Elkins, C., Long, T.E. and Wilkes, G.L. (2005). Electrospinning of linear homopolymers of poly (methyl methacrylate): exploring relationships between fiber formation, viscosity, molecular weight and concentration in a good solvent. *Polymer,* **46**(13), pp. 4799-4810.

Güther, V. and Otto, A. (1999). Recent developments in hydrogen storage applications based on metal hydrides. *Journal Of Alloys And Compounds,* **293**, pp. 889-892.

Hafizovic, J., Bjørgen, M., Olsbye, U., Dietzel, P.D., Bordiga, S., Prestipino, C., Lamberti, C. and Lillerud, K.P. (2007). The inconsistency in adsorption properties and powder XRD data of MOF-5 is rationalized by framework interpenetration and the presence of organic and inorganic species in the nanocavities. *Journal Of The American Chemical Society,* **129**(12), pp. 3612-3620.

Han, S.O., Son, W.K., Youk, J.H., Lee, T.S. and Park, W.H. (2005). Ultrafine porous fibers electrospun from cellulose triacetate. *Materials Letters,* **59**(24), pp. 2998-3001.

Henry, S.M., El-Sayed, M.E., Pirie, C.M., Hoffman, A.S. and Stayton, P.S. (2006). Ph-responsive poly (styrene-alt-maleic anhydride) alkylamide copolymers for intracellular drug delivery. *Biomacromolecules,* **7**(8), pp. 2407-2414.

Hirscher, M., Panella, B. and Schmitz, B. (2010). Metal-Organic Frameworks for hydrogen storage. *Microporous And Mesoporous Materials,* **129**(3), pp. 335-339.

Houghton, J. (2005). Global warming: the complete briefing. Cambridge University Press. *Reports On Progress In Physics,* **68**, pp. 1343-1403.

Houghton, J.T., Ding, Y., Griggs, D.J., Noguer, M., Van Der Linden, Paul J, Dai, X., Maskell, K. and Johnson, C. (2001). Climate change 2001: the scientific basis.

Hu, J., Chen, J., Sundararaman, S., Chandrashekhara, K. and Chernicoff, W. (2008). Analysis of composite hydrogen storage cylinders subjected to localized flame impingements. *International Journal Of Hydrogen Energy,* **33**(11), pp. 2738-2746.

Hua, T., Ahluwalia, R., Peng, J., Kromer, M., Lasher, S., Mckenney, K., Law, K. and Sinha, J. (2011). Technical assessment of compressed hydrogen storage tank systems for automotive applications. *International Journal Of Hydrogen Energy,* **36**(4), pp. 3037-3049.

Huang, Z., Zhang, Y., Kotaki, M. and Ramakrishna, S. (2003). A review on polymer nanofibers by electrospinning and their applications in nanocomposites. *Composites Science And Technology,* **63**(15), pp. 2223-2253.

Im, J.S., Jang, J. and Lee, Y. (2009). Synthesis and characterization of mesoporous electrospun carbon fibers derived from silica template. *Journal Of Industrial And Engineering Chemistry,* **15**(6), pp. 914-918.

Inayat, A., Knoke, I., Spiecker, E. and Schwieger, W. (2012). Assemblies of mesoporous FAU-type zeolite nanosheets. *Angewandte Chemie International Edition,* **51**(8), pp. 1962-1965.

Jacobs, V., Anandjiwala, R.D. and Maaza, M. (2010). The influence of electrospinning parameters on the structural morphology and diameter of electrospun nanofibers. *Journal Of Applied Polymer Science,* **115**(5), pp. 3130-3136.

Jain, I. (2009). Hydrogen the fuel for 21st century. *International Journal Of Hydrogen Energy,* **34**(17), pp. 7368-7378.

Jiménez, V., Ramírez-Lucas, A., Sánchez, P., Valverde, J.L. and Romero, A. (2012). Hydrogen storage in different carbon materials: influence of the porosity development by chemical activation. *Applied Surface Science,* **258**(7), pp. 2498-2509.

Jordá-Beneyto, M., Suárez-García, F., Lozano-Castelló, D., Cazorla-Amorós, D. and Linares-Solano, A. (2007). Hydrogen storage on chemically activated carbons and carbon nanomaterials at high pressures. *Carbon,* **45**(2), pp. 293-303.

Kandiah, M., Nilsen, M.H., Usseglio, S., Jakobsen, S., Olsbye, U., Tilset, M., Larabi, C., Quadrelli, E.A., Bonino, F. and Lillerud, K.P. (2010). Synthesis and stability of tagged UiO-66 Zr-MOFs. *Chemistry Of Materials,* **22**(24), pp. 6632-6640.

Kaye, S.S., Dailly, A., Yaghi, O.M. and Long, J.R. (2007). Impact of preparation and handling on the hydrogen storage properties of Zn_4O (1, 4-benzenedicarboxylate)$_3$ (MOF-5). *Journal Of The American Chemical Society,* **129**(46), pp. 14176-14177.

Kim, B., Park, H., Lee, S. and Sigmund, W.M. (2005a). Poly (acrylic acid) nanofibers by electrospinning. *Materials Letters,* **59**(7), pp. 829-832.

Kim, D., Park, S.H., Kim, B.C., Chin, B.D., Jo, S.M. and Kim, D.Y. (2005b). Electrospun polyacrylonitrile-based carbon nanofibers and their hydrogen storages. *Macromolecular Research,* **13**(6), pp. 521-528.

Klell, M. (2006). Hydrogen as future energy source. Na. HycentA Research GmbH, Inffeldgasse 15, A-8010 Graz, Austria *(Conference proceedings).*

Kyotani, T., Ma, Z. and Tomita, A. (2003). Template synthesis of novel porous carbons using various types of zeolites. *Carbon,* **41**(7), pp. 1451-1459.

Langmi, H., Book, D., Walton, A., Johnson, S., Al-Mamouri, M., Speight, J., Edwards, P., Harris, I. and Anderson, P., (2005). Hydrogen storage in ion-exchanged zeolites. *Journal Of Alloys And Compounds,* **404**, pp. 637-642.

Latroche, M., Surblé, S., Serre, C., Mellot-Draznieks, C., Llewellyn, P.L., Lee, J., Chang, J., Jhung, S.H. and Férey, G. (2006). Hydrogen storage in the giant-pore metal–organic frameworks MIL-100 and MIL-101. *Angewandte Chemie International Edition,* **45**(48), pp. 8227-8231.

Leach, M.K., Feng, Z., Tuck, S.J. and Corey, J.M. (2011). Electrospinning fundamentals: optimizing solution and apparatus parameters. *J vis exp,* **47**. (http://www.jove.com/video/2494/electrospinning-fundamentals-optimizing-solution-apparatus?sms_ss=delicious&at_xt=4d7f10290b719462,0). [accessed on 13 March 2015]

Lee, J., Farha, O.K., Roberts, J., Scheidt, K.A., Nguyen, S.T. and Hupp, J.T. (2009). Metal–organic framework materials as catalysts. *Chemical Society Reviews,* **38**(5), pp. 1450-1459.

Lee, K., Kim, H., Bang, H., Jung, Y. and Lee, S. (2003). The change of bead morphology formed on electrospun polystyrene fibers. *Polymer,* **44**(14), pp. 4029-4034.

Lee, S., Kim, J., Ku, B., Kim, J. and Joh, H. (2012). Structural evolution of polyacrylonitrile fibers in stabilization and carbonization. *Scientific Research*, **2**, pp. 275-282.

Li, L. and Hsieh, Y. (2005). Ultra-fine polyelectrolyte fibers from electrospinning of poly (acrylic acid). *Polymer,* **46**(14), pp. 5133-5139.

Li, J. and Wu, E. (2012). Chapter 5: storage of hydrogen in zeolites in zeolites: synthesis, chemistry and applications. Eds. Andreyev M K And Zubkov O L. Nova science publishers, inc. pp 149-170. Available online. [25 may 2015]

Li, W., Zhao, H., Teasdale, P., John, R. and Zhang, S. (2002). Synthesis and characterisation of a polyacrylamide–polyacrylic acid copolymer hydrogel for environmental analysis of Cu and Cd. *Reactive And Functional Polymers,* **52**(1), pp. 31-41.

Li, Y. and Yang, R.T. (2006). Hydrogen storage in low silica type X zeolites. *The Journal Of Physical Chemistry B,* **110**(34), pp. 17175-17181.

Li, Z. and Wang, C. (2013). Effects of working parameters on electrospinning. *One-dimensional nanostructures. Springer*, pp. 15-28.

Liaquat, A., Kalam, M., Masjuki, H. and Jayed, M. (2010). Potential emissions reduction in road transport sector using biofuel in developing countries. *Atmospheric Environment,* **44**(32), pp. 3869-3877.

Liu, D., Purewal, J., Yang, J., Sudik, A., Maurer, S., Mueller, U., Ni, J. and Siegel, D. (2012). MOF-5 composites exhibiting improved thermal conductivity. *International Journal Of Hydrogen Energy,* **37**(7), pp. 6109-6117.

Lowell, S., Shields, J.E., Thomas, M.A. and Thommes, M. (2012). Characterization of porous solids and powders: surface area, pore size and density. *Springer* science & business media.

Lund, H. (2007). Renewable energy strategies for sustainable development. *Energy,* **32**(6), pp. 912-919.

Lund, H. and Kempton, W. (2008). Integration of renewable energy into the transport and electricity sectors throughV2G. *Energy Policy,* **36**(9), pp. 3578-3587.

Ma, Y., Yan, C., Alshameri, A., Qiu, X. and Zhou, C. (2014). Synthesis and characterization of 13X zeolite from low-grade natural kaolin. *Advanced Powder Technology,* **25**(2), pp. 495-499.

Masika, E. and Mokaya, R. (2013). Preparation of ultrahigh surface area porous carbons templated using zeolite 13X for enhanced hydrogen storage. *Progress In Natural Science: Materials International,* **23**(3), pp. 308-316.

Mckee, M.G., Wilkes, G.L., Colby, R.H. and Long, T.E. (2004). Correlations of solution rheology with electrospun fiber formation of linear and branched polyesters. *Macromolecules,* **37**(5), pp. 1760-1767.

Megelski, S., Stephens, J.S., Chase, D.B. and Rabolt, J.F. (2002). Micro-and nanostructured surface morphology on electrospun polymer fibers. *Macromolecules,* **35**(22), pp. 8456-8466.

Mori, D. and Hirose, K. (2009). Recent challenges of hydrogen storage technologies for fuel cell vehicles. *International Journal Of Hydrogen Energy,* **34**(10), pp. 4569-4574.

Musyoka, N.M., Ren, J., Langmi, H.W., North, B.C. and Mathe, M. (2015). A comparison of hydrogen storage capacity of commercial and fly ash-derived zeolite X together with their respective templated carbon derivatives. *International Journal Of Hydrogen Energy,* **40**(37), pp. 12705-12712.

Nataraj, S., Yang, K. and Aminabhavi, T. (2012). Polyacrylonitrile-based nanofibers—a state-of-the-art review. *Progress In Polymer Science,* **37**(3), pp. 487-513.

Nguyen, J.G. and Cohen, S.M. (2010). Moisture-resistant and superhydrophobic metal–organic frameworks obtained via postsynthetic modification. *Journal Of The American Chemical Society,* **132**(13), pp. 4560-4561.

Nishihara, H., Hou, P., Li, L., Ito, M., Uchiyama, M., Kaburagi, T., Ikura, A., Katamura, J., Kawarada, T. and Mizuuchi, K. (2009). High-pressure hydrogen storage in zeolite-templated carbon. *The Journal Of Physical Chemistry C,* **113**(8), pp. 3189-3196.

Nishihara, H. and Kyotani, T. (2012). Templated nanocarbons for energy storage. *Advanced Materials,* **24**(33), pp. 4473-4498.

Nishihara, H., Yang, Q., Hou, P., Unno, M., Yamauchi, S., Saito, R., Paredes, J.I., Martínez-Alonso, A., Tascón, J.M. and Sato, Y. (2009). A possible buckybowl-like structure of zeolite templated carbon. *Carbon,* **47**(5), pp. 1220-1230.

O'malley, K., Ordaz, G., Adams, J., Randolph, K., Ahn, C.C. and Stetson, N.T. (2014). Applied hydrogen storage research and development: a perspective from the US Department of Energy. *Journal Of Alloys And Compounds,* **645**, pp.5419-5422.

O'neill, L.D., Zhang, H. and Bradshaw, D. (2010). Macro-/microporous MOF composite beads. *Journal Of Materials Chemistry,* **20**(27), pp. 5720-5726.

Ostermann, R., Cravillon, J., Weidmann, C., Wiebcke, M. and Smarsly, B.M. (2011). Metal–organic framework nanofibers via electrospinning. *Chemical Communications,* **47**(1), pp. 442-444.

Pegels, A. (2010). Renewable energy in South Africa: potentials, barriers and options for support. *Energy Policy,* **38**(9), pp. 4945-4954.

Rahaman, M.S.A., Ismail, A.F. and Mustafa, A. (2007). A review of heat treatment on polyacrylonitrile fiber. *Polymer Degradation And Stability,* **92**(8), pp. 1421-1432.

Ren, J., Langmi, H.W., North, B.C. and Mathe, M. (2015). Review on processing of metal–organic framework (MOF) materials towards system integration for hydrogen storage. *International Journal Of Energy Research,* **39**(5), pp. 607-620.

Ren, J., Langmi, H.W., North, B.C., Mathe, M. and Bessarabov, D. (2014). Modulated synthesis of zirconium-metal organic framework (Zr-MOF) for hydrogen storage applications. *International Journal Of Hydrogen Energy,* **39**(2), pp. 890-895.

Ren, J., Musyoka, N.M., Annamalai, P., Langmi, H.W., North, B.C. and Mathe, M. (2015). Electrospun MOF nanofibers as hydrogen storage media. *International Journal Of Hydrogen Energy,* **40**(30), pp. 9382-9387.

Ren, J., Musyoka, N.M., Langmi, H.W., Segakweng, T., North, B.C., Mathe, M. and Kang, X. (2014). Modulated synthesis of chromium-based metal-organic framework (MIL-101) with enhanced hydrogen uptake. *International Journal Of Hydrogen Energy,* **39**(23), pp. 12018-12023.

Ren, J., Musyoka, N.M., Langmi, H.W., Swartbooi, A., North, B.C. and Mathe, M. (2015). A more efficient way to shape metal-organic framework (MOF) powder materials for hydrogen storage applications. *International Journal Of Hydrogen Energy,* **40**(13), pp. 4617-4622.

Ren, J. and North, B.C. (2014). Shaping porous materials for hydrogen storage applications: a review. *Journal Of Technology Innovations In Renewable Energy,* **3**(1), pp. 12.

Richard-Lacroix, M. and Pellerin, C. (2013). Molecular orientation in electrospun fibers: from mats to single fibers. *Macromolecules,* **46**(24), pp. 9473-9493.

Ross, D. (2006). Hydrogen storage: the major technological barrier to the development of hydrogen fuel cell cars. *Vacuum,* **80**(10), pp. 1084-1089.

Sakintuna, B., Lamari-Darkrim, F. and Hirscher, M. (2007). Metal hydride materials for solid hydrogen storage: a review. *International Journal Of Hydrogen Energy,* **32**(9), pp. 1121-1140.

Schaate, A., Roy, P., Godt, A., Lippke, J., Waltz, F., Wiebcke, M. and Behrens, P. (2011). Modulated synthesis of Zr-based metal–organic frameworks: from nano to single crystals. *Chemistry–A European Journal,* **17**(24), pp. 6643-6651.

Schulte, I., Hart, D. and Van Der Vorst, R. (2004). Issues affecting the acceptance of hydrogen fuel. *International Journal Of Hydrogen Energy,* **29**(7), pp. 677-685.

Shenoy, S.L., Bates, W.D., Frisch, H.L. and Wnek, G.E. (2005). Role of chain entanglements on fiber formation during electrospinning of polymer solutions: good solvent, non-specific polymer–polymer interaction limit. *Polymer,* **46**(10), pp. 3372-3384.

Sherif, S., Zeytinoglu, N. and Veziroğlu, T. (1997). Liquid hydrogen: potential, problems, and a proposed research program. *International Journal Of Hydrogen Energy,* **22**(7), pp. 683-688.

Solomon, B.D. and Banerjee, A. (2006). A global survey of hydrogen energy research, development and policy. *Energy Policy,* **34**(7), pp. 781-792.

Somayajulu Rallapalli, P., Raj, M.C., Patil, D.V., Prasanth, K., Somani, R.S. and Bajaj, H.C. (2013). Activated carbon@ MIL-101 (Cr): a potential metal-organic framework composite material for hydrogen storage. *International Journal Of Energy Research,* **37**(7), pp. 746-753.

Srinivasan, D., Rao, R. and Zribi, A. (2006). Synthesis of novel micro-and mesoporous zeolite nanostructures using electrospinning techniques. *Journal Of Electronic Materials,* **35**(3), pp. 504-509.

Su, D.S. and Centi, G. (2013). A perspective on carbon materials for future energy application. *Journal Of Energy Chemistry,* **22**(2), pp. 151-173.

Subbiah, T., Bhat, G., Tock, R., Parameswaran, S. and Ramkumar, S. (2005). Electrospinning of nanofibers. *Journal Of Applied Polymer Science,* **96**(2), pp. 557-569.

Thambiran, T. and Diab, R.D. (2011). Air pollution and climate change co-benefit opportunities in the road transportation sector in durban, south africa. *Atmospheric Environment,* **45**(16), pp. 2683-2689.

Thomas, K.M. (2007). Hydrogen adsorption and storage on porous materials. *Catalysis Today,* **120**(3), pp. 389-398.

Thommes, M., Kaneko, K., Neimark, A.V., Olivier, J.P., Rodriguez-Reinoso, F., Rouquerol, J. and Sing, K.S. (2015). Physisorption of gases, with special reference to the evaluation of surface area and pore size distribution (iupac technical report). *Pure And Applied Chemistry,* **87**(9-10), pp. 1051-1069.

Treacy, M.M. and Higgins, J.B. (2007). Collection of simulated XRD powder patterns for zeolites fifth (5th) revised edition. Elsevier.

Turner, J.A. (2004). Sustainable hydrogen production. *Science (New York, N.Y.),* **305**(5686), pp. 972-974.

US DOE 2009
http://energy.gov/sites/prod/files/2015/05/f22/fcto_targets_onboard_hydro_storage_explanation.pdf [accessed on 25 January 2016].

Utgikar, V.P. and Thiesen, T. (2005). Safety of compressed hydrogen fuel tanks: leakage from stationary vehicles. *Technology In Society,* **27**(3), pp. 315-320.

Villalonga, S., Nony, F., Magnier, C., Yvernes, J., Thomas, C., Delmas, B. and Mazabraud, P. (2009). Composite 700 bar-vessel for on-board compressed gaseous hydrogen storage, *proc. Of 17th International Conference on Composite Materials, Edinburgh, UK,* 2009,.

Vitousek, P.M., Mooney, H.A., Lubchenco, J. and Melillo, J.M. (1997). Human domination of earth's ecosystems. *Science,* **277**(5325), pp. 494-499.

Wabiri, N. and Amusa, H. (2010). Quantifying South Africa's crude oil import risk: a multi-criteria portfolio model. *Economic Modelling,* **27**(1), pp. 445-453.

Wang, C., Chien, H., Hsu, C., Wang, Y., Wang, C. and Lu, H. (2007). Electrospinning of polyacrylonitrile solutions at elevated temperatures. *Macromolecules,* **40**(22), pp. 7973-7983.

Wang, T. and Kumar, S. (2006). Electrospinning of polyacrylonitrile nanofibers. *Journal Of Applied Polymer Science,* **102**(2), pp. 1023-1029.

Weitkamp, J., Fritz, M. and Ernst, S. (1995). Zeolites as media for hydrogen storage. *International Journal Of Hydrogen Energy,* **20**(12), pp. 967-970.

Wißmann, G., Schaate, A., Lilienthal, S., Bremer, I., Schneider, A.M. and Behrens, P. (2012). Modulated synthesis of Zr-fumarate MOF. *Microporous And Mesoporous Materials,* **152**, pp. 64-70.

WRI (World Resources Institute), (2014) http://www.wri.org//blog/2014/05/history-carbon-dioxide-emissions) [accessed on 13 January 2016].

Wu, H., Chua, Y.S., Krungleviciute, V., Tyagi, M., Chen, P., Yildirim, T. and Zhou, W. (2013). Unusual and highly tunable missing-linker defects in zirconium metal–organic framework UiO-66 and their important effects on gas adsorption. *Journal Of The American Chemical Society,* **135**(28), pp. 10525-10532.

Wu, Y., Li, F., Liu, H., Zhu, W., Teng, M., Jiang, Y., Li, W., Xu, D., He, D. and Hannam, P. (2012). Electrospun fibrous mats as skeletons to produce free-standing MOF membranes. *Journal Of Materials Chemistry,* **22**(33), pp. 16971-16978.

Yamane, A., Sawai, D., Kameda, T., Kanamoto, T., Ito, M. and Porter, R.S. (1997). Development of high ductility and tensile properties upon two-stage draw of ultrahigh molecular weight poly (acrylonitrile). *Macromolecules,* **30**(14), pp. 4170-4178.

Yang, C. and Yan, X. (2011). Metal–organic framework MIL-101 (Cr) for high-performance liquid chromatographic separation of substituted aromatics. *Analytical Chemistry,* **83**(18), pp. 7144-7150.

Yang, J., Sudik, A., Wolverton, C. and Siegel, D.J. (2010). High capacity hydrogen storage materials: attributes for automotive applications and techniques for materials discovery. *Chemical Society Reviews,* **39**(2), pp. 656-675.

Yang, S.J., Jung, H., Kim, T. and Park, C.R. (2012). Recent advances in hydrogen storage technologies based on nanoporous carbon materials. *Progress In Natural Science: Materials International,* **22**(6), pp. 631-638.

Yang, Z., Xia, Y. and Mokaya, R. (2005). Hollow shells of high surface area graphitic N-doped carbon composites nanocast using zeolite templates. *Microporous And Mesoporous Materials,* **86**(1), pp. 69-80.

Yürüm, Y., Taralp, A. and Veziroglu, T.N. (2009). Storage of hydrogen in nanostructured carbon materials. *International Journal Of Hydrogen Energy,* **34**(9), pp. 3784-3798.

Zeng, K. and Zhang, D. (2010). Recent progress in alkaline water electrolysis for hydrogen production and applications. *Progress In Energy And Combustion Science,* **36**(3), pp. 307-326.

Zhang, Z., Huang, S., Xian, S., Xi, H. and Li, Z. (2011). Adsorption equilibrium and kinetics of CO2 on chromium terephthalate MIL-101. *Energy & Fuels,* **25**(2), pp. 835-842.

Zhao, D., Yuan, D. and Zhou, H. (2008). The current status of hydrogen storage in metal–organic frameworks. *Energy & Environmental Science,* **1**(2), pp. 222-235.

Zhao, J., Lee, D.T., Yaga, R.W., Hall, M.G., Barton, H.F., Woodward, I.R., Oldham, C.J., Walls, H.J., Peterson, G.W. and Parsons, G.N. (2016). Ultra-fast degradation of chemical warfare agents using MOF–nanofiber kebabs. *Angewandte Chemie,* **128**(42), pp. 13418-13422.

Zhao, Q., Yuan, W., Liang, J. and Li, J. (2013). Synthesis and hydrogen storage studies of metal− organic framework UiO-66. *International Journal Of Hydrogen Energy,* **38**(29), pp. 13104-13109.

Zhao, T., Jeremias, F., Boldog, I., Nguyen, B., Henninger, S.K. and Janiak, C. (2015). High-yield, fluoride-free and large-scale synthesis of MIL-101 (Cr). *Dalton Transactions,* **44**(38), pp. 16791-16801.

Zhao, Z., Li, X. and Li, Z. (2011). Adsorption equilibrium and kinetics of p-xylene on chromium-based metal organic framework MIL-101. *Chemical Engineering Journal,* **173**(1), pp. 150-157.

Zheng, J., Liu, X., Xu, P., Liu, P., Zhao, Y. and Yang, J. (2012). Development of high pressure gaseous hydrogen storage technologies. *International Journal Of Hydrogen Energy,* **37**(1), pp. 1048-1057.

Zuo, W., Zhu, M., Yang, W., Yu, H., Chen, Y. and Zhang, Y. (2005). Experimental study on relationship between jet instability and formation of beaded fibers during electrospinning. *Polymer Engineering & Science,* **45**(5), pp. 704-709.